EPA/600/R-97/054
September 1997

Theoretical and Experimental Modeling of Multi-Species Transport in Soils Under Electric Fields

By

Yalcin B. Acar and Akram N. Alshawabkeh
Electrokinetics, Inc.
Baton Rouge, LA 70809

Randy A. Parker
National Risk Management Research Laboratory
U.S. Environmental Protection Agency
Cincinnati, OH 45268

Cooperative Agreement No. CR-816828-01-1

Project Officer:

Randy A. Parker
Land Remediation and Pollution Control Division
National Risk Management Research Laboratory
Cincinnati, OH 45268

National Risk Management Research Laboratory
Office of Research and Development
U.S. Environmental Protection Agency
Cincinnati, OH 45268

TECHNICAL REPORT DATA
(Please read Instructions on the reverse before completing)

1. REPORT NO.	2.	3. RECIPIENT'S ACCESSION NO.
EPA/600/R-97/054		PB97-193056

4. TITLE AN0 SUBTITLE

Theoretical and Experimental Modeling of Multi-Species Transport in Soils Under Electric Fields

5. REPORT 0 TE: September 1997

6. PERFORMING ORGANIZATION COOE

A7. AUTHOR(S)

Yalcin B. Acar[1], Akram N. Alshawabkeh', and Randy A. Parker [2]

8. PERFORMING ORGANIZATION REPORT NO,

9. PERFORMING. ORGANIZATION NAME AND ADRESS

Electrokinetics, Inc., 11552 Cedar Park Ave.
Baton Rouge, LA 70809
[2]National Risk Management Research Laboratory, USEPA
Cincinnati, OH 45268

10. PROGRAM ELEMENT NO.

11. CONTRACT/GRANT NO.

CR-816828-01-l

12. SPONSORING AGENCY NAME AN0 AOORESS

National Risk Management Research Laboratory
Office of Research and Development
U.S. Environmental Protection Agency
Cincinnati. OH 45268

13. TYPE OF REPORT AND PERIOD COVERED
Project Report, 8/90 - 8/94

14. SPONSORING AGENCY CODE

EPA/600/14

15. SUPPLEMENTARY NOTES

Project Officer: Randy A. Parker (5 13) 569-7271

16. ABSTRACT

Electrokinetics employs the use of electrodes implanted in soils-contaminated media. Electrodes are supplied with direct current (dc) facilitating ionic transport and subsequent, removal. This project investigates the feasibility and efficiency of electrokinetic transport of lead in soils at bench and pilot-scale. A theoretical model was developed using numerical algorithms based on differential and algebraic equations. The theoretical model is presented and compared with pilot-scale results.

17. KEY WOROS AN0 DOCUMENT ANALYSIS

a. DESCRIPTORS	b. IDENTIFIERS/OPEN ENDED TERMS	c. COSATI Field/Group
Emerging Technology Lead Soils	Electrokinetics Site Program	

8. DISTRIBUTION STATEMENT	19. SECURITY CLASS (THIS *Report)*	21. NO. OF PAGES
Release to Public	Unclassified	
	20. SECURITY CLASS *(This page)* Unclassified	22. PRICE

EPA Form 2220-I (Rev. 4-77 PREVIOUS EDITION OBSOLETE

DISCLAIMER

The U.S. Environmental Protection Agency through its Office of Research and Development partially funded and collaborated in the research described here under Cooperative Agreement No. CR 816828-01-0 to Electrokinetics, Inc. It has been subject to the Agency's peer and administrative review, and it has been approved for publication as an EPA document. Mention of trade names or commercial products does not constitute endorsement or recommendation for use.

FOREWORD

The U.S. Environmental Protection Agency (EPA) is charged by Congress with protecting the Nation's land, air, and water resources. Under a mandate of national environmental laws, the Agency strives to formulate and implement actions leading to a compatible balance between human activities and the ability of natural systems to support and nurture life. To meet this mandate, EPA's research program is providing data and technical support for solving environmental problems today and building a science knowledge base necessary to manage our ecological resources wisely, understand how pollutants affect our health, and prevent or reduce environmental risks in the future.

The National Risk Management Research Laboratory is the Agency's center for investigation of technological **and** management approaches for reducing risks from threats to human health and the environment. The focus of the Laboratory's research program is on methods for the prevention and control of pollution to air, land, water, and subsurface resources: protection of water quality in public water systems; remediation of contaminated sites and ground water: and prevention of indoor air pollution. The goal of this research effort is to catalyze development and implementation of innovative, cost effective environmental technologies; develop scientific and engineering information needed by EPA to support regulatory and policy decisions; and provide technical support and information transfer to ensure effective implementation of environmental regulations and strategies.

This publication has been produced as part of the Laboratory's strategic long-term research plan. It is published and made available by EPA's office of Research and Development to assist the user community and to link researchers with their clients.

E. Timothy Oppelt, Director
National Risk Management Research Laboratory

ACKNOWLEDGEMENTS

The pilot-scale studies reported herein are supported by the US Environmental protection Agency **(USEPA)** National Risk Management Research Laboratory (NRMRL) under the SITE-E03 program through the Cooperative Agreement CR81682801-1 with Electrokinetics Inc. of Baton Rouge, Louisiana. Don Sanning, Norma Lewis, Randy Parker and Guy Simes of **the SITE** program of NRMRL are gratefully acknowledged for their collaboration and cooperation during the course of this project

"Fundamental Aspects of Electrokinetic Remediation of Soils" is another project funded with Federal Funds as part of the program of the Gulf Coast Hazardous Substance Research Center (GCHSRC) which is supported under cooperative agreement R815197 with the United States Environmental Protection Agency. Monsanto Corporation partnered with GCHSRC through the Industrial Ties Program in partial support of some of the tasks in the pilot-scale testing and the theoretical development effort. We thank Alan Ford of GCHSRC and Sa Ho of Monsanto for their efficient input and collaboration.

We appreciate the materials and the labor donated in manufacturing the liners used in the pilot-scale boxes by the Gundle Corporation and Robert Johnson of this corporation.

The contents and opinions expressed in this report are those of the authors and do not necessarily reflect the views and policies of the USEPA and other sponsors.

TABLE OF CONTENTS

LIST OF TABLES

LIST OF FIGURES

LIST OF PLATES

EXECUTIVE SUMMARY

The feasibility and efficiency of transporting lead under electric fields are investigated at pilot-scale in three one ton Georgia kaolinite specimens spiked with lead nitrate solution and at an dectrode spacing of 72 cm. In order to establish the relation between chemistry and mechanics, enhancement methods such as cathode depolarization and/or catholyte neutralization techniques are not employed in processing. **A** constant direct current density of I33 $\mu A/cm^2$ is applied. Two of the tests are conducted on specimens spiked with lead at concentrations of 856 mg/kg and 1,533 mg/kg. The third test is conducted on a I : 1 mixture of compacted kaolinite/sand spiked with lead at a concentration of 5,322 mg/kg. pH distributions, electric potential distributions, lead transport, pore pressures and temperatures developed across the soil mass are presented, evaluated and discussed. The tests demonstrated that the lead was transported towards the cathode and precipitated at its hydroxide solubility value within the basic zone in direct contact with the cathode compartment. Subsequent to 2,950 h of proccssing and an energy expenditure of 700 kWh/m^3, 55 % of the lead removed across the soil was found precipitated within the last 2 cm close to the cathode, 15 % was left in the soi1 before reaching this zone, 20 % was found precipitated on the fabric separating the soil from the cathode compartment and 10% was unaccounted. The results demonstrate that heavy metals and species that are solubilized in the anodic acid front can be efficiently transported by electromigration under an electrica l field applied across electrodes placed in soils. The results also disclose the rdation between chemistry and mechanics in pore fluid transport and electroosmotic consolidation. In direct response to the changes in electrochemistry, suction and electroosmotic consolidation prevail in the soil even when egress and ingress of pore fluids into the soil are allowed at the electrodes.

A mathematical model also is presented for multi-component species transport under coupled hydraulic, electric, and chemical potential differences. Mass balance of species and pore fluid together with charge balance across the medium result in a set of differential equations. Sorption, aqueous phase and precipitation reactions are accounted by a set of algebraic equations. Instantaneous chemical equilibrium conditions are assumed. Transport of H^+, OH-, Pb^{2+} the associated chemicaI reactions, electric potential and pore pressure distribution across the electrodes in electrokinetic remediation are modeled. Model predictions of acid transport, lead transport, and pore pressure distribution display very good agreement with the pilot-scale test results validating

the formalisms offered for multi-component transport of reactive species under an electric field. The model also bridges the gap between the electrochemistry and mechanics in electroosmotic consolidation of soils.

This report was submitted in fullfillment of Cooperative Agreement CR81682801-1 between the National Risk Management Research Laboratory of the U. S. Environmental Protection Agency and Electrokinetics Inc. The accomptishment presented by the report covers a period from August 1990 to August 1994 and the work is completed as of June 1994.

Section **1**

INTRODUCTION

The impact of soil contamination on groundwater resources is becoming increasingly significant as the disclosed number of unengineered waste containment facilities and contaminated sites grow and remediation costs increase. The growing size of the problem has given way to a comprehensive national program that endeavors to encourage waste reduction, advance treatment, and disposal of hazardous wastes. As a result, a Resource Conservation and Recovery Act (RCRA) has been enacted in 1976 and amended several times since its enactment, most importantly by the Hazardous and Solid Waste Amendments of 1984 (HSWA). Over 500,000 companies and/or individuals in the United States who generate over 172 million metric tons of hazardous waste each year must comply with the RCRA regulatory program (Arbuckle et al. 1989). In 1980, Congress established the Comprehensive Environmental, Response, Compensation, and Liability Act (CERCLA), usually referred to as the Superfund, which is subsequently reauthorized by Superfund Amendments Reauthorization Act (SARA) of 1986. Both CERCLA and RCRA seek to provide a veil coverage of the hazardous waste problem. While RCRA is designed as a regulatory program for present and new hazardous waste sites, CERCLA establishes a comprehensive response program for the past hazardous waste activities. According to CERCLA,

> ... Whenever there is a release or substantial threat of release into the environment of any hazardous substance or pollutant or contaminant under circumstances where the pollutant or contaminant may present an imminent and substantial danger, EPA is authorized to undertake removal and/or remedial action

Removal and remedy differ in that removal is a short-time limited response to a more manageable problem while remedy is a longer-term more permanent and expensive solution for a complex problem.

From among the over 40,000 sites reported to United States Environmental Protection Agency (USEPA or EPA) which might need remedial action, about 2,000 sites are listed as Superfund sites. While the estimated remediation cost for the Superfund sites is 50 billion dollars, the total estimated cost for all the contaminated sites may run up to 350 billion dollars. Figure 1.1

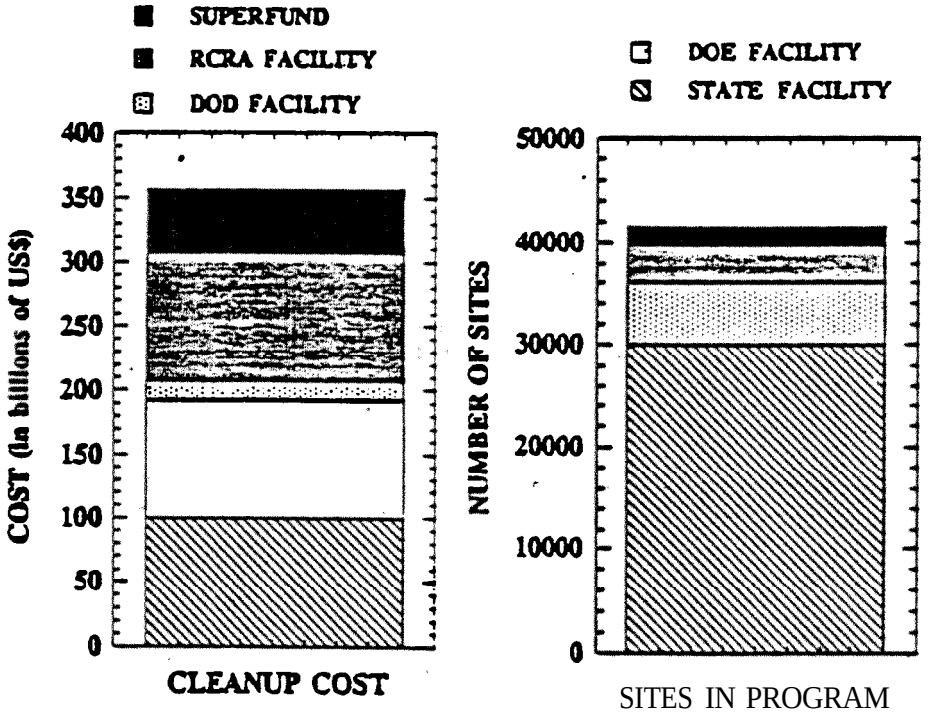

Figure 1.1: Estimated Number of Contaminated Sites and Clean-up Costs in the US (Adapted from Morse 1989).

presents an estimate of the number of contaminated sites and the associated cleanup cost reported by different state agencies in the United Stares (Morse, 1989).

In 1980, CERCLA has required EPA to develop and to provide criteria for determining priorities among sites that require remedial action and to devdop and maintain a National Priority List (NPL). Under EPA regulations, these sites are eligible for remedial action. Although 149 sites have been cleaned and removed from the NPL since Superfund's inception, the list continues to grow. Recently, EPA added 33 new sites bringing the NPL total to 1250 sites (Austin, 1993).

A variety of options may exist to select a cleanup remedy at a site; however, the efficiency and costs of these options may vary widely. Accordingly, the decision of "how clean is clean?" and "how expensive is expensive?" is taken independently for each site by the EPA Although conventional ground burial and land disposal are often economical, they do not provide the best solutions, and in some cases they are not necessarily the most effective solution. There exists an everlasting need to introduce new, innovative, and preferably in-situ remediation technologies. Several such schemes are introduced in the last decade including incineration, solidification/stabilization, bioremediation, dechlorination, flushing, vitrification, washing, thermal desorption, vacuum extraction, and chemical treatment (EPA 199 1). Each technology exhibits certain advantages and Iimitations in remediating a myriad of organic/inorganic contaminants encountered in different types of soil deposits. As an example there is a growing use of vacuum extraction technique for removing organic contaminants. This technology favors partially saturated deposits having relatively high hydraulic conductivities (silt and sand). The technique is ineffective in removing inorganic contaminants. There is not one specific technology that can be considered as a panacea to all types of contaminants and soil deposits (Acar et al. 1992a).

A major limitation of the most successful remediation technologies, such as vacuum extraction and soil flushing, is that they are restricted to soils with high hydraulic conductivity and hence, cannot be used for fine-grained deposits. Furthermore, they are not specifically effective in removing contaminants adsorbed on the soil particles (such as pump and treat). Such adsorption may pose threat for ground water and plant contamination.

The challenging demand to develop new, innovative and cost effective in-situ remediation technologies in waste management stimulated the vision to employ conduction phenomena under electrical currents as a soil remediation technology (Acar and Alshawabkeh 1993; Acar et al.

1993a). This technology uses low level DC electrical potential differences (ii the order of few volts per cm) or electrical currents (in the order of milliamps/cm^2 of soil cross sectional area) across a soil mass applied through inert electrodes placed in an open flow arrangement. The application of low level DC across electrodes placed in holes filled with fluid in a soil mass causes physicochemicai and hydrological changes in the soil-water-dectrolyte medium leading to contaminant transport and removal. The applied electric current (or electric potential difference) leads to electrolysis reactions at the electrodes generating an acidic medium at the anode and an alkaline medium at the cathode. The acid generated at the anode advances through the soil towards the cathode by different transport mechanisms including ion migration due to electrical **gradients,** pore fluid advection due to prevailing dectroosmotic flow, pore fluid flow due to any externally applied or internally generated hydraulic potential difference, and diffusion due to generated chemical gradients. The alkaline medium developed at the cathode will first advance towards the anode by ionic migration and diffusion; however, the mass transport of H+ will neutralize this base front, preventing its transport towards the anode. Acidification of the soil causes desorption of **the** contaminants. Species present in the soil pore fluid, or desorped from the soil surface, **are** transported towards the electrodes depending on their dectric charge. The driving mechanisms for species transport are the same as the acid-base transport mechanisms. As a result, cations are accumulated at the cathode and anions at the anode while there is a continuous transfer of hydrogen and hydroxyi ions into‘the medium. various bench scale. studies have shown that heavy metals and other cationic species can be removed from the-soil either with the effluent or deposited-at or dose to the cathode (Hamed 1990; Hamed et al. 1991; Eykholt 1992; Wittle and Pamukcu 1993; Acar et al. 1993).

The demonstrated feasibility of dectrokinetic soil remediation through bench-scale studies necessitates a pilot scale study investigating the effect of up-scaling bench scale experiments on the efficiency and performance of the process. Furthermore, a comprehensive theoretical model which accounts for the transport mechanisms and the physicochemical changes associated with the process is required. The predictions of the theoretical model should be compared with the results obtained in pilot-scale experimental model. The developed theoretical model is expected to provide the basis for a comprehensive design/analysis tool for the different boundary conditions, site specific contamination and variable soil profiling encountered in full scale implementation of the process. Such a theoretical model will also allow assessment of the principles of multi species transport under electric fields.

1.1 Ob jectives

The objectives of this study are identified as:

1. to investigate the feasibility and efficiency of field-scale electrokinetic soil remediation by conducting pilot-scale laboratory tests with Pb(II) loaded kaolinite and kaolinite/sand mixture. The size of the samples is chosen to simulate one-dimensional conditions and to represent an intermediate Scale between bench-scale and full-scale in-situ remediation,
2. to monitor and investigate the changes expected in electrical, chemical and hydraulic potentials, and geophysicochemical properties of the soil-water-electrolyte medium during processing,
3. to provide a theoretical model, numerical solution algorithm and a computer code for coupled transient transport of fluid, charge, and chemically reactive species under hydraulic, electric, and chemical gradients,
4. to evaluate the necessary soil properties and model parameters required by the. theotical model in predicting the pilot-scale experimental mode1 resuits, and
5. to evaluate the theoretical model developed for electrokinetic soil processing through comparisons of the **chemical, electrical,** and hydraulic potentials obtained from theoretical model with measurements made in the experimental model.

1.2 Scope

The study is aimed to investigate, theoretically and experimentally, the complexity of changes in chemical, electrical, and hydraulic potentials, and physicochemical properties of soil-water-electrolyte medium associated with removing contaminants by application of a DC current. Two bench-scale tests on Pb^{2+} spiked kaoiinite, two pilot-scale laboratory tests on Pb^{2+} loaded kaolinite, and one pilot-scale test on Pb^{2+} spiked kaolinite/and mixture are conducted. The size of these samples is chosen to simulate one-dimensional conditions and to represent an intermediate scale between bench-scale and full-scale in-situ remediation. One-dimensional conditions are selected since two-dimensional conditions wilI result in spatial variability in electrical gradients both due to the changing chemistry and also due to the electrode geometry unduly complicating

evaluation of the results. The effect of spatial variability in the electrical gradients due to the electrode configuration and geometry is not included as a variable in this study.

Tests are conducted for only removal of lead species from the specified soil samples. Lead is chosen for this study for the following reasons,

- it is the most identified species in hazardous waste sites listed in the NPL (Figure 1.2),
- bench-scale studies demonstrate that it can be removed successfully at relatively high concentrations (1,500 μg/g from kaolinite, Hamed et al. 1991; and 9,000 μG/g from fme argillaceous sand, Lageman 1989, 1993),
- it is highly retarded by clayey soils and it is hypothesized that lead removal by the process may implicate the feasibility of removing other less retarded ionic species. However, the validity of this hypothesis depends upon the chemistry of the species in the concern and surface chemistry of the soils,
- lead poisoning can occur by digestion or inhaling which would minimize the health and safety hazard in laboratory studies, specially pilot-scale tests, when comparing it with radionuclides or other contaminants, and
- current research work on electrokinetic soil remediation involves conducting field-scale remediation of a lead contaminated site at Ethyl Corporation, Baton Rouge. This makes the study a perfect link between bench-scale tests and the first field application of electrokinetic soil remediation in the United States.

Modeling lead removal by electrokinetics is chosen for this study in an attempt to evaluate the current understanding of the technology and to check the validity of the theoretical model presented. Though variouscations and anions might be present in the soil pore fluid at different concentrations, only four ions are included in this model. These are Pb^{2+} the contaminant of concern, NO_3^-, since lead nitrate salt is used for the experiment, and H^+ and OH^- because they are necessary in describing the acid/base distribution that has a great influence on the pore fluid chemistry. Dramatic changes in the concentration of these ions will result in different chemical reactions. Chemical reactions included in this mode1 are the reactions describing precipitation/dissolution of lead hydroxide ($Pb(OH)_2$) the water auto ionization reaction, and sorption reactions. Two approaches have been developed and used in the literature to describe chemical reactions; instantaneous equilibrium approach and kinetics approach.

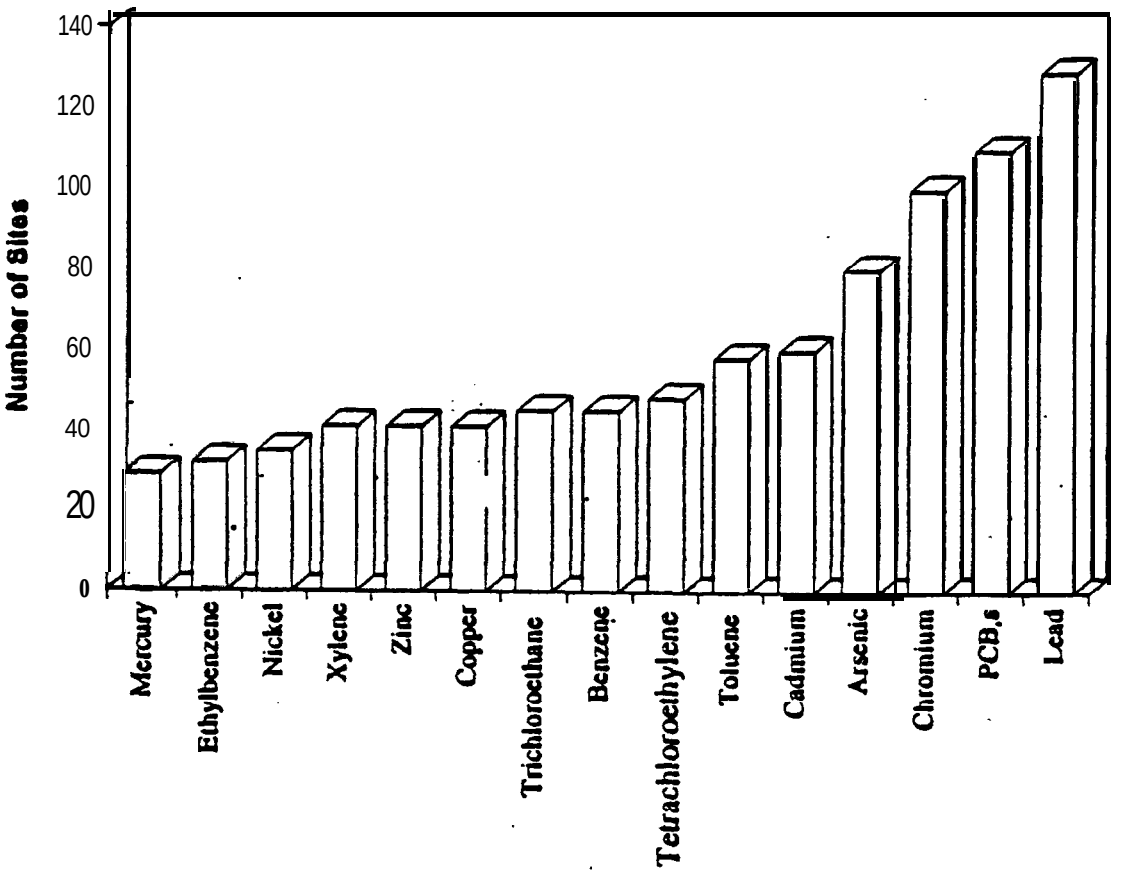

Figure **1.2:** **Most** Frequently Identified Species in Soils in the 1217 Sites Listed on the National Priority List in 1989 (Adopted from EPA 1991)

For several species, chemical reactions, specially precipitation/dissolution and sorption reactions, have been found to vary with time before reaching equilibrium. It may be more appropriate to use kinetics approach to model these reactions; however, this will unduly complicate the modeling effort and it will require an independent investigation of each reaction kinetics. Furthermore, chemical reactions involved in this study are expected to reach equilibrium at a very short time. Sorption reactions in low activity soils and precipitation reactions of heavy metals in solutions often take minutes to reach chemical equilibrium. On the other hand, processes related to the transport of these chemical species in fme grained deposits under electric, hydraulic and chemical gradients are siow compared to the rate of sorption or precipitation reactions. Consequently, the ratio of the rate of chemical reactions to the rate of transport of heavy metals in low activity fine grained deposits is expected to be high enough to meet the assumption of instantaneous equilibrium for these chemical reactions.

1.3 Organization of the Manuscript

The manuscript contains 8 (eight) Sections that covers the work conducted. A brief summary of the contents of these Sections is presented in this section.

Section 2 describes various electrokinetic phenomena, in soils and principles of electrokinetic soil remediation The effects of application of an electric current through a saturated soil **medium on the** physicochemicai properties of the medium are discussed. Electrolysis reactions at the electrodes, changes in the soil pH and their effect on sorption and precipitation/dissolution reactions, and transport mechanisms are addressed. Potential uses of electrokinetic phenomena in different aspects of environmental geotechnics are presented. This Section also summarizes available literature on electrokinetic soil remediation which is divided into two parts; experimental and theoretical. The experimental part covers bench-scale studies conducted by various researchers together with the feasibility and cost efficiency of the technique and limited pilot-scale studies conducted in the field. The theoretical part summarizes and reviews different attempts of numerical simulations of contaminant transport under electric fields.

Section **3** presents the theoretical development and mathematical formulation attained in electrokinetic soil processing. This Section describes the coupled fluxes of fluid, mass, and charge under hydraulic, electric, and chemical concentration gradients. Principles of conservation of

matter and energy are applied to these fluxes resulting in partial differential equations describing the coupled transient hydraulic, electric, and chemical potentials distributions. Chemical reactions in the soil pore fluid, such as sorption and precipitation/dissolution, are.decriribed by algebraic equations employing laws of mass action. The resulting differential/aIgebraic equations are summarized for a system of reactive chemical species in the soil pore fluid. Finally, this Section describes the resulting system of equations, initial and boundary conditions for modeling soil pH and modeling lead transport and removal by electrokinetic soil processing

Section 4 summarizes different numerical schemes that could be used to solve the developed system of differential and algebraic equations and explains the iterative scheme utilized for this study. This Section also describes the finite element approach and the variational formulation used to solve the system of differential equations. The isoparametric element used, formulation of local and global matrices, and the technique utilized for matrix inversion are summarized.

Section 5 presents design of the bench-scale and pilot-scale experiments conducted in this study. Size and shape 0f the container and soil samples together with type and configuration of the electrodes are described. The procedure used for mixing and compacting kaolinite with lead is discussed. A description of the probes and instruments used for measuring voltage distribution, soil suction, temperature, and pH is provided. The implemented data acquisition system is summarized and the procedures used for soil sampling and chemical analysis are presented.

Section 6 presents the results and analysis of the experimental work. Changes in soil, catholyte, and anolyte pH, final water content, and voltage distribution of all bench-scale and pilot-scale experiments are presented, analyzed, and discussed. This Section discusses the effects of the electrochemical changes during processing bench-scaie and piIot-scale specimens and their impact on the electric and hydraulic potential distributions. Significance of the different lead transport mechanisms under the applied electric gradient are discussed. Final lead distributions across the soil and removal efficiencies for these experiments are presented. Energy expenditure and-cost for these experiments are evaluated.

Section 7 describes the results of the numerical model and the results of the computer code developed for lead transport and removal under electric fieids. Comparisons between the results of

the model with the results of the pilot-scale experiment with initial lead concentration of 5322 μg/g are prcsentcd.

Section 8 summarizes the findings and conclusions of the study. Recommendations for future research are presented. Program listing, a list of t dh input and output files, and data generated in bench-scale and pilot-scale tests are presented in Appendices A through D.

Section 2

BACKGROUND

2.1 Introduction

Multi-species transport under electric fields is an area that is gaining increasing attention and interest. Species transport mechanisms under electric fields are envisioned to-be employed in remediating soils from inorganic and organic species (electrokinetic remediation), injection of microorganisms and nutrients in bioremediation, injection of grouts in soil stabilization and waste containment, soil and pore fluid characterization and species extraction using penetrating probes, diversion systems for contaminant plumes, and leak detection systems in containment barriers (Acar and Gale 1986, Acar et aL 1989). Bench-scale and limited pilot-scale studies in electrokinetic remediation demonstrate that the technique has significant potential. It becomes necessary to gain a better understanding of multi-species transport mechanisms both in an effort to critically evaluate the fundamental basis of the processes and also to develop the necessary design/analysis tools in engineering the implemented techniques.

2.2 Electrokinetic Phenomena in Soils

Generally, discrete clay particles have a negative surface charge that influences and controls the particle environment. This surface electric charge can be developed in different ways, including the presence of broken bonds and due to isomorphous substitution (Mitchell 1993). Thereupon, the clay particle-water-electrolyte system is usually considered to consist of three different zones; the clay particle with negatively charged surface, pore fluid with excess positive charge, and the free pore fluid with zero net charge (Figure 2.1). The net negative charge on the clay particle surfaces requires an excess positive charge (or exchangeable cations) distributed in the fluid zone adjacent to the clay surface forming the diffuse double Iayer. The quantity of these exchangeable cations required to balance the charge deficiency of clay is termed the cation exchange capacity (CEC), and expressed in milliequivalents per 100 grams of dry clay.

Several theories have been proposed for modeling charge distribution adjacent to clay surface. The Gouy-Chapman diffuse double layer theory has been widely accepted and applied to

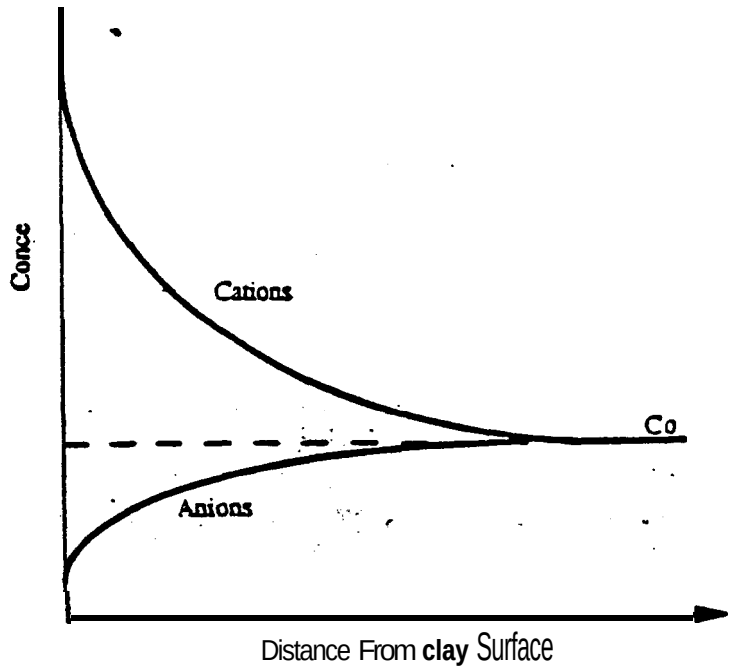

Figure 2.1: Charge Distribution Adjacent to Clay Surface (Mitchell 1993)

describe clay behavior. A detailed description of the diffuse double layer theories for a ***single flat*** plate is found in Hunter (1981), Stumm (1992), MitcheII(1993), and Yeung (1993).

Electrokinetics is defined as the physicochemical transport of charge, action of charged particles, and effects of applied electric potentials on formation and fluid transport in porous media. The presence of the diffuse double layer gives rise to several electrokinetic phenomena in soils, which may result from either the movement of different phases with respect to each other including transport of charge, or the movement **of** different phases relative to each other due to the application of electric field. The electrokinetic phenomena include electroosmosis, electrophoresis, streaming potential, and sedimentation potential. Electroosmosis is defined as fluid movement with respect to a solid wall as a result of an applied electric potential gradient. In other words, if the soil is placed between two electrodes in a fluid, the fluid will move from one side to the other when an electromotive force is applied. Electrophoresis is the movement of solids suspended in a liquid due to application of an electric potential gradient. Streaming potential is the reverse of electroosmosis. It difines the generation of an electric potential difference due to fluid flow in soils. Sedimentation (or migration) potential, known as Dorn effect (Kruyt 1952), is an electric potential generated by the movement of particles suspended in a liquid. Figure 22 dispiays the electrokinetic phenomena identified herein.

Under certain conditions, electroosmosis will have a significant role in electrokinetic soil remediation. Several theories are established to describe and evaluate water flow by electroosmosis; the most common being the Helmholtz-Smoluchowski theory, Schmid theory, Spiegler friction model, and ion hydration theory. Descriptions of these theories are given in Casagrande (1952) **, Gray** and Mitchell (1967), and Mitchell (1993). Helmholtz-Smoluchowski model is the most common theoretical description of electroosmosis and is based on **the** assumption **of** fluid transport in the soil pores due to transport of the excess positive charge in the diffuse double layer towards the cathode (Figure 2.3).

2.3 **Heavy Metals in Soils**

The term "heavy metals" is adopted as a group name for metals and metalloid that are associated with pollution and toxicity. The term also includes ***some*** **elements** which are essential for living organisms at low concentrations (Alloway 1990). General classification of heavy metals

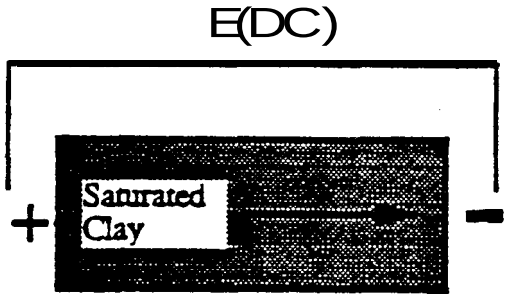

(a) Electric **Gradient**
Induces Water Flow

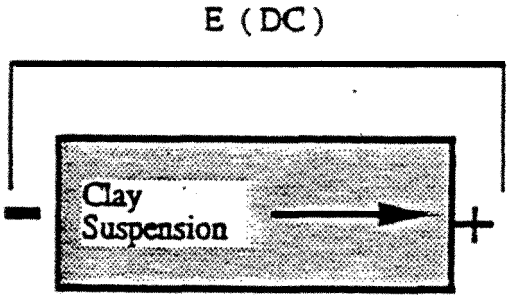

(c) Electrical **Gradient**
Induces Particle Movement

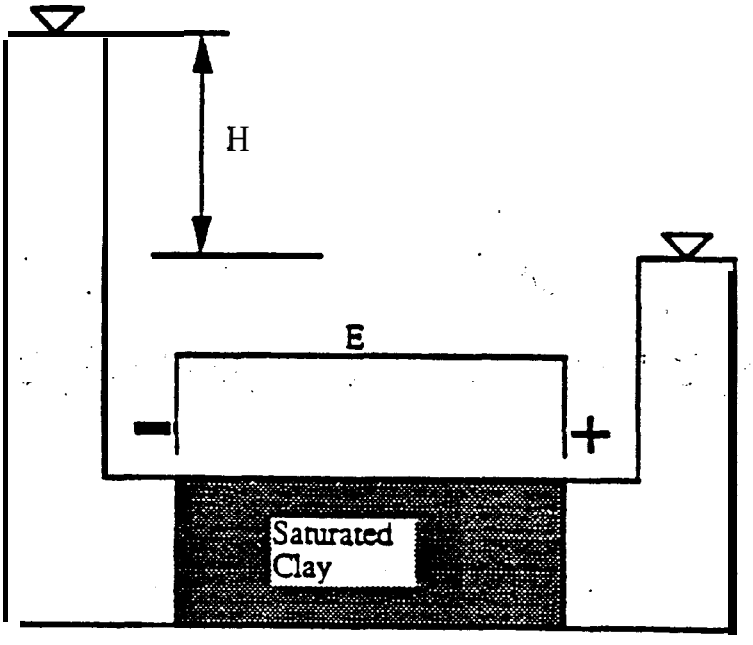

(b) Water Flow Induces
Electric Potential E

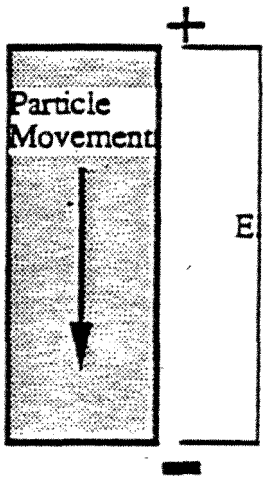

(d) Particle Movement
Induces Electric Potential

Figure 2.2: Electrokinetic Phenomena in Soils (Mitchell 1993)

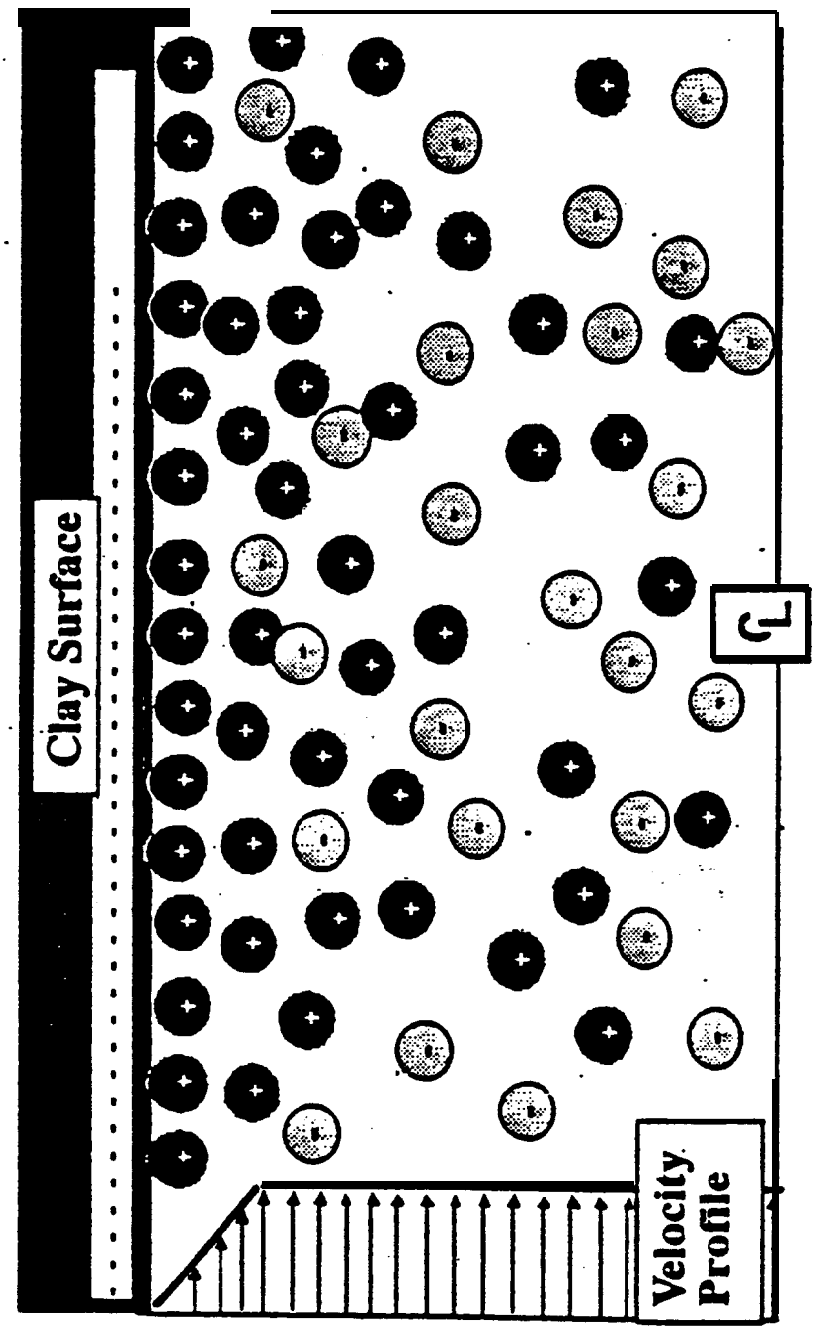

Figure 2.3: Schematic Diagram of Advection by Electroosmosis, Depicting the Excess Cations on the Clay Surface and an Approximate Velocity Profile Across the Pore Capillary (Acar et al. 1994b)

is based on the atomic density of 6 g/cm^3 or greater. Studies of heavy metals in ecosystems have indicated that many areas near urban complexes, metalliferous mines or major road systems contain anomalously high concentrations of these elements. In particular, soils in such regions have been polluted from a wide range of sources with Pb, Cd, Hg, As, and other heavy metals. Some recently have shown concerns that we may be experiencing a silent epidemic of environmental metal poisoning from the ever increasing amounts of metals discharged into the biosphere (Brady 1984; Alloway 1990).

As, Ag, Cd, Cu, Hg, Pb, Sh, and Zn are naturally encountered in the top (surface) horizons of the soil rather than the lower horizons due to the effect of cycling through vegetation, atmospheric deposition, and adsorption by the soil organic matter. Though natural concentrations of heavy metals in soils are not high, polluted or contaminated soils exist due to one or more of the following reasons (Alloway 1990),

* the use of leaded petrol for motor vehicles has been responsible for atmospheric pollution and consequently deposition in soils,

* the disposal of urban and industrial wastes can lead to soil contamination from the deposition of aerosol particles emitted by incineration of materials containing metals. The unauthorized dumping or disposal of items containing metals, ranging from miniature dry-cell batteries (Ni, Cd+ and Hg) to abandoned cars and car components, such as Pb-acid batteries, can give rise to small areas of very high metal concentrations in soils. The disposal of some domestic waste by burning on garden bonfires or burial in the garden can also result in localized high concentrations of metals, such as Pb, in soils used for growing vegetables,

* organic manures which include poultry manures that may contain high concentrations of Cu or As fed to improve food conversion efficiency. Sewage sludge usually contain relatively high concentrations of several metals, especially those from industrial catchments,

* contribution of metallurgical industries due to emissions of fumes and dusts containing metals which are transported in the air and eventually deposited onto soils and vegetations, effluent which may pollute soils when watercourses flood,

and creation of waste dumps from which metals may be leached and thus pollute underlying or nearby soils,

- the mining and smelting of non-ferrous metals have caused soil pollution which dates back to Roman times and earlier in some places, although most has occurred since the Industrial Revolution. Metals are dispersed in dusts, effluent and seepage water. Tailings discharged into watercourses have polluted alluvial soils downriver from mines during flooding especially when the dams in lagoons fail,

- the combustion of fossil fuels which results in the dispersion of many elements in the air over a large area. The disposal of ash is a further source of heavy metals, and

- agricultural fertilizers and pesticides which usually contain various combination of heavy metals, either as impurities or active constituents.

2.4 **Soil Contamination With Lead**

Soil contamination with lead has been documented to result from the use of different chemical forms of lead in petrol, paints, batteries, and pesticides, due to smelting of metals and mining, and due to disposal of lead-acid storage batteries (Harrison and Laxen 1981). Figure 1.2 displays that lead is the most frequently identified species in soils among the 1217 sites listed on the NPL in 1989. Soil contamination with lead at high concentrations such as 100,000 µg/g (10% by weight) is not uncommon.

Compared with most other contaminants, lead has a tendency of long residence time in soils. Together with its compounds, as lead accumulates in soils and deposits it remains accessible to the food chain and human metabolism far into the future. Detrimental effects associated with lead have been recognized for a long time. Lead is poisonous, and there are fears that body burdens below those at which clinical symptoms of lead toxicity appear may cause mental impairment in young children (Harrison and Laxen 1981). Clinical symptoms associated with lead poisoning include anemia, various digestive disorders, and central nervous system effects. Currently, no widely accepted remediation or treatment technology exists for lead-contaminated hazardous waste

sites. The most common treatment methods for lead contamination are containment or landfill disposal.

2.5 Principles of EIectrokinetic Soil Remediation

Electrokinetic soil remediation technology uses a low level direct current, in the order of milliamps per cm^2 of soil cross-sectionail area, to transport and remove species from soils. Upon application of a low level direct current the soil water-electrolyte system undergoes physicochemical and hydrological changes leading to contaminant transport and removal. The applied electric current (or electric potential difference) leads to electrolysis reactions at the electrodes, acid-base distribution drive by chemical, electrical, and hydraulic potential differences, adsorption/desorption and precipitation/dissolution reactions, transport of the pore fluid and ions, and electrodeposition. These on-going physico-chemical processes are reviewed in the following subsections.

2.5.1 Electrolysis Reactions

Application of direct electric current through electrodes immersed in water induces electrolysis reactions in the immediate vicinity of Electrodes. Oxidation of water at the anode generates an acid front while reduction at the cathode produces a base front by the following electrolysis reactions,

$$2H_2O - 4e^- \bullet O_2\,l + 4H^+ \quad E^0 = -1.229 \quad \text{(anode)} \quad (2.1)$$

$$2H_2O + 2e^- \cdot H_2\uparrow + 2OH^- \quad E^0 = -0.8277 \quad \text{(cathode)} \quad (2\text{-}2)$$

Secondary reactions may exist depending upon the concentration of available species, e.g.,

$$2H^+ + 2e^- \cdot H_2\uparrow \quad E^0 = 0.0 \quad \text{(reference)} \quad \textbf{(2.3)}$$

$$Me^{+n} + ne^- \cdot Me(s) \quad \textbf{(2.4)}$$

where E^0 is the standard reduction electrochemical potential, which is a measure of the tendency of

the reactants in their standard states to proceed to products in their standard states, and Me refers to metals. Table 2. I presents standard reduction electrochemical potentials for different electrolysis reactions in aqueous solution at 25° C. The prevailing of electrolysis reactions at the electrodes depends on the availability of chemical species and the eletrochemical potentials of these reactions. Although some secondary reactions might be favored at the cathode because of-their lower electrochemical potential, the water reduction half reaction (H_2O/H_2) is dominant at early stages of the process (the first two to three weeks of processing bench-scale tests). At later stages, the acid front advances towards the cathode carrying H+ and the cationic contaminants and half cell secondary reactions (H^+/H_2) or ($Me^{+n}/Me(s)$) arc expected to dominate. Within the first 100 hours of processing, electrolysis reactions will drop the pH at the anode to below 2 and increase it at the cathode to above 12, depending upon the total current applied (Acar et al. 1990,1993).

2.5.2 Changes in Soil pH

The acid generated at the anode will advance through the soil towards the cathode. This advance is governed by different transport mechanisms including ionic migration due to electrical gradients, pore fluid advection due to the prevailing electroosmotic flow, pore fluid advection due to any externally applied or internally generated hydraulic potential differences, and-diffusion due to concentration gradients. These transport mechanisms are discussed in more detail hereinafter. *The* alkaline medium developed at the cathode due to production of OH- will initially advance towards the anode by diffusion and ionic migration; however, the counterflow due to electroosmosis will retard this back-diffusion and migration:The advance of this front-towards the anode will be much slower than the advance of the acid front towards the cathode because of the counteracting *electroosmotic flow* and also because the ionic mobility of H^+ is about 1.76 times that of OH-. As a consequence, the acid front dominates the chemistry across the specimen (Acar et al. 1990; Alshawabkeh and Acar 1992; Acar and Alshawabkeh 1994). Figure 2.4 displays development of the acid/base profile across a 10 cm length cylindrical Georgia kaolinite specimen processed under one-dimensional conditions at a current density of 12.5 $\mu A/cm^2$ (Acar et al. 1990).

The decrease in pH value in the soil depends on the amount of acid generated at the anode (Acar et al. 1990,1993a) and the buffering capacity of the clay. Yong et al. (1990) investigated

Table 2. I: Standard Reduction EIectrochemical Potentials in Aqueous Solution at 25º *C(Kotz* and **Purcell 1987).**

Reduction Half Reaction	E° (V)
$F_2 + 2e^- \longrightarrow 2F^-$	+2.87
$H_2O_2(aq) + 2H^+(aq) + 2e^- \longrightarrow 2H_2O(l)$	+1.77
$Au^{3+} + 3e^- \longrightarrow Au(s)$	+1.50
$Hg^{2+} + 2e^- \longrightarrow Hg(l)$	+0.855
$Ag^+(aq) + e^- \longrightarrow Ag(s)$	+0.80
$Fe^{3+}(aq) + e^- \longrightarrow Fe^{2+}$	+0.771
$O_2(g) + H_2O(l) + 4e^- \longrightarrow 4OH^-$	+0.40
$Cu^{2+} + 2e^- \longrightarrow Cu(s)$	+0.337
$Sn^{4+} + 2e^- \longrightarrow Sn2+$	+0.15
$2H^+(aq) + 2e^- \longrightarrow H_2(g)$	0.00
$Sn^{2+}(aq) + 2e^- \longrightarrow Sn(s)$	-0.14
$Ni^{2+}(aq) + 2e^- \longrightarrow Ni(s)$	-0.25
$Cd^{2+}(aq) + 2e^- \longrightarrow Cd(s)$	-0.40
$Fe^{2+}(aq) + 2e^- \longrightarrow Fe(s)$	-0.44
$Zn^{2+}(aq) + 2e^- \longrightarrow Zn(s)$	-0.763
$2H_2O(l) + 2e^- \longrightarrow H_2(g) + 2OH^-(aq)$	-0.8277
$Al^{3+}(aq) + 3e^- \longrightarrow Al(s)$	-1.66
$Mg^{2+}(aq) + 2e^- \longrightarrow Mg(s)$	-2.37
$Na^+(aq) + e^- \longrightarrow Na(s)$	-2.714
$Li^+(aq) + e^- \longrightarrow Li(s)$	-3.045

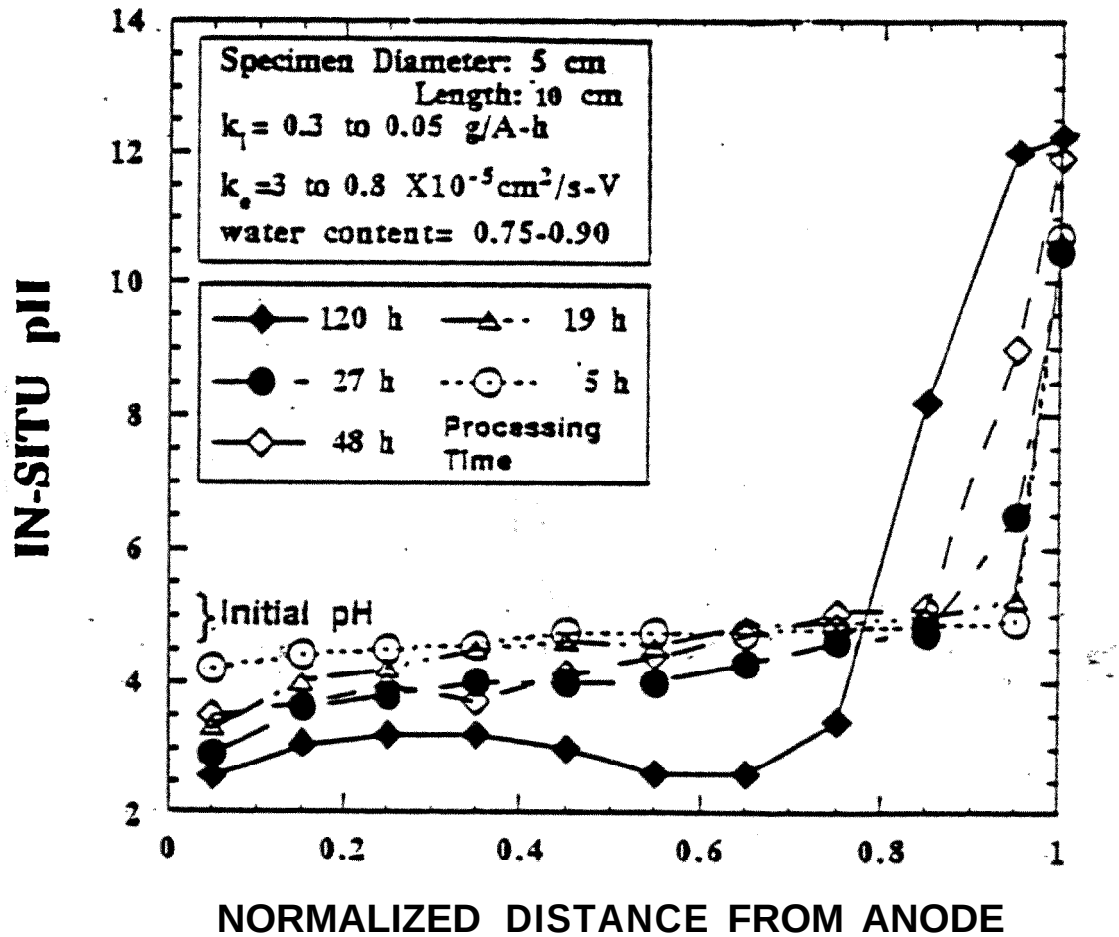

Figure 2.4: Acid/Base Distribution across Specimen of Slurry Consolidated Georgia Kaolinite Processed under an Electric Current of 12.5 $\mu A/cm^2$ (Acar et al. 1990).

the buffering capacity ofvarious types of clays and demonstrated that the cation exchange capacity and the organic content highly influence the soil PH. Furthermore, the study showed that kaolinite has low buffering capacity compared with different types of dayey soils.

2.5.3 Sorption Reactions

Heavy metals and other positively charged species are highly attracted and adsorbed on the negatively charged clay surfaces. Metals have different sorption characteristics and mechanisms that are also dependent upon the adsorbents. Sorption mechanisms include surface complexation (adsorption) and ion exchange. The adsorbents show differences in selectivity sequences for different metals. Table 2.2 demonstrates that Iead, compared to other metals, is highly attracted and adsorbed by various clay types.

Desorption of heavy metals from the clay is essential for the remedy to be efficient in contaminated fine-grained deposits. The adsorption/desorption mechanism depends upon the surface charge density of the clay mineral or CEC, characteristics and concentration of the cationic species, and existence of organic matter and carbonates in the **soil.** Furthermore, the adsorption/desorption mechanism is pH dependent. An increase in H+ concentration associated with a decrease in pH results in desorption of cations by an amount controlled by the soil type (Maguire et al. 1981 Harter 1983;and Yong et al. 1990). Therefore, acidification of the soil by the electrolysis reaction at the anode is a fundamental mechanism that assists in desorption of these species (Figure 2.5).

2.5.4 Precipitation/Dissolution

Dramatic changes in the soil electrochemistry throughout electrokinetic soiI processing results in different chemical reactions including precipitation/dissolution of salts and soil minerals. Species transport in soil pore fluid is highly influenced by formation and dissolution of these precipitates.

The base front generated by electrolysis at the cathode will cause precipitation of most heavy metals and actinides. The amount of precipitate differs from one species to another and it is

Table 2.2: Selectivity **of Different Soil Types** for **Divalent Metals** (Alloway **1990).**

Adsorbent	Selectivety Order
MontmorilIonite(Na)	***Ca>Pb>Cu>Mg>Cd>Zn>Ni***
Illite(Na)	***Pb>Cu>Zn>Ca>Cd>Mg***
Kaolinite(Na)	***Pb>Ca>Cu>Mg>Zn>Cd***
Smectitie, Vermiculite, and Kaolinite	***Zn*** > Mn.> ***Cd*** > ***Kg***
Albite, Labradorite	***Zn>Cd>Mn>Kg***
Mineral soil on marine clay,	***Pb>Cu>Zn>Cd>Ca***
Peat.	***Pb>Cu>Cd=Zn>Ca***

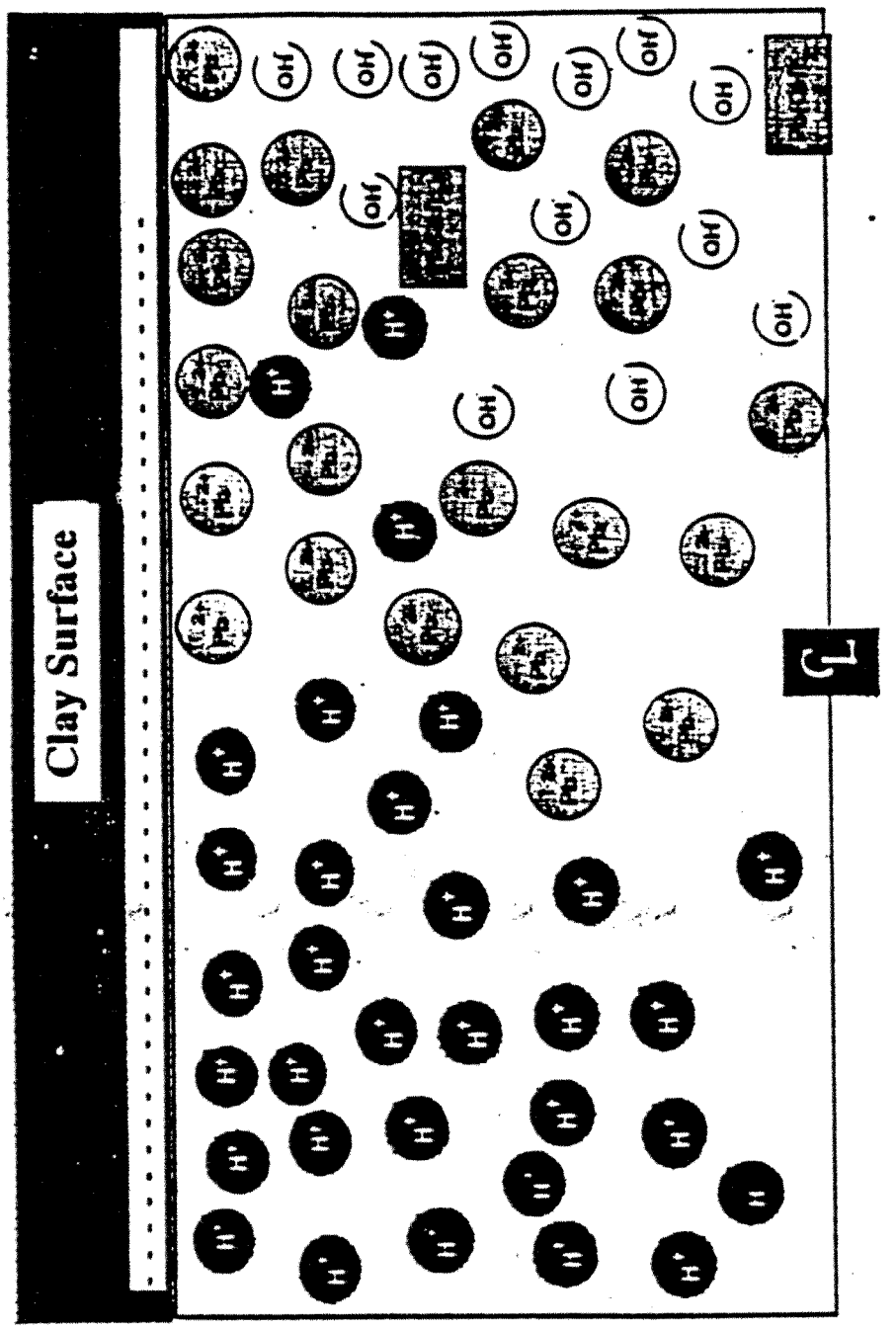

Figure 2.5: A Schematic Representation of Protons Displacing Lead from the Soil Surface and Transport of Both the Protons and Lead towards the Cathode (Acar et al. 1993).

highly dependent on soil and-pore fluid pH. Though the advance of the acid front generated at **the** anode will cause dissolution of most precipitates encountered, each precipitation or dissolution. reaction is treated independently depending upon the solubility product constant. Acar et al. (1993) and Acar and Alshawabkeh (1993) recommend the use of different enhancement techniques in order to remove these precipitates from the cathode tine. The advance of the acid front gcnerated at the anode is also expected to cause dissolution of day minerals. Kaolinite dissolution, which is pH dependant, generates different chemical forms of aluminum and silica. The impact of mineral dissolution on the efficiency of electrokinetic soil remediation has not yet been investigated. However, **Ugaz** et al. (1994) investigated the effect of using acid washed soil sections near the cathode on the efficiency of the process for *removal* of radionuclides from kaolinite. The study did not show any significant influence of acid washing soil sections near the cathode prior to processing on species transport.

2.5.5 **Contaminant Transport, Capture, and Removal**

Free chemical species present in the pore fluid and/or desorped from the soil surface will be transported towards the electrodes depending upon their charge. The primary driving mechanisms **of** species transport are the same as the acid or base transport mechanisms. Ion migration, advection, together with diffusion will contribute to the movement of species through the soil mass. At zones of high pH, both precipitation and sorption will retard species transport

As a result of transport of chemical species in the soil pore fluid, cations will collect at the cathode and anions at the anode. Heavy metals and other cationic species will be removed from the soil either with the effluent or they will be deposited at the cathode. Treatment of the effluent (such **as** ion exchange or resin columns) could be used for removal of the excess ions. Figure 2.6 presents a schematic diagram of in-situ electrokinetic soil remediation.

2.5.6. **Enhancement/Coditioning**

Acar et al. (1993a) recommend the use of different enhancement techniques in order to remove and/or avoid precipitation in the cathode compartment "envisioned enhancement schemes are expected to have the following characteristics; (a) the precipitate should be solubilized and/or

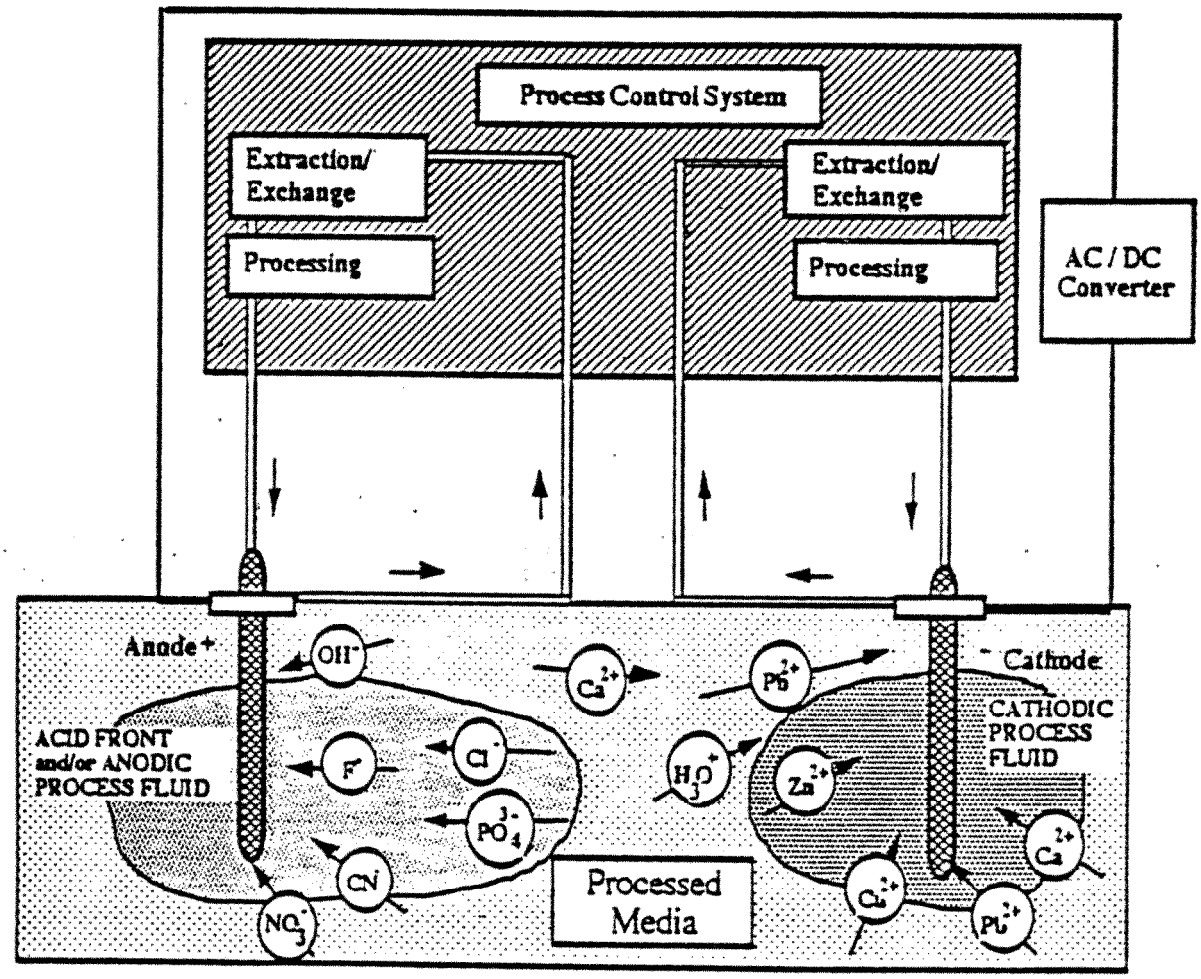

Figure 2.6 Schematic of Electrokinetic SoiI Processing Showing Migration of Ionic Species, Transport of Acid Front and/or Processing Fluid across the Processes Medium (Acar and Alshawabkeh)

precipitation should be avoided (b) preferably, ionic conductivity across the specimen should not increase excessively in a short period of time both to avoid a premature decrease in electroosmotic transport and to allow transference of species of interest, (c) the cathode reaction should possibly be depolarized to avoid generation of the hydroxide and its transport into the specimen, (d) such depolarization will also assist in decreasing the electrical potential difference across the electrodes leading to lower energy consumption, (e) if any chemical is used, the precipitate of the metal with this new chemical should be perfectly soluble within the pH ranges attained, and (f) any special chemicals introduced should not result in any increase in toxic residue in the soil mass" (Acar et al. 1993a).

Acar et al. (1993a) have investigated the depolarization of the cathode reaction by using an acid which forms a soluble salt with species in transport "Low concentrations of hydrochloric acid or acetic acid is introduced at the cathode to depolarize the cathode reaction. One concern with the introduction of hydrochloric acid is its possible electrolysis and formation of chlorine gas when it reaches the anode compartment. Acetic acid is environmentally safe, it does not fully dissociate and most acetate salts are soluble and therefore it is preferred." (Acar et al. 1993a).

Migration of the acid generated at the anode would generally aid in desorption of the species. However, when this process is considered in conjunction with migration of a species of interest, the substantial increase in hydrogen ion concentration and the complementing *increase* in the hydrogen ion transference number may hinder transport of other species (Acar and Alshawabkeh 1993). If hydrogen ion generation and supply at the anode is not controlled, most of the energy may be consumed by generation and migration of the proton across the cell rather than the transport of species of interest. Therefore, if it is desired to promote the transport of species in the pore fluid, it may be necessary to depolarize the anode reaction and/or control acid production and introduction into the soil mass (Acar and Alshawabkeh 1993). As discussed previously, desorption and dissolution reactions will dominate the advance of the acid front in the specimen. In an attempt to fully exploit the different conduction phenomena and transport processes in field implementation of electrokinetic remediation technique and to improve the efficiency under site conditions, it will be necessary to implement process optimization schemes (Acar and Alshawabkeh 1993).

2.6 Applications of Electrokinetics in Enviromental Geotechnics

Electrokinetic soil processing is an emerging technology in waste remediation and separation. It is envisioned that various electrokinetic phenomena in **soils,** described in previous sections, will give a chance for additional applications in the area of environmental geotechnics other than the extraction chemical species from soils.

2.6.1 Electrokinetic Flow Barriers

Electrokinetic barriers could be used in **clay** liners to oppose contaminant transport due to hydraulic and chemical gradients. Though compacted clay liners are designed to retard or minimize contaminant transport to the underlying soil and groundwater, sustained hydraulic and chemical gradient in landfills may result in transport and release of contaminant through liners. Figure 2.7a shows that application of electrical gradient through day liners could be used to generate electroosmotic flow opposing contaminant transport. Yeung (1990) and Yeung and Mitchell (1991) have demonstrated that electrokinetic flow barriers may be effective in retarding transport of cationic species but accelerate transport of anionic species. The feasibility of the proposed electrokinetic barrier requires study of the effect of electrochemicaI changes on the fabric and engineering characteristics (specificalIy hydraulic conductivity) of day liners (Alshawabkeh and Acar 1993).

2.6.2 Hydraulic Conductivity Measurements

Application of direct or alternating current in fine-rained soil mass generates electroosmotic flow from the anode to the cathode. If an impermeable anode is used (no flow at the anode) a negative pore water pressure (suction) will generate to compensate the electroosmotic flow at the anode. The amount of suction generated is dependent on the applied electric field, hydraulic conductivity, and coefficient of electroosmotic permeability of the soil mass. Using known values of the coefficient of electroosmotic permeability and electric potential gradients, measurements of the suction generated could be used to back calculate the hydraulic conductivity of the soiI (Finno et al. 1994).

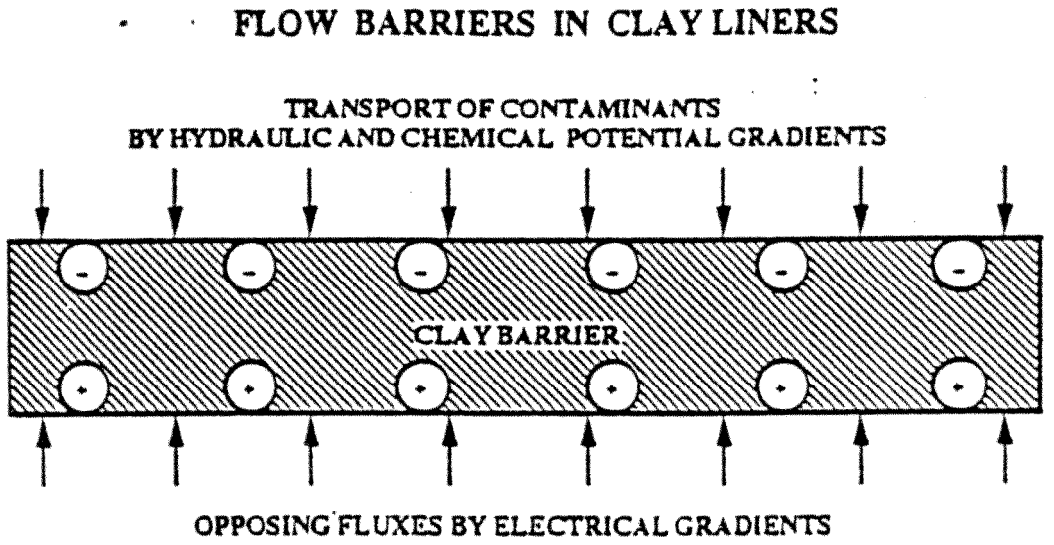

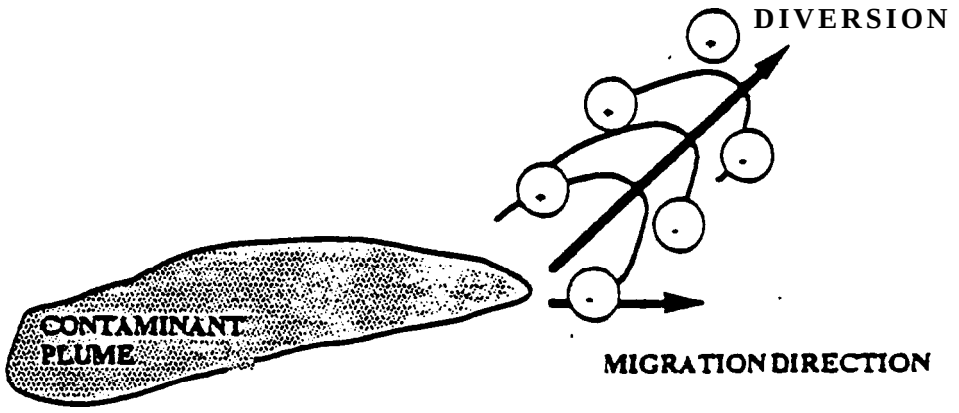

Figure 2.7: (a) Electrokinetic Flow Barriers and (b) Plume Diversion Scheme.

2.6.3 **Concentration and Dewatering**

Waste sludge and degraded spoil material are usually stored in ponds which continually threaten the environment. Electrophoresis could be first used for concentration of the solid particles, followed by electroosmotic consolidation and ion migration to separate and extract contaminants (Mitchell 1986). The feasibility of using electrokinetics for dewatering waste sludge and coal/washery slimes has been demonstrated by limited bench-scale studies (Krizek 1976; Lockhart 1981; Lockhart and Stickland 1984).

2.6.4 Plume Diversion Schemes

Contaminant transport in subsurface soil may threaten the groundwater contamination. This might require short-term immediate solutions by either retarding or changing flow directions. Migrational mass flux and electroosmotic water flow could be generated towards any required direction by application of direct current (or electric gradient) to the soil mass as shown in Figure 2.7b (Acar and Gale 1986; Acar et al. 1989; Acar and Hamed 1991). Though the feasibility of this technique has not been investigated yet, bench-scale results of electrokinetic soil processing demonstrate the significance of the applied electrical gradients on the amount and the direction of water and contaminant fluxes.

2.6.5 Hydrofracturing/EIectrokinetics/Bioremediation

Electrokinetics could be used in combination with hydrofracturing and bioremediation for removal of organic contaminants from soils (Ho et al.1993). Hydrofracturing Could be applied in contaminated fine-grained deposits to introduce layers of sand and carbon as shown in Figure 2.8. Electric potentials could be applied through the sand/carbon layers to cause electroosmotic water flow in fine-grained deposits to transport contaminants to the cathode, where they can be adsorbed by the carbon. Microorganisms might also be introduced for biodegradation of the captured organic contaminants. Problems with soil hydrofracturing include generation of vertical cracks in regions close to the surface (when the over consolidation ratio, OCR $\geq$ 4 (By 1992)).

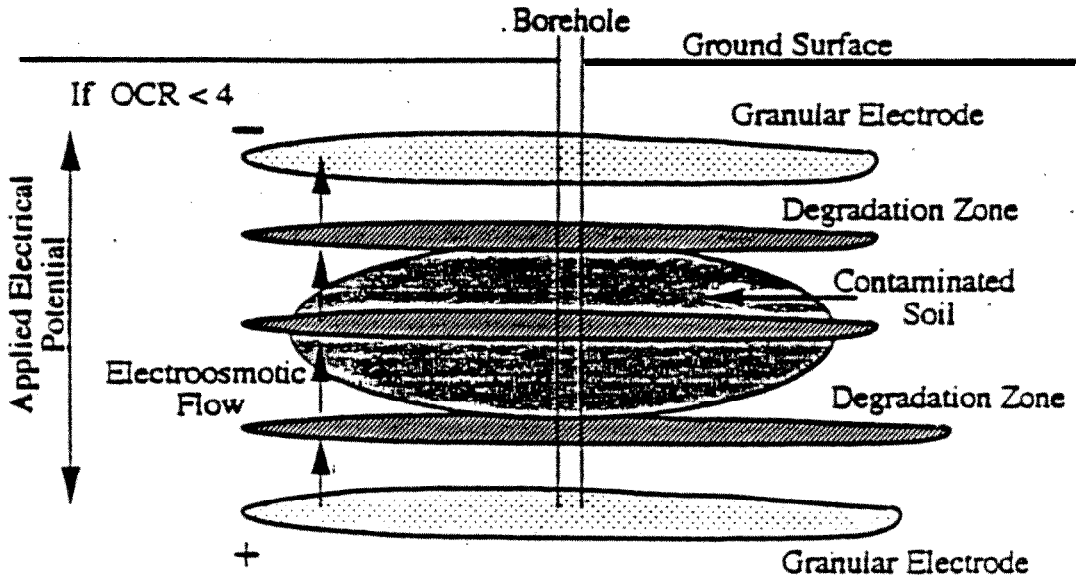

Figure 2.8: Hydrofracturing/Electrokinetics/Biodegradation in Soil Remediation (Ho 1993)

Other uses of eletrokinetics in environmental geotechnics include injection of grouts, cleanup chemicals or nutrients for growth **of microorganisms essential to** biodcgradation of specific wastes,contaminant detection, monitoring the physicochemical soil profiling (Acar and Gale 1986; Mitchell 1986; Acar et al. 1989; Acar and Hamed 199 1), and the use of electrophoresis for sealing impoundment leaks (Yeung et a. 1994).

2.7 Feasibility Studies On Eletrokinetic Soil Remediation

The uses of direct electric currents for electroosmotic consolidation and stabilization of fine-grained deposits-have been investigated by geotechnical engineers since the late 1930's. Effective applications of the processes have been demonstrated for slope stabilization, chemical alteration of day soils, concentration, separation, and stabilization of polluted dredging, soil consolidation and dewatering, reduction of negative skin friction of piles, and increasing the capacity of friction piles (Casagrande 1952a, 1983; Casagrande et al. 1961; Gladwell 1965; Mise 1961; Esrig 1968; Wan and MitchelI 1976; Gray and Somogyi 1977; Johnston and Butterfield 1977; Banerjee and Mitchell 1980a, 1980b). Most of this research has shown feasibility in geotechnical engineering applications; however, the effects of the application of electric gradients and electroosmosis on electrochemical changes of the soil medium have entertained limited attention. Gray and Schlocker 1969) investigated the effect of pH in controlling changes in soil composition and the feasibility of pH buffering during electrochemical treatment Their results demonstrated that composition and physical properties of clayey soils are altered when aluminum is introduced in the anolyte. Lockhart (1983) demonstrated that when the pore fluid of the soil has high electrolyte concentrations, strong electrolyte polarization occurs resulting in limited electroosmotic flow. However, Lockhart (1983) concluded that reasonable concentrations of electrolytes are not necessarily detrimental to electroosmotic dewatering (the meaning of reasonable concentrations is not defined). Putnam (1988) and Acar et al. (1989) discussed the effect of electrolysis reactions at the electrodes on soil pH. Acar et al. (1989) showed that the acid generated at the anode sweeps across the soil specimen ultimately decreasing the soil pH at the cathode.

Feasibility and cost effectiveness **of electrokinetics** for the extraction of heavy metals such as copper, zinc, and cadmium from soils have been demonstrated through bench-scale laboratory studies (Runnels and Larson 1986; Hamed 1990; Pamukcu et al. 1990; Acar et al. 1992 and 1993). A comprehensive treatise on the removal of Pb^{2+} from soils is reported by Hamed (1990), and

Hamed et al. (1991). Kaolinite samples are loaded with Pb^{2+} at various concentrations below and above the cation exchange capacity of the clay. As presented in Figure 2.9, the process removed 75% to 95% of Pb^{2+} at concentrations up to 1,500 $\mu g/g$ across the test specimens at an energy **expenditure of** 29 to 60 kWh/m^3 of soil processed. **Most** of the removed lead is found eletrodeposited at the cathode. This study clearly demonstrated that the removal is due to the transport of the acid front generated at the anode by the primary electrolysis reaction The study is the first to demonstrate the development of a nonlinear electric potential **across the** soil mass. Hamed (1990) also investigated the effect **of the initial** concentration and current density on the efficiency **of** removal. Higher current densities result in removal efficiencies similar to lower current densities, however, the energy requirement and cost of processing increases exponentially. Acar **et al.** (1994) demonstrated 90% to 95% removal of Cd^{2+} from bench-scale kaolinite specimens with initial concentration of 99-l14 $\mu g/g$. Acar and Alshawabkeh (1993) and Acar et al. (1994) showed higher removal rates of charged species can be achieved by electric migration rather than electroosmotic flow.

Figure 2.10 presents the results of enhanced electrokinetic remediation tests conducted on soil from a contaminated site (Acar et al. 1993). **"Calcium** and lead are mostly removed from the leading sections of the specimen first by dissolution then by the transport processes described. Close to 60% of the total lead (42 g) is precipitated in the middle sections (123 g of dry soil) clogging the soil pores and preventing further transport of the species. In such soils, it may be necessary to further enhance the processes by complementing the anodic acid with another introduced in the processing fluid" (Acar and Alshawabkeh 1993).

Runnels and Wahli (1993) emphasized the use of ion migration combined with soil washing for removal of Cu^{2+} and SO_4^{2-} from fine sands. Pamukcu and Wittle (1992) and Wittle **and** Pamukcu (1993) demonstrated removal of Cd^{2+}, Co^{2+}, Ni^{2+}, and Sr^{2+} from different **soil types** at variable efficiencies. The results showed that kaolinite, among different types of soils, had the highest removal efficiency followed by sand with 10% Na-montmorillonite, while Na-montmorillonite showed the lowest removal efficiency. Furthermore, their results demonstrated that lower initial concentrations of cadmium result in higher electroosmotic efficiency; however, removal efficiencies are higher for samples with higher initial concentrations. Other laboratory studies reported by Lageman (1989), Banerjee et al. (1990), Eykholt (1992), and Acar et al.

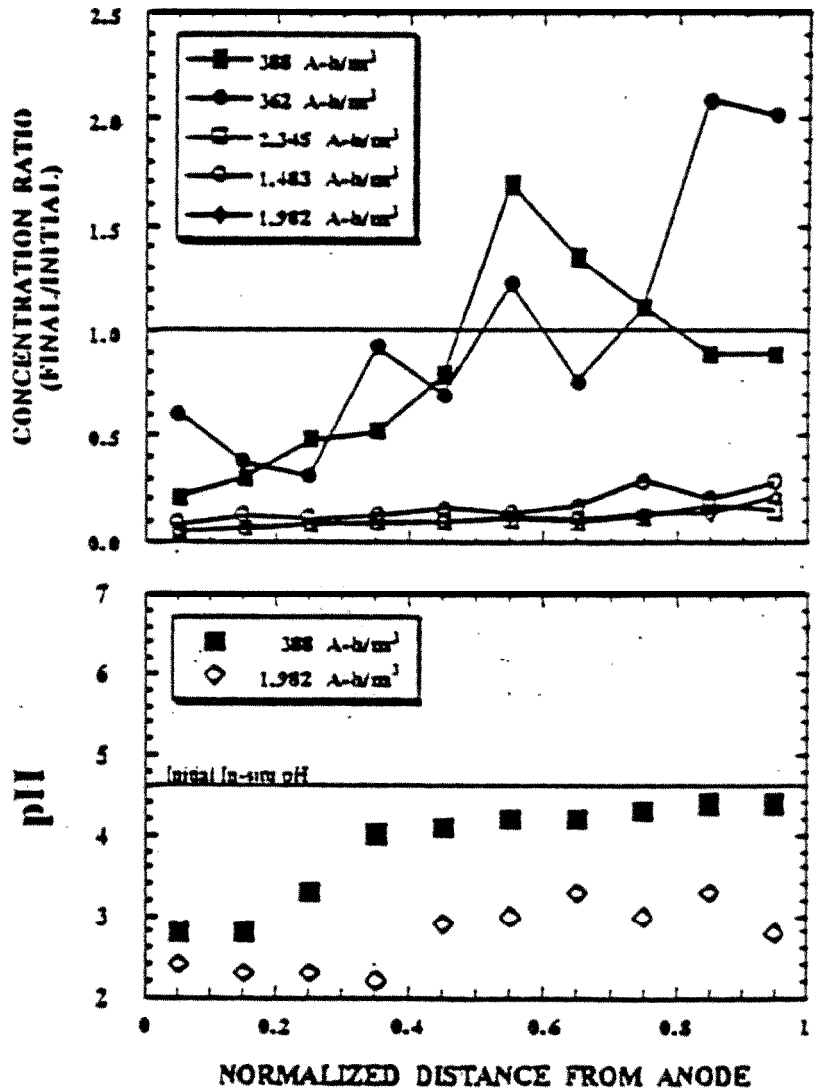

Figure 2.9: *Pb* Removal by Electrokinetics (Hamed 1990)

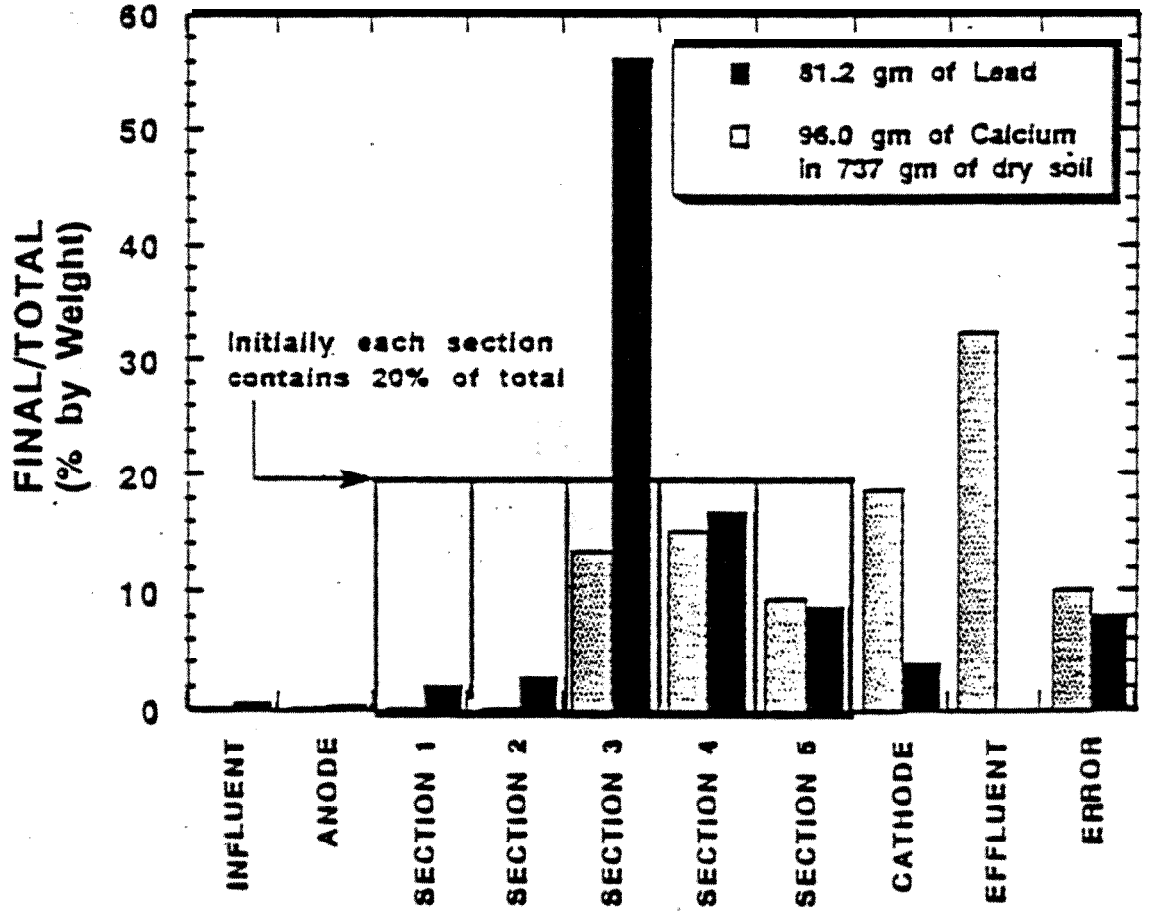

Figure 2.10: Post Treatment Distribution of Lead and Calcium across Specimens from a Site Processed with Acetic Acid Enhanced Electrokinetic Treatment (500 $\mu A/cm^2$ Current Density for 2,320 h with Average Gradient of 5.0 V/cm (Acar and 1993)

(1993) further substantiate the applicability of the technique to a wide range of heavy metals in soils.

The process can potentially remove radionuclides from clayey soil samples (Ugaz et al 1994, Acar et al. 1992c). Bench-scale tests displayed that uranium at 1,000 pCi/g of activity is efficiently removed from kaolinite. Figure 2.11 shows the change in uranium activity after different processing periods. Removal decreased from the anode towards the cathode due to the increase in pH values. A yellow uranium hydroxide precipitate was encountend in sections close to cathode. Enhanced electrokinetic processing showed that 0.05M acetic acid is just enough to depolarize the cathode reaction and overcome uranium precipitation close to the cathode compartment (Figure 2.12). Most uranyl ion was found precipitated at the cathode while more was in the catholyte in the acetic acid enhanced experiments (Acar et al. 1993b). The efficiency and feasibility of using this and other enhancement techniques are currently under investigation (Acar et al 1993b; Acar and Alshawabkeh 1993).

Other radionuclides, such as thorium and radium, have shown limited removal (Acar et al. 1992c). In the case of thorium, it is postulated that precipitation of these radionuclides at their hydroxide solubility limits at the cathode region formed a gel that prevented their transport and extraction. Limited removal of radium is believed to be either due to precipitation of radium sulfate or because radium strongly binds to the soil minerals causing its immobilization (Acar et al. 1992c).

Kaolinite specimens prepared with organic molding fluids demonstrated successful application of the process in transport of the BTEX (benzene, toluene, ethylene and m-xyiene) compounds in gasoline and trichloroethylene loaded on kaolinite specimens at concentrations below the solubility limit of these compounds (Bruell et al. 1992; Segal et al. 1992). High degrees of removal of phenol and acetic acid (up to 94%) also were achieved by the process (Shapiro et al. 1989; Shapiro and Probstein 1993). Acar et al. (1992) reported removal of phenol from saturated kaolinite by the technique. Figure 2.12 demonstrates two pore volumes were sufficient to remove 85% to 95% of phenol at an energy expenditure of 19 to 39 kWh/m^3. Wittle and Pamukcu (1993) investigated the feasibility of removal of organics from different synthetic soil types. Tests were conducted on kaolinite, Na-montmorillonite, and sand samples mixed with different organics. Their results showed the transport and migration of acetic acid and acetone towards the cathode. Samples mixed with hexachlorobenzene and phenol are reported to show accumulation at the center

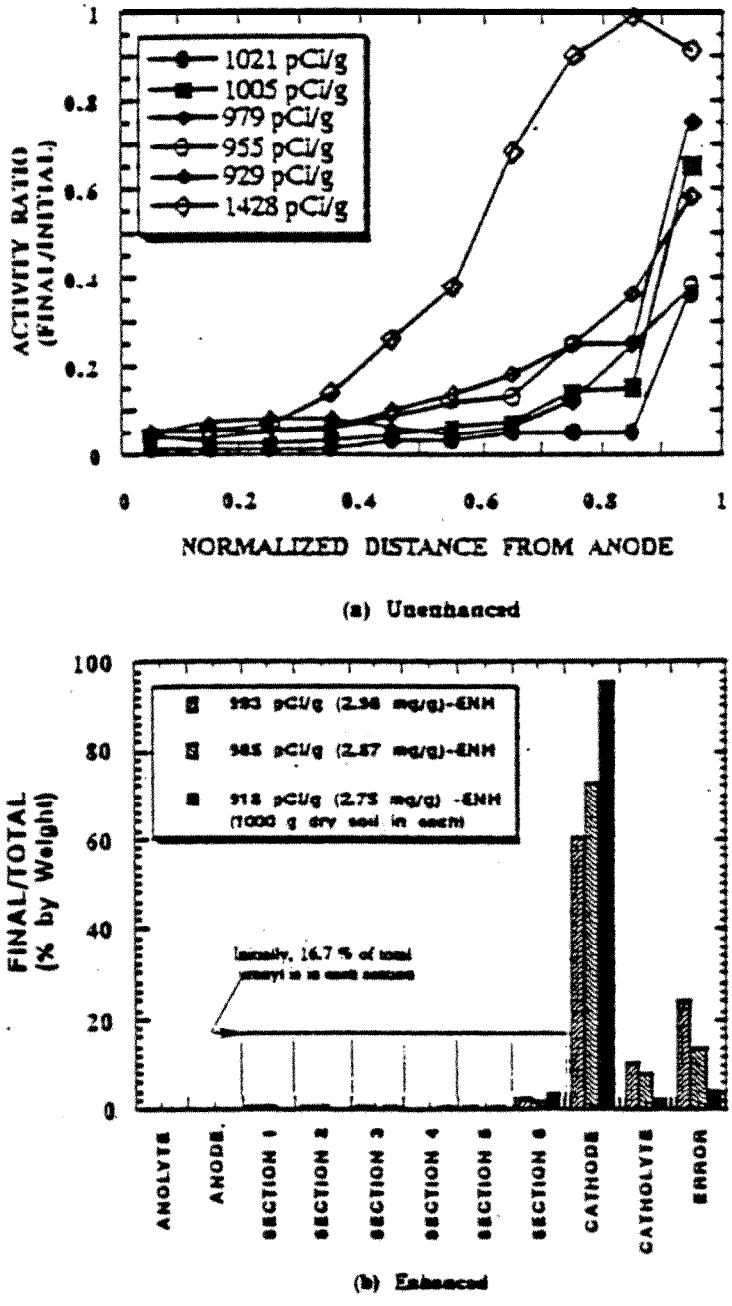

Figure 2.11: Post-Treatment Distribution of Uranyl Ion across the Specimen in Unenhanced Electrokinetic Experiments (Acar et al. 1992c). (b) Post-Treatment Mass Balance in Acetic Acid Enhanced Electrokinetics Remediation Experiments for Uranyl Ion Removal from Kaolinite Specimens (Acar et al. 1993b)

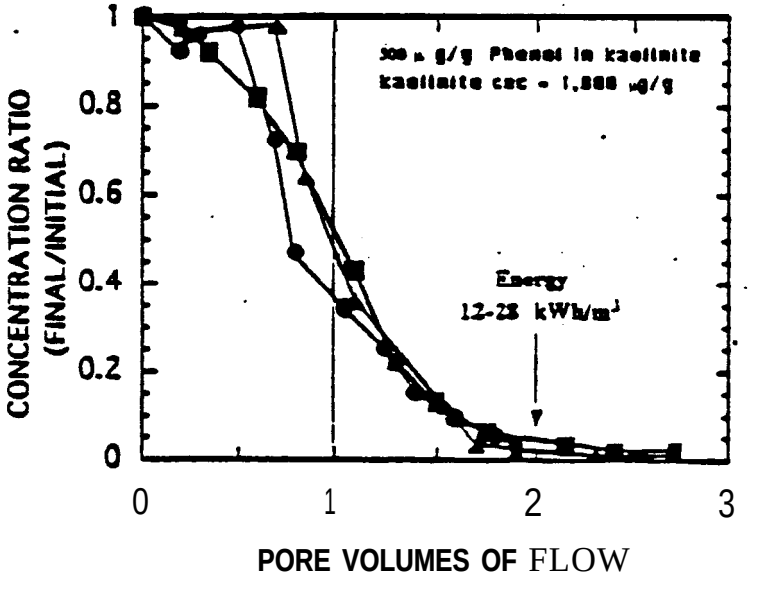

Figure 2.12: Phenol Removal by Electrokinetics (Acar et al. 1992)

of each samples. The results of some of these experiments were inconclusive, either because contaminant concentrations were below detection limits or because the samples were processed for only 24 hrs which might not be sufficient to demonstrate any feasibility in electrokinetic soil remediation.

Although removal of free phase non-polar organics is questionable, Mitchell (1990) stated that this could be possible if they would be present as small bubbles (emulsions) that could be swept along with the water moving by electroosmosis. Acar et al. (1993) stated that unenhanced electrokinetic remediation of kaolinite samples loaded up to 1,000 ug/g hexachlorobutadiene has been unsuccessful. Acar et al. (1993) also reported that hexachlorobutadiene transport was encountered only when surfactants are used. Figure 2.13 shows hexachlorobutadiene transport through compacted kaolinite using sodium dodecyl sulfate (SDS) in the anode compartment. The surfactants form charged micelles which migrate across the soil mass under an electric field. Studies are ongoing at Louisiana State University on the use of this technique in removing TNT from soils.

Field studies of soil decontamination by electrokinetics are limited. Lageman (1989) and (1993) reported the results of field studies conducted in the Netherlands. Figure 2.14 presents a schematic diagram of the reported field Process. These studies demonstrated 73% removal of Pb at a concentration of 9000 μg/g from fine argillaceous sand, 90% removal of As at 300 μg/g from day and varying removal rates ranging between 50% to 91% of Cr, Ni, Pb, Hg, Cu, and Zn from fine argillaceous sand. Cd, Cu, Pb, Ni, Zn, Cr, Hg, and As at concentrations of 10 to 173 μg/g also were removed from a river sludge at efficiencies of 50 to 71%. The energy expenditures ranged between 60 to 220 kWh/m^3 of soil processed. A field study reported by Banerjee et al. (1990) investigated the feasibility to use electrokinetics in conjunction with pumping to decontaminate a site from chromium. Although the effluent chromium concentrations increased slightly, the results of this study are inconclusive as the investigators monitored only the effluent concentrations and did not scrutinize removal across the electrodes.

The laboratory studies reported by Runnels and Larson (1986), Lageman (1989), Acar et al. (1989), Shapiro et al. (1989), Pamukcu et al. (1990), Hamed (1990), Bruell et al. (1990), Acar et al. (1990), Hamed et al. (199 I), Eykholt (1992), Ugaz et al. (1994), Runnels and Wahil (1993), Acar et al. (1993), and Acar et al. (1994) together with the pilot-scale study conducted by Lageman (1989) display the feasibility of the process in removing inorganic species and low level organic

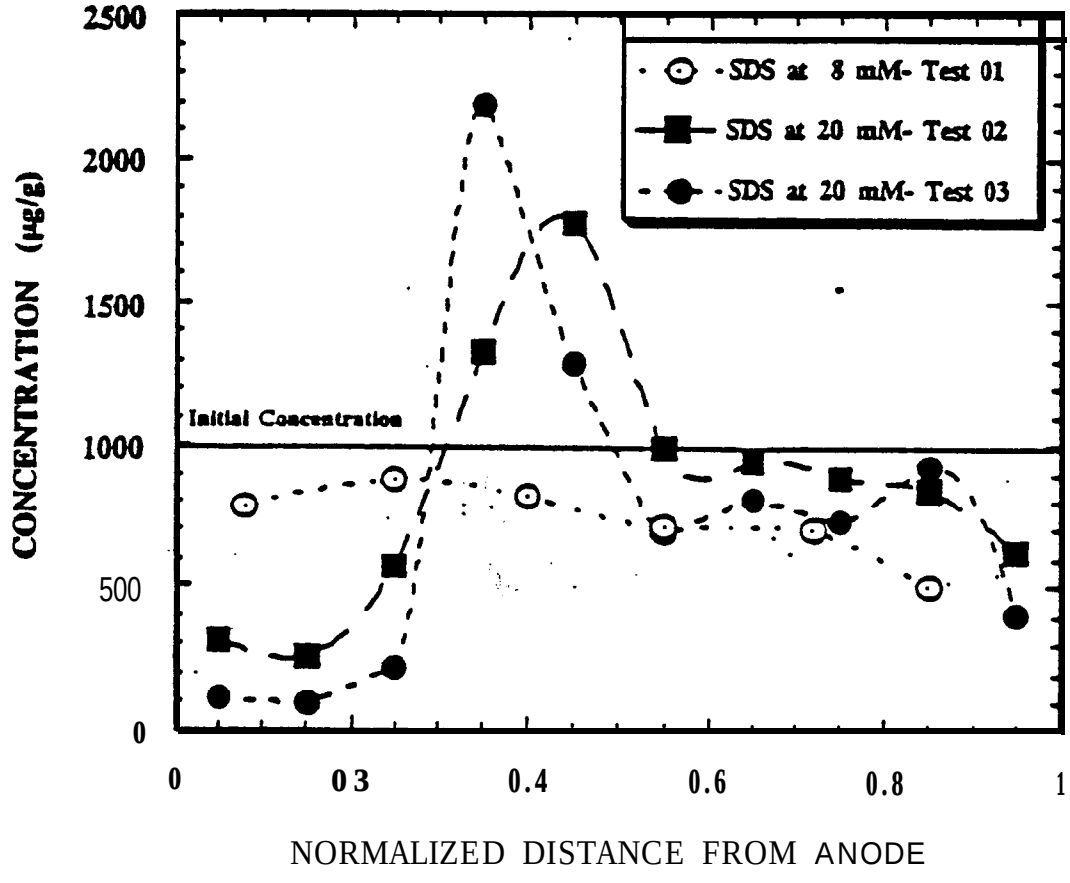

Figure 2.13: Hexachlorobutadiene Transport under Electric Gradients (Acar et al. 1993)

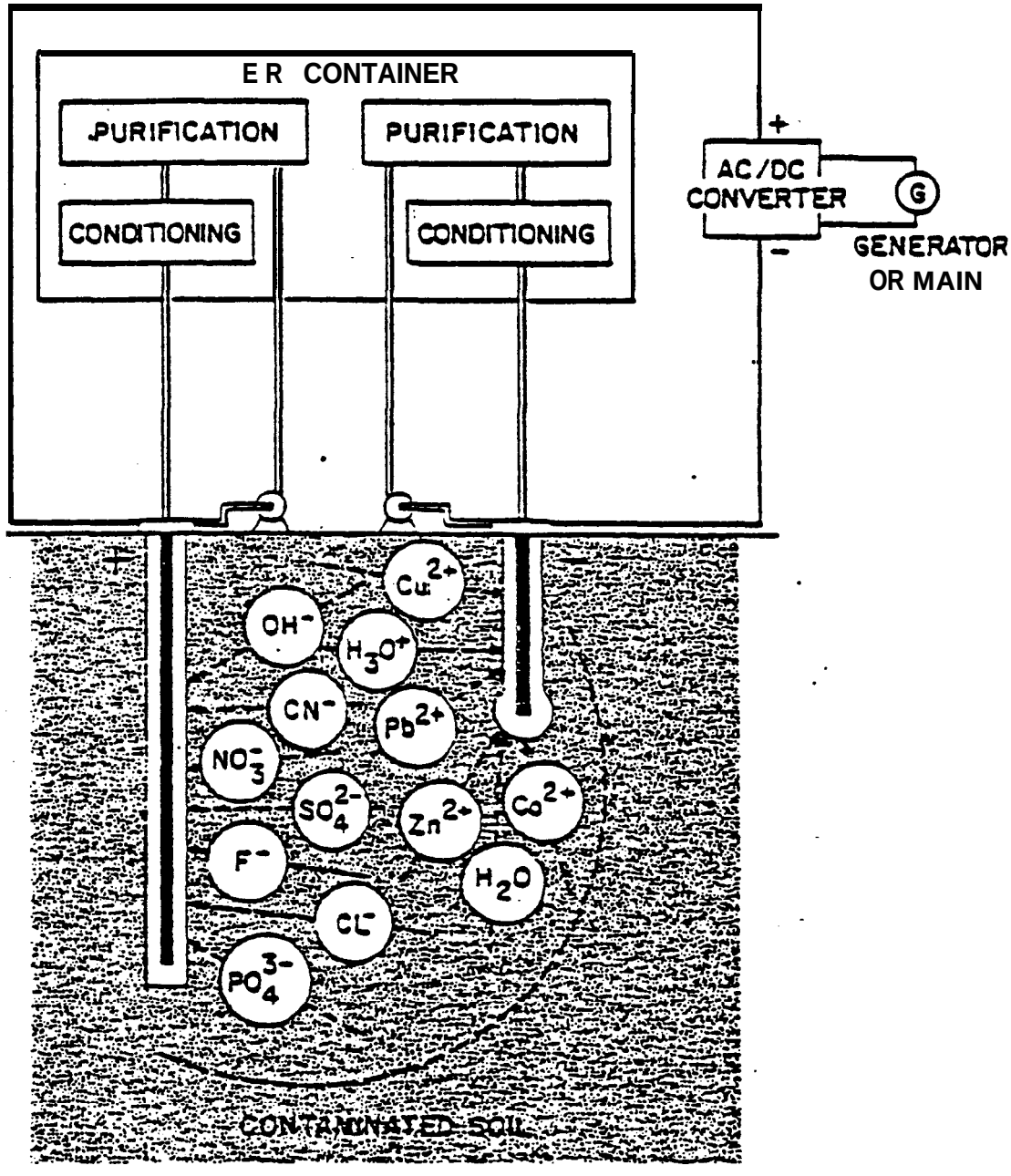

Figure 2.14: **A Schematic Diagram** of the Field System Reported by Lagernan (1989)

contaminants from soils. Table 2.3 summarizes the laboratory data reported for removal of chemical species from soils by electrokinetics and the references used are listed in Table 2.4.

2.8 Theoretical Modeling of Electrokinetic Soil Processing

Modeling coupled transport of fluid, charge, and chemically reactive species is based on generally accepted set of transient (time-dependent) coupled partial differential equations that maintain conservation of matter and energy and the principles of continuum. A set of nonlinear algebraic equations accompanies these partial differential equations to describe the chemical reactions among the constituent species.

For electro-osmotic consolidation of soft clay deposits, models which assume constant electrical potential gradient across the soil mass are proposed and analytical/numerical solutions are presented (Esrig 1968, Wan et al. 1976, Lewis et al. 1973, 1975, Bruch 1976, Banerjee et al., 1980a, 1980b). These models do not involve the chemistry associated with the process.

Theoretical treatise and pertinent solutions to multidimensional contaminant transport equations and hydrochemical transport equations in groundwater due to chemical and hydraulic gradients have shown significant progress in the last decade. Mangold and Tsang (1991) have presented a summary of the geochemical, contaminant transport, hydrochemical models, their solutions and limitations. Yeh and Tripathi (1991) have developed and demonstrated a detailed two-dimensional finite element hydrogeochemical transport model for reactive multispecies solute transport. The described model can be applied to heterogeneous, anisotropic, and saturated/unsaturated media, and can simultaneously account for chemical processes of complexation, dissolution/precipitation, adsorption/desorption, ion exchange, redox, and acid/base reactions.

Contaminant transport models which incorporate electrical gradients are limited. Acar et al. (1988) and Acar et al. (1989) presented a one dimensional pioneering model used to estimate the pH distribution during electrokinetic soil processing. The model provides reasonably good qualitative agreement with experimental evaluation of H^+ transport and distribution. This model considers the electrochemistry of the process. However, it neglects the time dependent changes in electrical and hydraulic gradients, disregards the coupling of electrical gradients with hydraulic

Table A 2.3: Synthesis of Laboratory Data Reported by Various Investigators on the Removal of Chemical Species from Soils

Ref.	Soil Type	Pore Fluid	Species	Initial Conc.	Current Density	Voltage	Duration (hrs)	Energy kWh/m^3	Removal (%)	Remarks
1	Silty Sand	NA	Cu	617	.01-.05 mA/cm^2	0.165 V/cm	24-72	NA	50	Cylindrical Specimens (D=0.75in, L=6 in.). Final concentration 290-543 mg/kg.
2,3	Kaolinite	DIW	Pb	100-1064 mg/kg	0.012-0.123 mA/cm^2	2.5 V/cm	100-1285	29-60	75-95	Bench-scale tests conducted on kaolinite samples loaded with Pb at concentrations below and above the CEC. Demonstrates the effect of pH changes on the process.
2,4	Kaolinite	DIW	Cd Cr	100-140 mg/kg	0.037 mA/cm^2	2-2.5 V/cm	480-1600	50-120	92-100 65-70	Bench-scale tests demonstrate the feasibility of the process. The study demonstrates the development of nonlinear electric potential distribution due to the electrochemical changes across the sample.
5	Silty Clay	GW	Cr	150-1500 mg/kg	NA	0.1-1.0 V/cm	24-168	NA	NA	Field specimens are used (D=5.1 cm, L=2.5cm to 6.7 cm). Hydraulic and electric potentials are used simultaneously.

DIW: Deionized Water, DW: Distilled Water, GW: Ground Water, HS: HumicSolution, TW: Tap Water, NA: Not Available.

Table A 2.3: Synthesis of Laboratory Data Reported by Various Investigators on the Removal of Chemical Species from Soils (cont'd)

Ref.	Soil Type	Pore Fluid	Species	Initial conc.	Current Density	Voltage	Duration (hrs)	Energy	Removal (%)	Remarks
6	Kaolinite	D I W	Cu $Cu(NO_3)_2$ sol.	1.3 meq/kg	0.3-2.0 mA	0.25 V/cm	16-48	4.5-7.4	NA	Demonstrates that buffering theanoderesultsinhigher electroosmotic flow than buffereing the cathode. Citrate treatment was not effictive in removing precipitated copper from the cathode zone.
7, 19	Kaolinite	D W	Cd. co, Ni, Sr	400-700 mg/kg	NA	30 v 4 *V/cm*	2430	NA	85-95	Conducted bench-scale tests *on the* feasibility of the process. The results display that removal efficiencies (or %removal) *is higher* for high *inilial* concentrations. The results show that kaolinite has the highest removal followed by clayey sand while Na-monimorillonite shows the lowest removal efficiency
	Kaolinite	HS.	Cd. Co, Ni, Sr	600-750 mg/kg	NA	30v 4 *V/cm*	2430	NA	85-95	
	Kaolinite	GW	Cd, Co, Ni. Sr	550-1100 mg/kg	NA	30 v 4 V/cm	24-50	NA	85-95	
	Na-Montm.	DW	Cd, Co, Ni, Sr	4500-8600 mg/kg	NA	30 v 4 *V/cm*	24-50	NA	85-95	
	Sand + 10% Na-Montm.	DW	Cd, Co, Ni, Sr'	400-I500 mg/kg	NA	30 v 4 *V/cm*	24-50'	NA	85-95	

DIW: Deionized Waler, DW: Distilled Water, GW: Ground Waler, HS: Humic Solution, TW: Tap waler, NA: Not Available.

Table A 2.3: Synthesis of Laboratory Data Reported by Various Investigators on the Removal of Chemical Species from Soils (cont'd)

Ref.	Soil Type	Pore Fluid	Species	Initial Conc.	Current Density	Voltage	Duration (hrs)	Energy kWh/m 3	Removal (%)	Remarks
8	Kaolinite Kaolinite	Deion. Water Deion. Water	Uranium Thorium	1000 pCi/g 41-313 pCi/g	0.127 mA/cm^2 0.127 mA/cm^2	0.5-12 V/cm 0.5-12 V/cm	85-550 144-785	50-300 kWh/m^3 100-300 kWh/m^3	85-95 20-75	The results demonstrate the feasibility of removing radionuct ides from bench-scale kaolinlte sampler. Thorium and radium removal were incomplete due to formation of (horuim hydroxide and radium sulphate.
9	Unsat. Sand	0.005M $CaSO_4$	Chrom-ate	100 mg/kg	0.35 mA/cm^2	89-150 V 4-7 V/cm	22	NA	NA	Demonstartes the efficiency of using the process for partially saturated samples. Rale of ion-migration Is 20 times the rate of electroosmosis.
10	Unsat. Sand	NA	Cu ($CuSO_4$ sol.)	617 mg/l	NA	2 V 0.13 V/cm	3, 5, 7, and 9 days	NA	NA.	Fully saturated samples showed higher removal efficiencies than unsaturated samples.
11	Sand	DW	$CuSO_4$	0.001M $CuSO_4$ (65 mg/l Cu Sol.)	NA	2.5 V 0.2 V/cm	7-48	NA	NA	Demonstartes the efficiency of using ion-migration for preconcentration of tons that are difficult to remove by pump-and-treat
12, 13	Altamont Caly (Illite)	NaCl Sol.	NaCl	0.02N NaCl	NA	10 V 0.1 V/cm	500 day	NA	NA	Investigates the feasibility of using electrokinetic clay barriers.

DIW: Deionized water, DW: Distilled Water. GW Ground Waler, HS: Humic Solution TW: Tap Waler, NA: Not Available.

Table A 2.3: Synthesis of Laboratory Data Reported by Various Investigators on the Removal of Chemical Species from Soils (cont'd)

Ref.	Soil Type	Poro Fluid	Species	Initial Conc.	Current Density	Voltage	Duration (hrs)	Energy kWh/m 3	Removal (%)	Remarks
14. 15. I6	Kaolinite Kaolinite	NA	acetic acid Phenol	0.5 M, 0.1 M 450 ppm 45 ppm	NA NA	2s v 0.62 V/cm	20-100 days up 10 60 days	3.7 Kwh/t 5.3-260 kwh/t	95 45 9s 75	0. IM NaCl purging solution was used to optimize the process.
I7	Kaolinite	DIW	Phenol	500 mg/kg	0.037 mA/cm^2	0.4-2.4 V/cm	78-144	18-39	85-95	Most of the phenol removed from the sample was collected with the effluent.
18	Kaolinite	TW	BTXs Comp.	l-150 mg/kg	NA	0.4 'V/cm	NA'	NA	see remarks	Different organics (TCE 150 mg/kg. bcnzcnc I30 mg/kg. tolucnc 70 mg/kg. m-xylene 30 mg/kg) showed transport and removal horn cylindrical bench-scale samples (L-30cm) by electroormosis.
I9	Kaolinite Na-Monl Sand	DW GW HS	Aceton (see remarks)	100-6800 ppm	NA	30 v 4 V/cm	24-50	NA	Varies 5.8-100	Different organics (aceltic acid, aceton, phenol, and hexachlorobenzene) showed transport and accumulation at center and towards the cathode.

DIW: Deionized Water: DW: Distilled Water, GW: Ground Water, HS: HumicSolution, TW: TapWater, NA Not Availa

Table 2.4: References for Data Presented in Table 2.3

1 Runnels and Larson (1986)
2 Hauled (1990)
3 Hamed, Acar, and Gale (1991)
4 Acar, Hamed, Alshawabkeh, and Gale (1994)
5 Banerjee, Horng, Ferguson, and Nelson (1990)
6 Eykholt (1992)
7 Pamukcu and Wittle (1992)
8 Ugaz, Puppala, Gale, and Acar (1994)
9 Lindgren, Mattson, and Kozak (1992)
10 Dabab, Kelly, and Godaya (1992)
11 Runnels and Wahli (1993)
12 Yeung (1990)
13 Mitchell and Yeung (1991)
14 Shapiro, Renauld, and Probstein (1989)
15 Shapiro and Probstein (1993)
16 Probstein and Hicks (1993)
17 Acar, Li, and Gale (1992b)
18 Bruell, Segal, and Walsh (1992)
19 Wittle and Pamukcu (1993)

gradients and does not incorporate the complicated chemistry and reactions associated with the process.

Yeung (1990) and Mitchell and Yeung (I99 I) have proposed another model in a study of the feasibility of using electrical gradients to retard or stop migration of contaminants across earthen barriers. Principles of irrversible thermodynamics were employed by these authors and a one dimensional model is developed for transport of contaminants across the liner. The integral finite difference method was used to solve the problem and the model reasonably predicted the transport of sodium and chloride ions across the liner. The limitations of this model are similar to those of Acar et al. (1989). Furthermore, the complicated chemistry of the electrode reactions (acid/base distributions) were not included and nonlinear changes in electrical and hydraulic potentials are neglected.

Shapiro et al. (1989) and Shapiro and Probstein (1993) incorporated the electrochemistry of the process and developed a model for transport of chemical species under electrical gradients. The model couples the transport equations of chemical species together with the charge flux equation and accounts for the chemical reactions in the soil pore fluid. A steady state electroosmotic flux was assumed and calculated by averaging the electrical gradient and zeta potential across the soil sample. Shapiro and Probstein (1993) reported that the numerical solution is achieved using finite element method in the spatial domain and Adams-Bashforth integration in time. The results were compared with the experiments for the case of constant voltage at the boundaries (the current changes with time depending upon the electrical conductivity of the soil sample). Comparisons displayed a good agreement in one case of acetic acid removal from a kaolinite specimen of 40 cm length. Other experiments did not show good agreement with the model results. The model integrates the charge flux equation to evaluate the electric potential distribution and did not solve the equation describing preservation of the electric charge. The model assumes incompressible soil medium, disregards the changes in the hydraulic potential distribution, and also does not account for any sorption reactions.

Eykholt (1992) attempted to model the pH distribution during the process using a mass conservation equation accompanied by empirical relations to account for the nonlinearity in the process. One transport differential equation is formed by subtracting the equation describing OH- transport from the equation describing H+ transport and assuming that hydrogen and hydroxyl ions have the same diffusion coefficients and ionic mobilities. The approach of using a dummy

concentration of the difference between H^+ and OH- concentrations has been widely used in modeling contaminant trasport in groundwater to eliminate the rate of chemical reactions, actions, such as the water autoionization reaction, from the differential equations (Miller and Benson 1983). However, it is confusing to use this approach in the case of species transport under electric gradients, even when the equal ionic mobility assumption is made for these species; in an electric field, OH- migrates in a direction opposite to that of H+ migration because of their opposite electric charge. This study showed that a negative pore water pressure may develop in soil due to changes in zeta potential. The development of negative pore water pressure is modeled based on zeta potential measurements made by Lorenz (1969) for kaolinite at different pH values. The modified Smoluchowski equation (developed by Anderson and Idol 1986) was used together with the proposed empirical relations to predict changes in the electric potential distribution.

Corapcioglu (1991) has presented a formulation of the system of equations governing the coupled transport of mass, charge, and fluid under electrical, chemical and hydraulic gradients assuming a nonreactive mass transport. Alshawabkeh and Acar (1992) have described a system of differential/algebraic equations for the process accounting for the chemical reactions of adsorption/desorption, precipitation/dissolution, and acid/base reactions. Acar and Alshawabkeh (1994) have modeled the changes in soil and effluent pH during electrokinetic soil processing. Two transient transport equations for hydrogen and hydroxy1 ions are used together with the water autoionization equation. This attempt also assumes linear electric and hydraulic gradients throughout the process and disregards the coupling of these components. Furthermore, in these models no special treatise is provided for the effect of conservation of electrical neutrality on transport of the chemical species present.

A comprehensive theoretical model is required for electrokinetic soil processing. This model should account for coupled multicomponent species transport under electric, hydraulic and chemical gradients. Chemical reactions in the soil pore fluid, such as sorption, precipitation/dissolution, aqueous phase, water autoionization, and electrolysis reactions, also should be included. This model is expected to provide the basis for a comprehensive design/analysis tool for the different boundary conditions, site-specific contamination and variable soil profiling encountered in full scale implementation of the process. Such a theoretical model also would allow assessment of the principles of multispecies transport under electric fields.

Section 3

THEORETICAL DEVELOPMENT

3.1 Introduction

Electrokinetic soil remediation encompasses a sundry of physico-chemical processes that cause species transport and removal. Theoretical understanding and simulation of the technology demand a grasp of the mathematical formulation of these processes. These processes are controlled by such variables as electrolysis reactions at the electrodes, pH and soil-surface chemistry, equilibrium chemistry of the aqueous system, electrochemistry of the contaminants, and geotechnical/hydrological characteristics of the porous medium. The complexity of the processes involved necessitates simplifying assumptions which would allow numerical simulation within the proposed time frame.

3.2 Assumptions

The following assumptions are employed in the theoretical development presented in this study

I The soil medium is isotropic and saturated.

2. The soil medium consists of clay particles with negatively charged surface, the fluid region with the excess cations, and the pore free fluid with N number of chemically reactive species.

3. All fluxes are linear homogeneous functions of all driving forces (or potential gradients).

4. Isothermal conditions prevail (coupled heat transfer is neglected).

5. All the applied voltage is effective in fluid and charge transport.

6. Electrophoresis is not present
7. Hydraulic conductivity, coefficient of eletroosmotic permeability, and coefficient of volume compressibility are constant in time and space.
8. The chemicoosmotic coupling is negligible.
9. The chemical reactions (precipitation/dissolution, aqueous phase reactions, and sorption) are at instantaneous equilibrium (rate kinetics are ignored).
10. Soil particles are treated as electrically nonconductive (insulators).
11. Surface conductance and streaming potential are negligible.

Most of the stated assumptions are reasonable and they are made in an attempt to accomplish the identified objectives within the scope and time frame available for this study. Other assumptions were also necessary since a limited understanding of the mathematical formulation of the physical or chemical specific processes exists. Justification of some of these assumptions is presented below while further discussion is presented throughout the manuscript.

Specific amount of the applied electric energy might be consumed in generation of heat, which might generate thermal gradients. The effect of the generated thermal gradient on the transport processes and performance and efficiency of electrokinetic processing is not included herein and is yet to be investigated. Therefore, an isothermal system is assumed where all the applied electrical energy is available for transport.

Electrophoresis is a significant transport mechanism for clay suspensions. In the case of compacted or even soft clay deposits, electrophoresis will have a minor contribution in charge transport under electric currents. The assumption of no electrophoresis is, therefore, assumed to be valid in this study.

Generation and dissipation of pore water pressure in soils result in consolidation, and changes in soil porosity. Coefficients of hydraulic conductivity, electroosmotic permeability, and soil compressibility are expected to change in time and space as a result of soil consolidation. In

some cases, such as consolidation of slurries, consolidation greatly affects porosity, hydraulic conductivity, and soil compressibility; however, in compacted clays, changes in hydraulic conductivity are not expected to be significant. The effects of these changes are not accounted for in this study because the uncertainty in evaluating these parameters would be more than the changes expected in their values.

The assumption of no chemicoosmosis is justified by the fact that this component becomes significant only in the presence of large chain molecules and in very active clay deposits (Mitchell et al. 1973).

3.3 Transport Processes

Application of hydraulic, electric, chemical, and/or thermal gradients to a homogeneous medium of soil-water-electrolyte results in transport of matter and energy. The resulting fluxes of fluid, charge, mass, and/or heat through the soil medium, their changes with time, and their effects on the properties and composition of the soil medium are significant in various geotechnical/geoenvironmental problems.

The fluxes of matter and/or energy through soil-water-electrolyte media could be categorized into two types; uncoupled fluxes and coupled fluxes. Direct spontaneous uncoupled fluxes result from application of a potential gradient of the same type of the matter transported (conjugated driving forces). Examples of direct fluxes are fluid transport due to a -hydraulic gradient (Darcy's law), charge transport due to an electric gradient (Ohm's law), mass transport due to a chemical gradient (Fick's raw), and heat transport due to a thermal gradient (Fourier's law). Coupled fluxes result from transport of matter and/or energy due to a potential gradient of different type than the matter and/or energy transported (non-conjugated driving forces). The nature of the soil-water-electrolyte system with the presence of the diffuse double layer gives arise to spontaneous coupled transport fluxes. Examples of coupled fluxes in soil-water-electrolyte system are water transport due to an electric gradient (electroosmosis), heat transport due to a chemical gradient (Dufour effect), and charge transport due to a thermal gradient (Soret effect). Table 3.1 summarizes various coupled and uncoupled direct fluxes identified as a result of

Table 3.1: Direct and Coupled Flow Phenomena

Flux J	Hydraulic Gradient	Chemical Gradient	Electrical Gradient	Thermal Gradient
Fluid Flux	Hydraulic Conduction	Chemico-Osmosis	Electro-Osmosis	Thermo-Osmosis
Mass Flux	Filtration	Diffusion	Migration Mass Flux	Thermo-Diffusion
Charge Flux	Streaming current	Diffusional current	Migrational current	Thermo-current
Heat Flux	Thermo-Filtration	Thermo-Diffusion	Thermo-Migration	Thermal Flux

application of hydraulic, electric, chemical, and thermal gradients to a system of soil-water-electrolyte.

Assuming that all fluxes are linear homogeneous functions of all their applied and/or generated driving forces (or potential gradients), the following equation is used to define a system of m fluxes, J(m), due to m conjugate driving forces, F(m),

$$J(m)=L.F(m) \tag{3.1}$$

where L is (m x m) matrix of coefficients Lij relating the flux J_i to a force F_j. The coefficients L_{ii}, L_{jj},..., in the main diagonal of the matrix are named straight (diagonal or uncoupled) coefficients, since they relate the fluxes to their conjugated forces. The other coefficients are called coupling (or cross) coefficients, as they relate the fluxes to the non-conjugated forces. The flux J_i is, therefore, described by m

$$J_i = \sum_{j=1}^{m} L_{ij} F_j \qquad j = 1, \ldots . M \tag{3.2}$$

3.3.1 Fluid Flux

Fluid flux results from application of a hydraulic gradient (Darcy's law), an electric gradient (electroosmosis) and/or a chemical gradient (chemicoosmosis). Chemicoosmosis is not included because, as stated in the assumptions, it is significant only in the presence of large chain molecules and in very active clay deposits.

3.3.1.1 Darcy's Law of Advection

Fluid flux due to a hydraulic gradient, $J_w^h (LT^{-1})$ is given by Darcy's law as,

$$J_w^h = k_h \nabla (-h) \tag{3.3}$$

where k_h is the coefficient of hydraulic conductivity (LT^{-1}), h (L) is the hydraulic head $(h = u / \gamma_w)$,

u is the hydraulic potential (F/L^{-2}), and γ_w in the unit **weight of the** pore fluid ($F\text{-}L^{-3}$). Numerous methods exist for evaluating the hydraulic conductivity of fine-grained soils. Daniel (1989) and (1993) summarize various laboratory and field methods and equipment that can be used for measurement of the hydraulic conductivity of different soil types.

Extensive research has been carried out on the hydraulic conductivity of fine-grained soils with **a** relatively good understanding of the fundamental factors affecting its value (Lambe 1954, 1958; MitchelI et al. 1965; Olson and Daniel 1981; Boynton and Daniel 1985; Acar and Olivieri 1989). These studies indicate that microstructure and fabric are among the factors that highly influence fluid transport in fine-grained deposits. Dispersed micro-structure generally results in lower hydraulic conductivity than flocculated micro-structure. Acar and Olivieri (1989), in a study on the effect of pore fluid chemistry on fabric and hydraulic conductivity of compacted clays, show that a change in the hydraulic conductivity occurs when organic fluids are permeated through them in response to changes in the diffise double layer, particle interactions and consequently soil fabric. Other **factors that affect** k_h, include soil porosity and pore size distribution. The presence of uniformly distributed fine size pores results in lower hydraulic conductivity, while the presence of macro pores results in higher hydraulic conductivity, even if soil porosity is the same in both **Cases.**

Electrokinetic soil remediation induces changes in the pore fluid chemistry, diffuse doubIe layer, soil fabric and consequently the hydraulic **conductivity.** Furthermore, electroosmotic consolidation is expected to take place and influence the hydraulic conductivity value. In attempting to model electrokinetic soil remediation in this study, hydraulic conductivity is assumed to be constant in time and space because of the following reasons; (a) there is no clear mathematical formalism that can describe the effect of pore fluid chemistry on soil fabric and consequently the hydraulic conductivity, and (b) the uncertainties in evaluating the hydraulic conductivities are more significant than the changes expected in their values.

3.3.1.2 Electroosmotic Fluid Flux

The Helmholtz-Smoluchowski theory for electroosmosis is the most commonly adopted theoretical description of fluid transport through soils due to electrical gradients. Similar to the hydraulic conductivity, this theory introduces the coefficient of electroosmotic permeability, k_e

$(L^2V^{-1}T^{-1})$, as the volume rate of fluid flowing through a unit cross sectional area due to a unit electrical gradient. Hence, the electroosmotic flow rate, $J_w^e\ (LT^{-1})$, is expressed by an empirical relation similar to Darcy's relation,

$$J_w^e = k_e \nabla(-E) = k_i I \tag{3.4}$$

where E is the electric potential (V), I is the electric current density $(CL^{-2}T^{-1})$, and $k_i\ (L^3C^{-1})$ is the electroosmotic coefficient of fluid transport given by,

$$k_i = \frac{k_e}{\sigma^*} \tag{3.5}$$

$\sigma^*\ (CV^{-1}T^{-1}L^{-1})$ is the effective electrical conductivity of the soil medium.

Although Equation 3.4 can provide an estimate of the flow rate for known value of the coefficient of electroosmotic permeability and electric conductivity under constant current conditions, it assumes constant electrical gradient across the electrodes. Applying an electric current through the soil medium will generate a zone of high electrical conductivity at the anode and a zone of low electrical conductivity at the cathode (Hamed 1990; Acar et al. 1993). Figure 3.1 presents a comparison of the pH and conductivity profiles across a soil specimen upon a complete sweep of the acid front generated at the anode compartment. Figure 3.2 presents a typical profile of electrical potential difference across the soil specimen in a test conducted for Cr^{3+} removal. As depicted in Figure 3.2, the electrical potential drop is mostly realized in the cathode region, resulting in higher electroosmotic flow in that region rather than the anode region.

The value of k_e is widely accepted to be a function of zeta potential, viscosity of the pore fluid, porosity and electrical permittivity of the soil medium. When the soil pores are treated as capillary tubes, the coefficient of electroosmotic permeability is given by,

$$k_e = \frac{\varepsilon\varepsilon_o\zeta}{\eta} n$$

where ε is the permittivity of the medium $(Farad/L^{-1})$, ζ is the zeta potential (v), n is the porosity (L^3L^{-3}), and η is the viscosity (FTL^{-2}). While hydraulic conductivity, k_h, is significantly

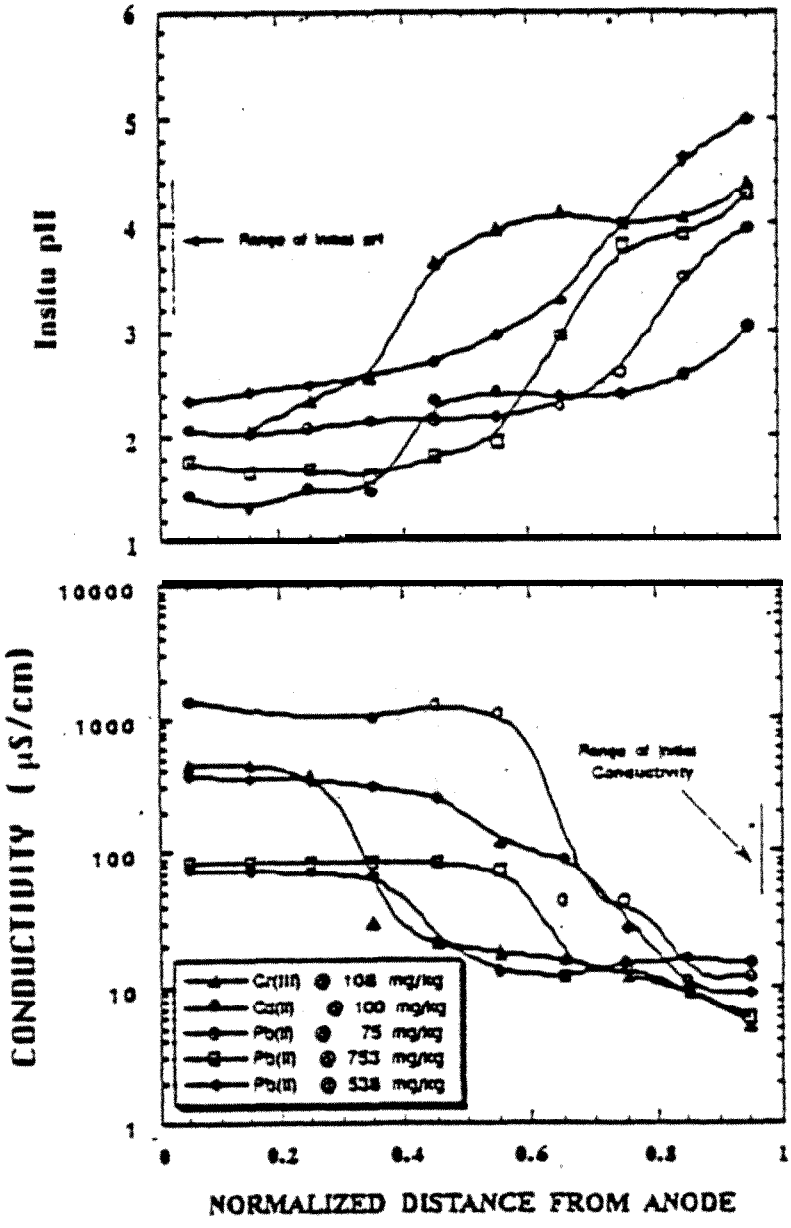

Figure 3.1: A Comparison of pH and Conductivity Profiles across a Specimen (Acar et al. 1992b)

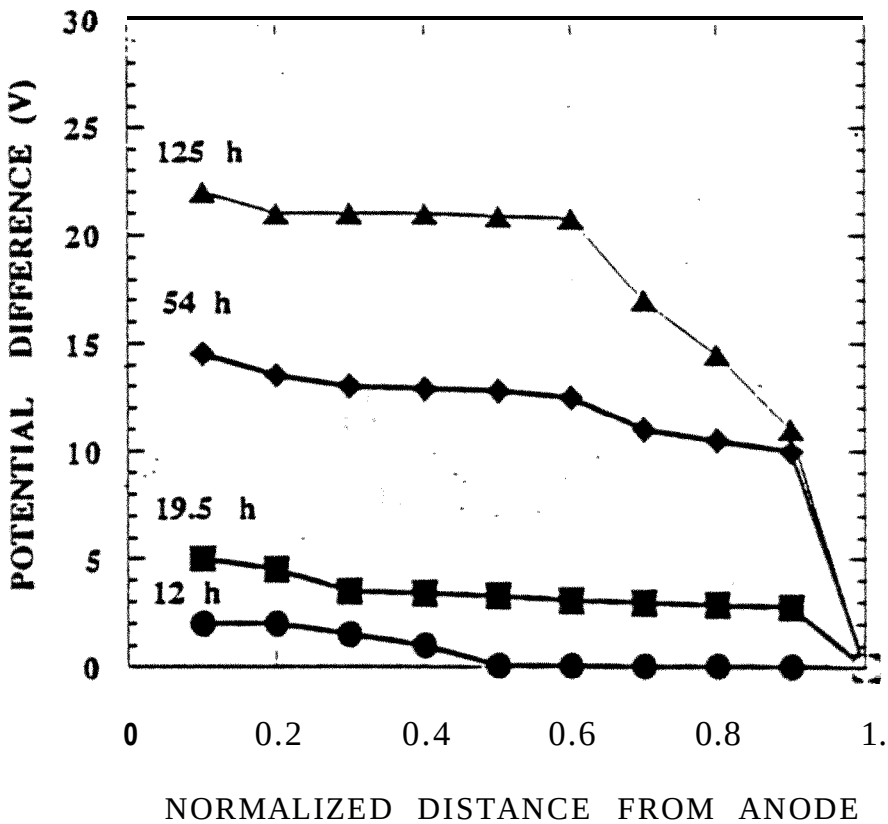

Figure 3.2: Electrical Potential Profile across a Specimen in Cr^{3+} Removal Test (Hamed,

influenced by the pore **size** and distribution in the medium (Acar and Olivieri 1989), the electroosmotic coefficient of permeability, k_e according to the Heimhoitz-Smoluchowski theory is dependent mainly on porosity and zeta potential. The value of k_e has been assumed to be constant during the electrokinetic process as long as there is no change in the concentration of ions or pH of the pore fluid. This was not a good assumption in the studies reported by Gray and Mitchell (1967), Lorenz (1969), and Hunter (1981).

Extensive research has been carried out on the zeta potential of the glass-water interface. There is a good qualitative agreement in the results of different studies. Hunter (1981) in an extensive summary of theoretical and experimental treatise of the zeta potential in colloid science, displays the effect of pH and ion concentration in the pore fluid on zeta potential. Figure 3.3 shows that the zeta potential decreases linearly with the decrease of logarithm of electrolyte concentration (Kruyt 1952; Hunter 1981) and/or the pH of the soil medium. The effect of electrolyte chemistry on zeta potential could therefore represented by (Kruyt .1952), (3.7)

$$\zeta = A - B \log C_o$$

where, A and B are two constants that are evaluated experimentally, and C_o (M/L^3) is the total electrolyte concentration

It is hypothesized that the drop in pH of the soil due to electrokinetic processing will cause a decrease in the coefficient of electroosmotic permeability associated with the drop in zeta potential; hence, the electroosmotic flow will start to decrease and eventually stop at later stages of the process. The results of Acar et al. (1989), Hamed et al. (1991), and Acar et al. (1993) demonstrate the decrease and cessation of electroosmosis upon continued testing. Consequently, the k_e value determined in one-dimensional tests is time-dependent and controlled by the chemistry generated at the electrodes.

3.3.1.3 Total Fluid Flux

Adding Equation 3.3 and Equation 3.4, the total fluid flux, J_w, is **given** by, (3.8)

$$J_w = k_h \nabla(-h) + k_e \nu(-E)$$

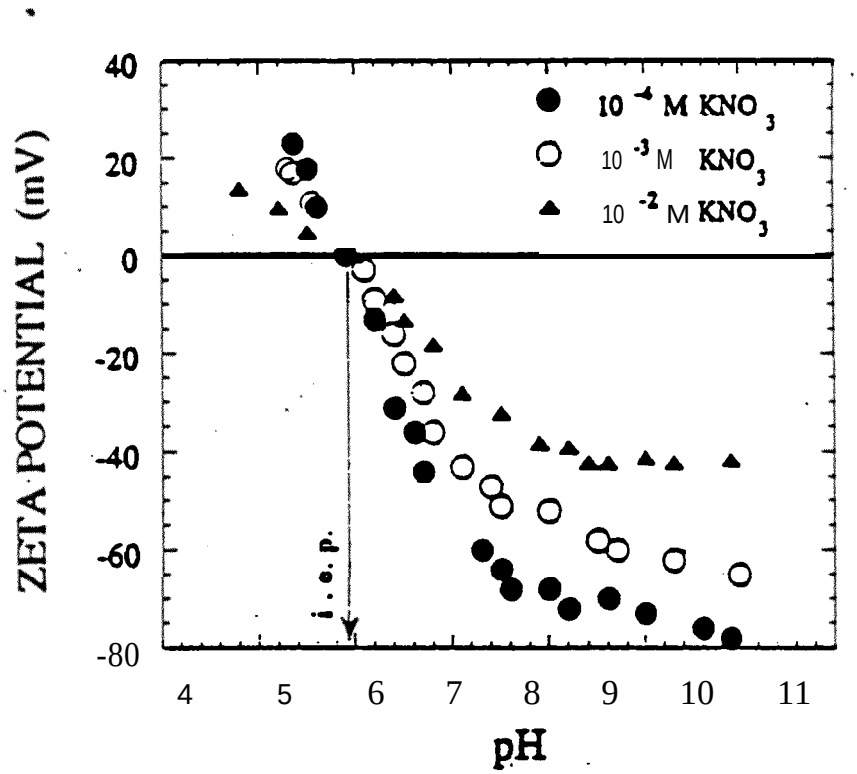

Figure 3.3: The Effect of pH and Ion Concentration on Zeta potential of Colloidal TiO_2 (iep is the isoelectric point) (Hunter, 1981)

The total one-dimensional fluid flux is,

$$J_w = -k_h \frac{\partial h}{\partial x} - k_e \frac{\partial E}{\partial x} \qquad (3.9)$$

3.3.2 Mass Flus

Mass flux of different chemical species relative to pore fluid is a consequence of different coupled potential gradients. Hydrodynamic dispersion is mass transport due to a chemical concentration gradient. Migrational mass flux is mass transport of charged species due to an electric potential gradient. Filtration or ion sieving is mass (or species) transport due to a hydraulic gradient (Groeneveit and Bolt 1969). Filtration is neglected in this study because it occurs only in soils with very fine pores where the resistance against passage of water molecules is much smaller than that for dissolved larger molecules. Total mass flux of dissolved species also includes the advective component due to species transport by the flowing fluid.

3.3.2.1 Fick's Law of Diffusion

Hydrodynamic dispersion, the phenomenon of mass transport of chemical species due to a concentration gradient, is a result of two basic phenomena; mechanical dispersion and molecular diffusion. While mechanical dispersion occurs as a result of velocity variation within the porous medium, molecular diffusion is mass transport due to the difference in thermal kinetic energy of the molecules. Perkins and Johnston (1963), Bear (1972), and Rowe (1987) indicate that mechanical dispersion is a significant mechanism in contaminant transport in ground water because of the relatively high hydraulic conductivity and advective hydraulic flow in such deposits (higher than $1.0 * 10^{-7}$ cm/sec). On the other hand, molecular diffusion is the primary process that controls hydrodynamic dispersion in clay deposits due to the low advective hydraulic flow in these deposits.

The diffusive mass transport of chemical species in a saturated soil medium under chemical concentration gradients is described by Fick's first law,

$$J_i^d = D_i^* \nabla(-c_i) \qquad (3.10)$$

where $J_i^d (ML^{-2}T^{-1})$ is the diffusive mass flux of the ith chemical species per unit cross sectional

area of the porous medium, $c_i (ML^{-3})$ is the molar concentration of the ith chemical species, and $D_i^* (L^2T^{-1})$ is the effective diffusion coefficient of the ith chemical species. The effective diffusion coefficient in the porous medium, D_i^*, is related to the respective diffusion coefficient in free solution, D_i, by (Bear, 1972; Gillham and Dherry, 1982; Shackelford and Daniel, 1991),

$$D_i^* = D_i \tau n \tag{3.11}$$

where $\tau (L^2/L^2)$ is an empirical coefficient accounting for the tortuosity of the medium. Values of τ span over a wide range for different saturated and unsaturated soils. Experiments are often necessary to determine its value for a specific soil type. Shackelford and Daniel (1991 a) have summarized various values of τ for different soil types reported by various authors (Table 3.2). These values are as low as 0.01 and as high as 0.84, mostly ranging between 0.2 to 0.5.

Diffusion coefficients for different ions at infinite dilution have been evaluated and reported by various authors. Tables 3.3 and 3.4 present absolute values of diffusion coefficients for representative cations and anions attained under ideal conditions. Many factors might affect the molecular diffusion coefficient such as the electroneutrality requirement concentration, and electrolyte strength (Shackeiford, 1991). Irreversible thermodynamics could be used to evaluate molecular diffusion coefficient for a single ion with respect to a counter ion in a single electrolyte. Utilizing preservation of electrical neutrality, nolecular-diffusion for a single electrolyte, D_o, is evaluated as,

$$D_o = \frac{D+D-(z_+ - z_-)}{z_+ D_+ - z_- D_-} \tag{3.12}$$

where D_+ and D_- are the diffusion coefficients of the particular cation and anion, respectively, and z_+ and z_- are the charges of the cation and anion, respectively. Table 3.5 shows representative diffusion coefficients for single electrolytes. Limited research is encountered for multicomponent diffusion coefficient of a solution of more than one electrolyte. Multicomponent describes ion diffusion due to coupled concentration gradients of other ions present in the solution.

Table 3.2: Representative Tortuosity Factors (Adapted from **Schackelford and** Daniel, 1991).

Soil	Tracer	Saturation	r
50% Sand:Bentonite Mixture	^{36}Cl	Saturated	0.08-0.12
Bentonite :Sand Mixture	^{36}Cl	Saturated	0.04-0.49
Bentonite:Sand Mixture	^{36}Cl	Saturated	0.59-084
Silt Loam	^{36}Cl	Unsaturated	0.05-0.55
Sand	^{36}Cl	Saturated	0.28
Loam	^{36}Cl	Saturated	0.36
Clay	^{36}Cl	Saturated	0.31
Clayey Till	Cl-	Saturated	0.15
Silty Clay	Cl-	Saturated	0.13-0.3
Silty clay	Cl-	Saturated	0.1
Sandy Loam	Cl-	Unsaturated	0.21-0.35
Silty Clay Loam; Sandy Loam	Cl-	Saturated	0.08-0.22
Kaolinite	Cl-	Saturated	0.12-0.5
Smectite Clay	Cl-	Saturated	0.07-0.24
Clay	$Cl^- \& SO_4^{2-}$	Saturated	0.55
Silty Clay Loam; Sandy Loam	Br^-	Saturated	0.19-0.3
Kaolinite	Br^-	Saturated	0.15-0.42
Smectite Clay	Br^-	Saturated	0.08
Sandy Loam	Br^-	Saturated.	0.25-0.35
Bentonite:Sand Mixtures	^3H	Saturated	0.01-0.22
Bentonite:Sand Mixtures	^3H	Saturated	0.33-0.7

Table 3.3: Absolute **Values** of Diffusion Coefficients and Ionic Mobilities for Representative Cations as Infinite Dilution at 25° C (Adapted from Dean, 1985).

Cation	D_jx10^6 cm^2/ sec	u_jx10^5 cm^2/V/sec	Cation	D_jx10^6 cm^2/sec	u_jx10^5 cm^2/V/sec
Ag^+	16.47	64.1	K^+	19.58	76.2
AL^{3+}	5.41	63.2	La^{3+}	6.18	72.1
Ba^{2+}	8.50	66.2	Li^+	10.30	40.1
Be^{2+}	5.99	46.6	Mg^{2+}	7.07	55.0
Ca^{2+}	7.93	61.7	Mn^{2+}	7.12	55.4
Cd^{2+}	7.19	56.0	NH_4^+	19.58	76.2
Ce^{3+}	6.21	72.5	$N_2H_5^+$	15.70	61.1
Co^{3+}	4.70	54.9	Na^+	13.33	51.9
$Co(NH_3)_6^{3+}$	8.87	103.6	Nd^{3+}	6.18	72.1
$Co(en)_3^{3+}$	6.63	77.4	Ni^{2+}	6.65	51.8
Cr^{3+}	5.94	69.4	Pb^{2+}	9.46	73.6
Cs^+	20.84	80.1	Pr^{3+}	6.1	72.1
Cu^{2+}	7.32	57.0	Ra^{2+}	8.89	69.2
D^+ (18°C)	55.57	221.5	$Rb+$	20.71	80.6
Dy^{3+}	5.83	68.1	Sc^{3+}	5.74	67.0
Er^{3+}	5.86	68.4	Sm^{3+}	6.08	71.0
Eu^{3+}	6.03	70.4	Sr^{2+}	7.91	61.6
Fe^{2+}	7.19	56.0	Tl^+	20.25	78.8
Fe^{3+}	6.04	70.5	Tm^{3+}	5.82	67.9
Gd^{3+}	5.98	69.8	UO_2^{2+}	4.27	33.2
$H+$	93.13	362.5	Y^{3+}	5.50	64.2
Hg^{2+}	7.05	54.9	Yb^{3+}	5.79	67.6
Ho^{3+}	5.88	68.7	Zn^{2+}	7.03	54.7

Table 3.4: Absolute Values of Diffusion Coefficients and Ionic Mobilities for Representative Anions at Infinite Dilution at 25° C (Adaptel from Dean, 1985).

Anion	Dix106 cm^2/sec	$u_i x10^5$ $cm^2/V/sec$
$Au(CN)_2^-$	13.31	51.8
$Au(CN)_4^-$	9.58	37.3
$B(C_6H_5)_4^-$	5.60	21.8
Br^-	20.78	80.9
Br_3^-	11.46	44.6
BrO_3^-	14.85	57.8
Cl^-	20.32	79.1
ClO_2^-	13.85	53.9
ClO_3^-	17.19	66.9.
ClO_4^-	18.09	70.4
CN^-	20.76	80.8
CO_3^{2-}	9.58	74.6
$Co(CN)_6^{3-}$	8.78	102.5
CrO_4^{2-}	11.32	88.1
F^-	14.49	56.4
$Fe(CN)_6^{4-}$	7.39	115.0
$Fe(CN)_2^{3-}$	8.97	104.7
$H_2AsO_4^-$	9.04	35.2
HCO_3^-	11.84	46.1
HF_2^-	19.96	77.7
HPO_4^{2-}	7.59	59.1
$H_2PO_4^-$	8.79	34.2
$H_2PO_2^-$	12.25	47.7

Anion	$D_i x10^6$ cm^2/sec	$u_i x10^5$ $cm^2/V/sec$
HS^-	17.32	67.4
HSO_3^-	13.31	51.8
HSO_4^-	13.31	51.8
$H_2SbO_4^-$	8.25	32.1
I^-	20.45	49.6
IO_3^-	10.79	42.0
IO_4^-	14.52	56.5
$N(CN)_2^-$	14.52	56.5
NO_2^-	19.11	74.4
NO_3^-	19.01	74.0
$NH_2SO_3^-$	12.95	50.4
N_3^-	18.37	71.5
OCN^-	17.19	66.9
OH^-	52.87	205.8
PF_6^-	15.16	59.0
PO_3F^{2-}	8.43	65.6
PO_4^{3-}	6.12	71.5
$P_2O_7^{4-}$	5.42	84.3
$P_3O_9^{3-}$	7.42	86.6
$P_3O_{10}^{5-}$	5.81	113.0
ReO_4^-	14.57	56.7
SCN^-	17.57	68.4
$SeCN^-$	17.21	67.0

Table 3.5: Limiting Free-Solution Diffusion Coefficients for Representative Simple Electrolytes at 25° C (Schackelford and Daniel, 1991).

Electrolyte	$D_o x10^6$ cm^2/sec
HCl	33.36
HBr	34.0
$LiCl$	13.66
$LiBr$	13.77
$NaCl$	16.10
$NaBr$	16.25
NaI	16.14
KCl	19.93
KBr	20.16
KI	19.99
$CsCl$	20.44
$CaCl_2$	13.35
$BaCl_2$	13.85

Shackelford and Daniel (1991b) investigated the effective diffusion coefficients, D^*, of different inorganic chemicals in compacted clay. Their results demonstrate that molding water content and compaction methods have little effect, if any, on the effective diffusion coefficients. Generally, changing molding water content in compaction tests results in significant changes in the compacted soil microstructure (Mitchell 1993): According to the results by Shackelford and Daniel (1991b) the change in compacted clay microstructure due to different molding water contents will have little effect on the effective diffusion coefficient of different chemicals.

3.3.2.2 Mass Flux by Ion Migration

The migrational mass flux of the free ionic species in the soil pore fluid due to the applied electric field is given by,

$$J_i^* = u_i^* c_i \nabla(-E) \tag{3.13}$$

where $J_i^*(ML^{-2}T^{-1})$ is the migrational mass flux of the ith species, and $u_i^*(L^2T^{-1}V^{-1})$ is the effective ionic mobility of the ith species. The effective ionic mobility, u_i^*, defines the velocity of the ion in soil pores under unit electric field. There is no method yet devised to directly measure the single ionic mobilities (Koryta 1982); however, u_i^*, can be estimated theoretically by assuming that the Nernst-Townsend-Einstein relation between D_i^*, the molecular diffusion coefficient, and u_i holds for ions in the pore fluid of soils (Holmes, 1962);

$$u_i^* = n\tau u_i = \frac{D_i^* z_i F}{RT} \tag{3.14}$$

where u_i is the ionic mobility of species I at infinite dilution, z_i is the charge of the ith species, F is Faraday's constant (96,485 C/mol electrons), R is the universal gas constant (8.3144 J/Kmol), and T is the absolute temperature. Note that each of u_i in this case has a value and a sign that reflects the charge of species i (i.e. the ionic mobilities and effective ionic mobilities, u_i and u_i^*, will have negative values for anions and positive values for cations). The signs are included in the ionic mobilities, of cations and anions to simplify the mathematical equations. Tables 3.3 and present absolute values of ionic mobilities for representative ions at infinite dilution.

3.3.2.3 Advective Mass FIux

The other important mechanism of species flux is advection by the soil pore fluid. The advective mass flux of species i relative to the soil particles is,

$$J_i^{w} = c_i J_w \tag{3.15}$$

where c_i, is the molar concentration of water (- 1).

3.3.2.4 Total Mass Flux

Adding Equations 3.10, 3.13, and 3.15, the total flux is given by;

$$J_i = D_i^{*} \nabla(-c_i) + c_i (u_j^{*} + k_,) \nabla(-E) + c_i k_h \nabla(-h) \tag{3.16}$$

For one-dinensional applications, the total mass flux of species i is given by,

$$J_i = -D_i \frac{\partial c_i}{\partial x} - c_i (u_i^{*} + k_,) \frac{\partial E}{\partial x} - c_i k_h \frac{\partial h}{\partial x} \tag{3.17}$$

This equation demonstrates that the electrical gradient has two transport components, ion migration and electroosmotic advection. It also explains that for cations both components will act in the same direction since the values of u_i^{*} and k_e have the same algebraic sign; however, for anions these components will act in opposite directions since u_i^{*}, is negative for anions while k_e, is positive.

Figure 3.4 conceptualizes the transport mechanisms of positively charged and negatively charged species, from a soil mass with c_0 initial concentration, due to the different potential gradients given in Equation 3.16.

3.3.3 Charge Flux

Applying a DC potential across a soil-water-electrolyte medium generates an electric field causing charge transport. Figure 3.5 shows a schematic diagram of the mechanisms by which charge is transported through a soil-water-electrolyte medium. Seven paths are identified in Figure

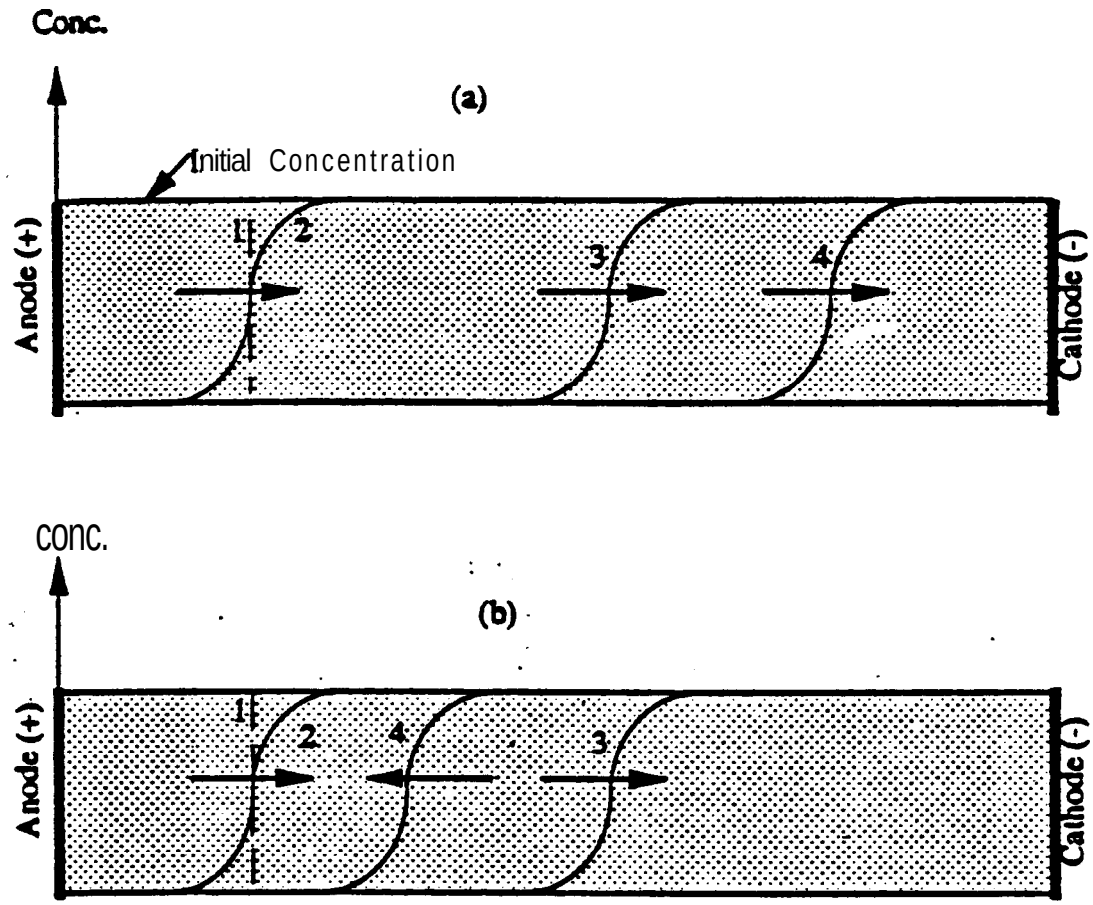

(1) Hydraulic Advection (2) Diffusion

(3) Eletroosmosis (4) Ion Migration

Figure 3.4: A Schematic Diagram of Concentration Profiles in Transport of (a) Positively Charged and (b) Negatively Charged Species

3.5 for charged transport through saturated clay; these are (a) through soil solids, (b) soil solids/diffuse double layer, (c) diffuse double layer, (d) diffuse double layer/free pore fluid, (e) pore fluid, (f) pore fluid/soil solids, and (g) soil solids/pore fluid/diffuse double layer. These charge transport mechanisms are based on the assumption that the soil pores are interconnected and, at the same time, the soil solids are interconnected, with at least several continuous paths that connect the medium pores from one side to the other and several continuous paths that connect the soil solids from one side to the other. This assumption is made to make it possible for the electric charge to move from one side of the medium to the other, either through the pore fluid and/or through the soil solids. Furthermore, charge transport through the soil pore fluid is divided into two components, one due to the migration of the counter ions and co-ions of the diffuse double layer and the second is due the migration of the free ions present in the free pore fluid.

The contribution of each path on charge transport vary widely for different types of soil-water-electrolyte media. With the assumption that soil solids are non conductors, a simplified model that accounts for only charge transport through the diffuse double layer and pore fluid (paths ℓ and ℓ respectively) is shown in Figure 3.5 (ii). Figure 3.5 (iii) represents these components by an electric circuit. Only when the soil pore fluid has a relatively high ionic strength, the contribution of the free pore fluid dominates the other charge transport mechanisms. To simplify the calculations below, the contributions of the soil solids and the diffuse double layer ions on charge transport are neglected.

3.3.3.1 Migrational Charge Flux

The simplest form of electrical conductance of the soil is governed by Ohm's law describeng the current density (charge transport) in the pore fluid due to electrical gradients,

$$I = \sigma^{*} \nabla(-E) \tag{3.18}$$

The migrational charge flux can be related to the migrational mass flux of species by using Faraday's law for equivalence of mass flux and charge flux,

$$I^{*} = \sum_{j=1}^{N} z_j F J_j^{*} \tag{3.19}$$

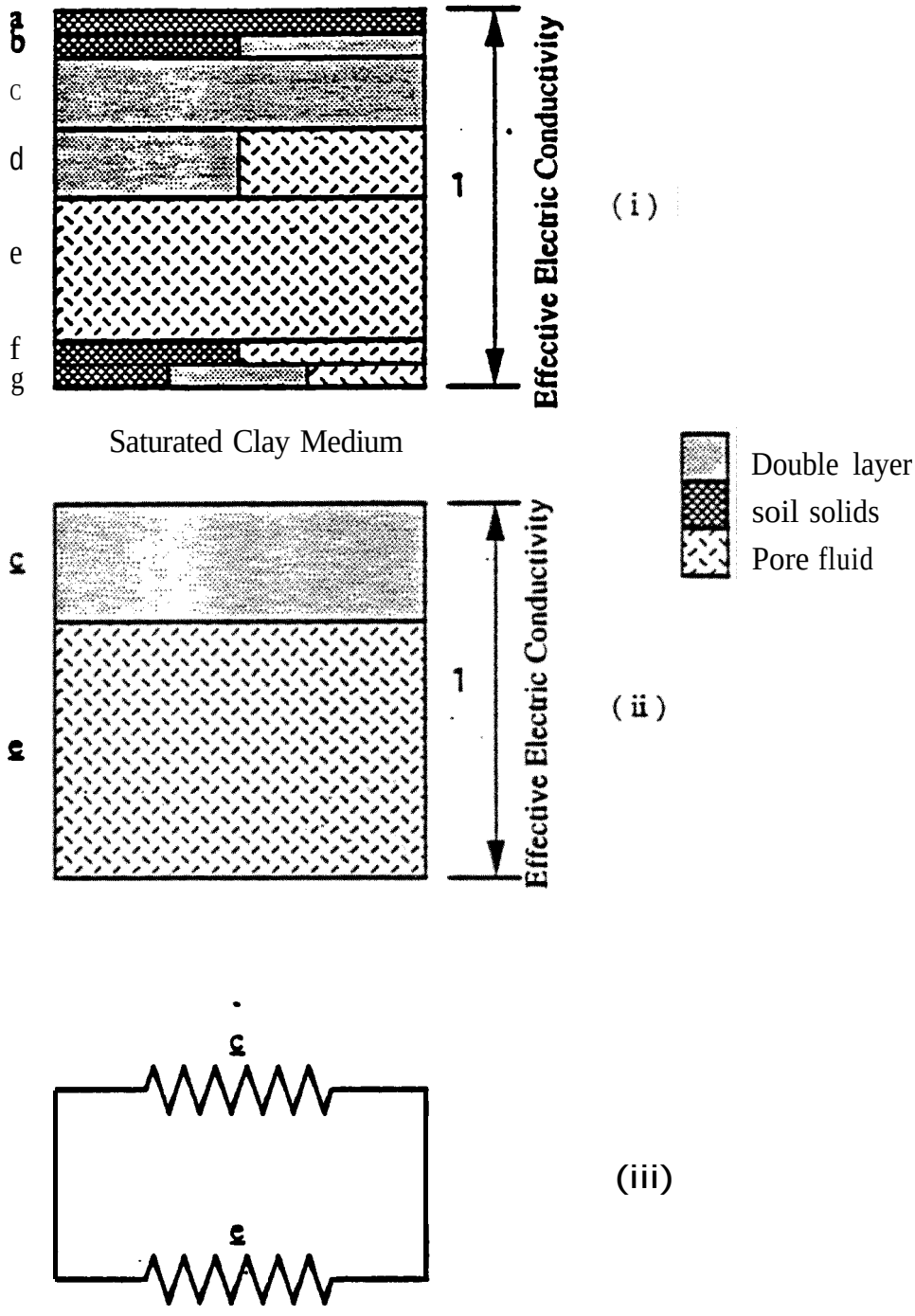

Figure 3.5: A Schematic Diagram of Possible Paths of an Electric Charge through a Soil-Water Electrolyte Medium (i) All Possible Paths, (ii) Simplified Case Accounting only for the DDL and Pore Fluid, and (iii) Electric Circuit for Case (ii)

Substituting Equation 3.13 into Equation 3.19, the migrational charge flux is given by,

$$I^{\bullet} = \sum_{j=1}^{N} z_j F u_j^{\bullet} c_j \nabla(-E) \qquad (3.20)$$

Comparing **Equation** 3.20 with Equation 3.18, and assuming that the migrational charge flux is equal to the total charge flux, the effective electrical conductivity of the soil bulk due to migrational charge flux is evaluated by,

$$\sigma^{\bullet} = \sum_{j=1}^{N} z_j F u_j^{\bullet} c_j \qquad (3.21)$$

3.3.3.2 **Transport Number**

Analogous to the total current density, the partial current density that represents the contribution of the ith charged species to the overall current density, I_i, is evaluated by applying Faraday's law of the equivalence of mass and charge,

$$I_i = F z_i J_i = F z_i u_i^{\bullet} c_i \nabla(-E) \qquad (3.22)$$

Constant current has been used in most experimental work at Louisiana State University on electrokinetic soil processing. Therefore, from Equation 3.18, the electric gradients will change depending upon the bulk electrical conductance of the soil,

$$\nabla(-E) = \frac{I}{\sigma^{\bullet}} \qquad (3.23)$$

Substituting Equation 3.23 in Equation 3.22

$$I_i = \frac{F z_i u_i^{\bullet} c_i}{\sigma^{\bullet}} I = t_i I \qquad (3.24)$$

where t_i is the transport (or transference) number of the ion i, giving the contribution of the ith ion to the total effective electric conductivity,

$$I_i = \frac{F z_i u_i^{\bullet} c_i}{\sigma^{\bullet}} I = t_i I \qquad (3.25)$$

The transport number of the ith ion thus depends on its ionic mobility, its concentration, and the total electrolyte concentration (or the electrolyte ionic strength). Table 3.6 lists examples of

Table 3.6: Transport Numbers of Cations at Various Concentrations (Koryta and Dvorak, 1987).

Electrolyte	C_o					
	0	0.01	0.02	0.05	0.1	0.2
HCl	0.8209	0.8251	0.8266	0.8292	0.8314	0.8337
CH_3COONa	0.5507	0.5537	0.5550	0.5573	0.5594	0.5610
CH_3COOK	0.6427	0.6498	0.6523	0.6569	0.6609	-
KNO_3	0.5072	0.5084	0.5087	0.5093	0.5103	0.5120
NH_4Cl	0.4909	0.4907	0.4906	0.4905	0.4907	0.4911
KCl	0.4906	0.4902	0.4901	0.4899	0.4898	0.4894
KI	0.4892	0.4884	0.4883	0.4882	0.4883	0.4887
KBr	0.4849	0.4883	0.4832	0.4831	0.4833	0.4841
$AgNO_3$	0.4643	0.4648	0.4652	0.4664	0.4682	-
$NaCl$	0.3963	0.3918	0.3902	0.3876	0.3854	0.3821
$LiCl$	0.3364	0.3289	0.3261	0.3211	0.3168	0.3112
$CaCl_2$	0.4380	0.4264	0.4220	0.4140	0.4060	0.3953
$\frac{1}{2}Na_2SO_4$	0.386	0.3848	0.3836	0.3829	0.3823	0.3828
$\frac{1}{2}K_2SO_4$	0.479	0.4829	0.4848	0.4870	0.4890	0.4910
$\frac{1}{3}LaCl_3$	0.477	0.4625	0.4576	0.4482	0.4375	0.4233

transport numbers for cations in a single electrolyte solution It should be noted that the summation of transport numbers of all ions in the soil pore fluid is equal to one,

$$\sum t_i = 1 \qquad \textbf{(3-26)}$$

The transport number of a specific species will increase as the ionic concentration of that species increases. This implies that when a concentration of a species decreases relative to the total electrolyte concentration in the pore fluid, its transport number and removal under electric currents will be less efficient. Therefore, it is reasonable to assume that the efficiency of removal of a specific species will decrease in time as its concentration in the pore fluid decreases.

3.3.3.3 Diffusional Charge Flux

Similar to the migrational charge flux, the diffusional charge flux due to the diffusional mass flux of charged: species is evaluated using Faraday's law of the equivalence of mass flux and charge flux,

$$I^d = \sum_{j=1}^{N} z_j F J_j^d \qquad \textbf{(3.27)}$$

Substituting Equation 3.10 in Equation 3.27, .

$$I^d = \sum_{j}^{N} z_j F D_j^* \nabla(-c_j) \qquad (3.28)$$

3.3.3.4 Advective Charge Flux

Applying Faraday's Law to advective mass flux will result in the advective charge flux,

$$I^w = \sum z_j F \frac{c_j}{c} J^w \qquad (3.29)$$

Employing the preservation of electrical neutrality,

$$\sum_{j=1}^{N} c_j z_j = 0 \qquad \textbf{(3.30)}$$

Accordingly there is no contribution of the advective fluid transport in charge transport (I^w =0).

3.3.3.5 TotaI Charge Flux

The resulting total, migrational and diffusional, charge flux is,

$$I = F \sum_{j=1}^{N} z_j D_j^* \nabla(-c_j) + \sigma^* \nabla(-E) \tag{3.31}$$

For one-dimensional applications, the total charge flux is given by,

$$I = -F \sum_{j=1}^{N} z_j D_j^* \frac{\partial c_j}{\partial x} - \sigma^* \frac{\partial E}{\partial x} \tag{3.32}$$

3.4 Conservation of Mass and Charge

There are two approaches in describing the position variable in a system; the Lagrangian approach and the Eulerian approach. In the Lagrangian approach the coordinates of a moving particle are represented as a function of time (this approach describes the history of individual particles, material coordinates). On the other hand, the Eulerian approach describes the flux changes by referring to specific points that are fixed in space (spatial coordinates). The Eulerian approach, used in this formulation, requires a definite fixed volume in space that has an arbitrary shape, termed as the control volume (Bear 1972). The boundaries of the control volume always form a closed surface in space. Though the flux of matter in a control volume may change with time, the shape and position of the control volume must remain fixed.

Consider a finite control volume of dimensions $\Delta x, \Delta y, \Delta z$, around a point $O(x,y,z)$ in the porous medium. The change in amount of matter or energy transported through a control volume could be described by,

$$-\nabla . J + R \tag{3.33}$$

where R is a source/sink term. Principles of conservation of matter or energy require that the Term 3.33 equals the amount which matter or energy are stored in the control volume during ^t

time. Consequently, time dependent equations for consevation of mass, charge, and energy are used to develop the partial differential equations for transient changes in hydraulic head, electric potential, and concentration of the chemical species presented in the pore fluid.

3.4.1 **Soil Consolidation**

Applying the Conservation equation to fluid flux in a saturated soil medium (Terzaghi's consolidation theory),

$$\frac{\partial \varepsilon_v}{\partial t} = -\nabla . J_w \tag{3.34}$$

where ε_v is the volumetric strain of the soil mass. In consolidation of fine-grained soils the volumetric strain is equivalent to the change in void ratio per unit volume,

$$\frac{\partial \varepsilon_v}{at} = \frac{1}{1+e}\frac{\partial e}{\partial t} \tag{3.35}$$

where e is the void ratio. The change in void ratio, ∂ e, due to the increase in effective stress is,

$$\partial e = -a_v \partial \sigma' = a_v \partial u \tag{3.36}$$

where a, is the coefficient of compressibility, u is the pore water pressure, and σ' is the effective stress. Substituting Equation 3.36 in Equation 3.35,

$$\frac{\partial \varepsilon_v}{\partial t} = \frac{a_v}{1+e}\frac{\partial u}{\partial t} = m_v \frac{\partial u}{\partial t} \tag{3.37}$$

where, m_v is the coefficient of volume compressibility. Substituting $(u = h\gamma_w)$, the consolidation Equation is given by

$$(m_v \gamma_w)\frac{\partial h}{\partial t} = -\nabla . J_w \tag{3.38}$$

3.4.2 Conservation of Mass

The partial differential equation describing transient mass transport of species i is developed by applying the law of mass conservation of species i,

$$\frac{\partial nc_i}{\partial t} = -\nabla . J_i + nR_i \qquad (3.39)$$

where, R_i $(ML^{-3}T^{-1})$ is the production rate of the ith aqueous chemical species per unit fluid volume due to chemical reactions such as sorption, precipitation-dissolution, oxidation/reduction, and aqueous phase reactions.

3.4.3 Conservation of Charge

Applying conservation of charge to the charge flux equation,

$$\frac{\partial T_e}{\partial e} = -\mathrm{v} . \mathbf{I} \qquad (3.40)$$

where T_e is the volumetric charge density of the soil medium (CL^{-3}). The electric potential is related to the volumetric charge density by,

$$\frac{\partial T_e}{\partial t} = C_p \frac{\partial E}{\partial t} \qquad (3.41)$$

where C_p has the units of the electrical capacitance per unit volume (farad L^{-3}) and measures the ability of soils to hold electric charge. Substituting into Equation 3.40,

$$C_p \frac{\partial E}{\partial t} = -\nabla . \mathbf{I} \qquad (3.42)$$

3.4.4 Chemical Reactions

Equation 3.39 may be simplified by expanding the production term, R_i, to account for sorption reactions (surface complexation and ion exchange), aqueous phase reactions and precipitation/dissolution reactions,

$$R_i = R_i^s + R_i^{aq} + R_i^p \qquad (3.43)$$

where R_i^s is a term for sorption, similarly R_i^{aq} is a term for aqueous phase reactions and R_i^p, for

precipitation/dissolution reactions. Two approaches have been developed and used in the literature to describe chemical reactions; instantaneous equilibrium approach and kinetics approach. In instantaneous equilibrium reactions, be it sorption, precipitation/dissolution, or aqueous phase reactions, species concentrations are assumed to reach equilibrium instantaneously whereby in kinetic reactions approach concentrations in solution are assumed to be time dependent and change before they roach chemical aquilibrium.

For several species, chemical reactions, specially precipitation/dissolution and sorption reactions, have been found to vary with time before reaching equilibrium. It may be more appropriate to use kinetics approach to model these reactions; however, this will unduly complicate the modeling effort and it will require an independent investigation of each kinetics. Furthermore, chemical reactions involved in this study are expected to reach equilibrium at a very short time. Sorption reactions in low activity soils and precipitation/dissolution reactions of heavy metals in solutions often take minutes to reach chemical equilibrium. On the other hand, transport processes of these chemical species in fine-grained deposits under electric, hydraulic and chemical gradients are slow compared to the rate of sorption or precipitation reactions. Consequently, the ratio of the rate of chemical reactions to the rate of transport of heavy metals in low activity fine-grained deposits is expected to be high enough to satisfy the assumption of instantaneous equilibrium for these chemical reactions.

3.4.4.1 Sorption Reactions

The following general term has been widely considered for evaluation of sorption of species on thi soil particles,

$$R_i^s = -\frac{P}{n}\frac{\partial s_i}{\partial t} = -\frac{\rho}{n}\frac{\partial s_i}{\partial c_i}\frac{\partial c_i}{\partial t} \qquad i = I,2\ ,.....,\ N \qquad (3.44$$

where ρ is the bulk dry density of the soil, s_i is the adsorbed concentration of the component i per unit mass of the soil solids (mole/M) The reversible term $(\partial s_i / \partial t)$ is often used to describe the sorption rate. The equilibrium partitioning between the adsorbed phase and the aqueous phase of the chemical components are commonly measured under controlled temperature and applied pressure, and the resulting correlations of s_i versus c_i are callled adsorption isotherms. Several equilibrium models (linear, Freundlich, and Langmuir models) have been used to describe sorption

of heavy metals on soils. Assuming instantaneous equilibrium in sorption reactions and linear isotherms, the change in concentration of the sorped phase of species i is linearly related to the change in concentration of the aqueous phase,

$$\frac{\partial s_i}{\partial c_i} = K_{di} \qquad (3.45)$$

where K_{di} is called the distribution coefficient K_d, of species i. A retardation factor, R_{di}, have been introduced and used in modeling species transport accounting for linear sorption as,

$$Rd_i = 1 + \frac{\rho K_{di}}{n} \qquad (3.46)$$

The retardation factors of species i, Rd_i, define the relative rate of transport of a nonsorped species to that of a sorped species. For a nonsorped species , Rd = 1.

Recently other methods have been used to account for R_i' in contaminant transport equations because the previous method ignores the effect of pH, ionic strength, redox reactions, competitive adsorption, and the mechanism of adsorption. These methods include isotherm equations, mass action models, and surface complexation models proposed by Langmuir (1987), Kirkner and Reeves (1988); Yeh and Tripathi (19891, Mangold and Tsang (1991), and selim (1992), among others.

3.4.4.2 Aqueous Phase Reactions

In the following formulation, it is assumed that the N number of chemically reactive aqueous species is divided into N_c number of components and N_x, number of complexes. In aqueous phase reactions, any complex j is the product of i's reactants components, i.e.:

$$\sum_{i=1}^{N_c} a_{ji}\, \overline{c_i} \cdots \overline{x_j} \qquad j = I, \ldots\ldots, N_x \qquad (3.47)$$

where $\overline{c_i}$ is the chemical formula for component i, $\overline{x_j}$, is the chemical formula for the complex j, a_{ji} is the stoichiometric coefficient in complex j for component i. The law of mass action implies that:

$$x_j = K_j^{aq} \prod_{i=1}^{N_c} c_i^{a_{ij}} \qquad j = 1,\ldots,N_x \qquad (3.48)$$

where K_j^{aq} is the equilibrium constant for aqueous reaction j. From Equation 3.47, the rate accumulation of component I due to aqueous reaction R_{ji}^{aq}, is:

$$R_{ji}^{a} = -a_{ji} R_j \qquad (3.49)$$

where R_j, is the rate of accumulation of complex j due to the chemical reaction j. The total rate of accumulation of component i due to all aqueous reactions, R_i^{aq}, is:

$$R_i^{aq} = \sum_{j=1}^{N_x} R_{ji}^{aq} = -\sum_{j=1}^{N_x} a_{ji} R_j \qquad (3.50)$$

Consequently, evaluation of R_i^{aq} requires evaluation of N_x number of R_j $(j = 1, \ldots . N_x)$ and therefore, N_x number of equations is required. These equations are obtained from Equation 3.50 for j = $1,\ldots,N_x$. Note that Equation 3.48 requires known values of the equilibrium constant K_j^{aq} for $j = 1, \ldots . N_x$.

3.4.4.3 **Precipitation/Dissolution Reactions**

Bench-scale studies conducted at Louisiana State University involving removal of Pb^{2+}, Cr^{3+} Cd^{2+} and uranium by electrokinetics have shown that these metal ions precipitate close to the cathode at pH values corresponding to their hydroxide solubility. It is necessary to account for the precipitation/dissolution reactions in the formulation of mass transport equations. In precipitation reactions, the chemical components are assumed to be composed of products,

$$\overline{p_j} \cdot\cdot \sum_{i=1}^{N_c} b_{ji} \overline{c_i} \qquad j = 1, \ldots, N_p \qquad (3.51)$$

where $\overline{p_j}$ is the chemical formula for precipitate j, b_{ji} is the stoichiometric coefficient in precipitate j for component i, and N_p is the number of precipitates for component i. The production of the

precipitate will **not occur until the** solution is saturated. **Therefore, the** law of mass action is written as,

$$K_j^{sp} \geq \prod_{i=1}^{N_c} c_i^{b_{ij}} \qquad j = 1, \ldots\ldots N_p \qquad (3.52)$$

Where K_j^{sp} is the solubility product equilibrium constant for precipitate j. By the same rationalization of previous formulations, the total rate of production **of** component i due to precipitation/dissolution reactions R_i^p, is,

$$R_i^p = \sum_{j=1}^{N_p} R_{ij}^p = -\sum_{j=1}^{N_p} b_{ji} R_j^p \qquad (3.53)$$

where R_{ij}^p is the rate of accumulation of component i due to precipitation reaction j and R_j^p is the rate of production of precipitate j.

Similar to the case of the aqueous phase reactions, evaluation of $\mathbf{R^P}$ requires evaluation of $\mathbf{N_p}$ number of R_j^p. $\mathbf{N_p}$ equations for this case are obtained from Equation *3.52* for j = 1,..,$\mathbf{N_p}$. Solubility product equilibrium constants K_j^p are available for any **jth** precipitation/dissolution **reaction.**

3.5 General System for Modeling Species Transport

The theoretical formalism presented in this Section results in a mathematical system of equations describing the transient reactive coupled muiticomponent species transport under hydraulic, electric, and chemical gradients. The resulting system consists of differential equations for transport processes and algebraic equations for chemical reactions. The objectives of this study involve one-dimensional application of electrokinetic soil processing **therefore, the** formulations are summarized in this section only for the one-dimensional transport of matter and energy.

The differential equations describing transport of N number of chemical species are obtained by substituting the total mass flux, Equation 3.17, in Equation 3.39, which describes conservation of mass. The resulting one-dimensional equation is,

$$\frac{\partial nc_i}{\partial t} = D_i^* \frac{\partial^2 c_i}{\partial x^2} + c_i \left[(u_i^* + k_e) \frac{\partial^2 E}{\partial x^2} + k_h \frac{\partial^2 h}{\partial x^2} \right]$$

$$+ \frac{\partial c_i}{\partial x} \left[(u_i^* + k_e) \frac{\partial E}{\partial x} + k_h \frac{\partial h}{\partial x} \right] + nR_i \qquad (3.54)$$

for I = 1,2 „„, N .

Note that for the case of nonreactive solute transport ($R_i = 0$), steady state fluid flux ($\partial h/\partial x$ = *const.*) and no electrical gradient, Equation 3.54 becomes,

$$\frac{\partial nc_i}{at} = D_i \frac{\partial^2 c_i}{\partial x^2} + \frac{\partial c_i}{\partial x} k_h \frac{\partial h}{\partial x} \qquad (3.55)$$

Usually, the advective fluid flux under hydraulic gradients is referred to by the **advective velocity, v,** i. e.,:

$$v = -k_h \frac{\partial h}{\partial x} \qquad (3.56)$$

Substituting the advective velocity in Equation 3.55,

$$\frac{\partial nc_i}{\partial t} = D_i^* \frac{\partial^2 c_i}{\partial x^2} - v \frac{\partial c_i}{\partial x} \qquad (3.57)$$

which is the diffusive advective solute transport equation widely used to describe nonreactive solute transport

Changes in the electric potential distribution across the soil as a result of changes in the chemistry of the soil pore fluid is formulated by substituting the charge flux equation in the charge conservation equation (Equation 3.32 in Equation 3.42),

$$C_p \frac{\partial E}{\partial t} = F \sum_{j=1}^{N} z_j D_j^* \frac{\partial^2 c_j}{\partial x^2} + \sigma^* \frac{\partial^2 E}{\partial x^2} + \frac{\partial^2 \sigma^*}{\partial x} \qquad (3.58)$$

where, the soil effective electric conductivity, σ^*, and its gadicnt are evaluated by,

$$\sigma^* = F\sum_{j=1}^{N} z_j c_j u_j^* \tag{3.59}$$

$$\frac{\partial \sigma^*}{\partial x} = F\sum_{j=1}^{N} z_j u_j^* \frac{\partial c_j}{\partial x} \tag{3.60}$$

Assuming zero electrical capacitance ($C_p = 0$),

$$0 = F\sum_{i=1}^{N} z_i D_i \frac{\partial^2 c_i}{\partial x^2} + \sigma^* \frac{\partial^2 E}{\partial x^2} + \frac{\partial \sigma^*}{\partial x}\frac{\partial E}{\partial x} \tag{3.61}$$

Note the fact that Equation 3.61 gives the relation between electrical and concentration gradients.

As to fluid transport, substituting the fluid flux equation (Equation 3.9) in Equation 3.38 and considering only one-dimensional conditions,

$$\frac{\partial h}{\partial t} = c_v \frac{\partial^2 h}{\partial x^2} + \frac{k_*}{m_v \gamma_*}\frac{\partial^2 E}{\partial x^2} \tag{3.62}$$

The total number of differential equations which describe by this system are n + 2 which are n equations for species transport, one equation for charge conservation, and one equation for soil consolidation. The unknowns described in this system are n species concentrations c_i, one electric potential E, one hydraulic potential h, and n unknowns for the rate of i chemical reactions. Therefore 2n + 2 unknowns are described by n + 2 differential equations. The other n number of equations required for this system are the mass balance equations for the chemical reactions.

3.5.1 Initial and Boundary Conditions

Differential equations describing any physical system require initial and boundary conditions to develop the required solution. Initial value differential equations require initial conditions while boundary value problems require boundary conditions. First order boundary value problems demand one boundary condition, second order boundary value problems demand two boundary conditions, and so on.

The resulting partial differential equations describing the coupled transport of matter and energy are initial-boundary value equations. Initial condition and two boundary conditions are necessary for every transient transport differential equation present. Initial conditions for every dependent variable (or potential) are evaluated according to the initial state of potential and/or potential gradient distribution different types of boundary conditions can be specified for solution of the transport differential equations; these are Dirichlet boundary conditions, homogeneous boundary **conditions, mixed** boundary conditions, and Neumann boundary conditions (Zwillinger 1989). The type of boundary conditions used differ from one case to another.

3.5.2 Preservation of Electrical Neutrality

. According to Faraday's law for the equivalence of mass and charge, the rate of change in the electric charge for a unit volume of the soil medium equals to the total rate of change of chemical species concentrations, times their charge, times Faraday's constant,

$$\sum_{j=1}^{N} z_j F \frac{\partial n c_j}{\partial t} \tag{3.63}$$

Preservation of eIectrical neutrality requires that the rate of change of the electric charge per unit volume must equal zero. Substituting Equation 3.39 in Equation 3.63,

$$\sum_{j=1}^{N} z_j F \frac{\partial n c_j}{\partial t} = - \sum_{j=1}^{N} z_j F \nabla . \mathbf{J}_j + n \sum_{j=1}^{N} z_j F R_j \tag{3.64}$$

The total rate of chang of all chemical species under chemical reactions times their charge is zero,

$$\sum_{j=1}^{N} z_j R_j = 0 \tag{3.65}$$

In other words, for any chemical reaction,

$$A \cdot\cdot mB^{+I} + ID^{-m} \tag{3.66}$$

one mole of A will produce m moles of B^{+I} and I moles of D^{-m}. The total change in B^{+I} concentration times its charge is (m moles of B^{+I} x (+1)) = ml. The total change in D^{-m} concentration times its charge is (I moles of D^{-m} x (-m)) = -ml. Therefore, the total change in electric charge is ml-ml=0.

For one dimensional applications, substituting Equation 3.17 for mass flux of species i and Equation 3.65 in Equation 3.64,

$$\sum_{j=1}^{N} z_j F \frac{\partial nc_j}{\partial t} = \sum_{j=1}^{N} z_j F D_j^* \frac{\partial^2 c_j}{\partial x^2} + \sum_{j=1}^{N} z_j F c_j \left[(u_j^* + k_e) \frac{\partial^2 E}{\partial x^2} + k_h \frac{\partial^2 h}{\partial x^2} \right] + \sum_{j=1}^{N} z_j F D_j^* \frac{\partial c_j}{\partial x} \left[(u_j^* + k_e) \frac{\partial E}{\partial x} + k_h \frac{\partial h}{\partial x} \right] \quad (3.67)$$

However, Equation 3.61, already describes the right hand side of Equation 3.71 to be equal to zero. Substituting $\sum z_j c_j = 0$,

$$\sum_{j=1}^{N} F z_j \frac{\partial nc_j}{\partial t} = \sum_{j=1}^{N} F z_j D_j^* \frac{\partial^2 c_j}{\partial x^2} + \sum_{j=1}^{N} F z_j c_j u_j^* \frac{\partial^2 E}{\partial x^2} + \sum_{j=1}^{N} F z_j u_j^* \frac{\partial c_j}{\partial x} \frac{\partial E}{\partial x} \quad (3.68).$$

Note that,

$$\sigma^* = F \sum_{j=1}^{N} z_j c_j u_j^* \quad (3.69)$$

$$\frac{\partial \sigma^*}{\partial x} = F \sum_{j=1}^{N} z_j u_j^* \frac{\partial c_j}{\partial x} \quad (3.70)$$

Equation 3.68 is therefore described by

$$\sum_{j=1}^{N} F z_j \frac{\partial nc_j}{\partial t} = \sum_{j=1}^{N} F z_j D_j^* \frac{\partial^2 c_j}{\partial x^2} + \sigma^* \frac{\partial^2 E}{\partial x^2} + \frac{\partial \sigma^*}{\partial x} \frac{\partial E}{\partial x} \quad (3.71)$$

However, Equation 3.61 already describes the right hand side of Equation 3.71 to be equal to zero. Therefore,

$$\sum_{j=1}^{N} F z_j \frac{\partial nc_j}{\partial t} = 0 \quad (3.72)$$

In other words, the change in chemical concentration of species present in the soil pore fluid due to different transport mechanisms will occur in a way to preserve the electrical neutrality.

Theoretically, preservation of electrical neutrality results from redistribution of the electrical potential across the sample. The electrical potential undergoes a change in its distribution to account for the electrical potential component that results from the concentration gradients of the charged chemical species. This implies that the electrical gradient is not described by Ohm's Iaw any more, but includes **a diffusional** component that is a result of concentration gradients within the soil pore fluid . Failure to account for diffusional charge flux in charge transport equation results in failure to preserve the electrical neutrality.

Modeling Acid/Base Distribution

The effect of soil acidity or alkalinity, represented by the soil pH, is significant in heavy metal-soil interactions and sorption. Changes in soil pH influence sorption reactions in various ways. Literature reviewed in soil science and colloid chemistry demonstrates that surface charge, and therefore cation exchange capacity, increases with increasing soil pH resulting in different sorption characteristics. (Pratt 1961; Lorenz 1969; Hunter 1981; Maguire et al. 1981; Stumm 1992). Different sorption characteristics might be attributed to changes in the soil cation exchange capacity. Furthermore, sorption by ion exchange is dependent on the availability of various cations competing to balance the surface charge on clay particles. At low pH values; H^{1+} ions, behaving like polyvalent ions, will replace adsorbed metals by ion exchange. The rates of ion exchange reactions are dependent on ion concentration, pH, and the selectivity coefficient of each ion.

As described elsewhere, application of direct electric current through a soil mass oxidizes the water at the anode, generating a local acidic medium, and reduces the water at the cathode, generating an alkaline medium. Accordingly, soil pH decreases at the anode and increases at the cathode. Furthermore, the acid front at the anode will advance towards the cathode with time by the different transport mechanisms discussed, The changes in the soil pH will greatly influence the soil-water-electrolyte interactions and consequently contaminant transport and removal. It is therefore essential to model the changes in soil pH in modeling contaminant transport and removal.

Utilizing the theoretical development described earlier for species transport and interactions, a system of partial differential equations and algebraic equations is developed for modeling soil pH. The differential equations are for transport of H+ ion, OH- ion, pore fluid, and charge. The algebraic equations account for the water electrolysis reaction. All equations are

nondimensionalized in distance by the following transform,

$$X = \frac{x}{L} \quad \frac{ax}{\partial x} = \frac{1}{L} \tag{3.73}$$

where L is the spacing between the anode and cathode. The anode is at X = 0 and the cathode is at X =1.

3.6.1 H+ Transport

Ion migration, advection, and diffusion are the processes considered in modeling transport in this study. The differental equation describing one-dimensional transport of the hydrogen ion is therefore described by,

$$Rd_H \frac{\partial nc_H}{\partial t} = \left(\frac{D_H^*}{L^2}\right)\frac{\partial^2 c_H}{\partial X^2} + c_H\left[\left(\frac{u_H^* + k_e}{L^2}\right)\frac{\partial^2 E}{\partial X^2} + \frac{k_H}{L^2}\frac{\partial^2 h}{\partial X^2}\right] + \frac{\partial c_H}{\partial X}\left[\left(\frac{u_H^* + k_e}{L^2}\right)\frac{\partial E}{\partial X} + \frac{k_h}{L^2}\frac{\partial h}{\partial X}\right] - R_H^{eq} \tag{3.74}$$

Boundary conditions for the hydrogen ion transport equation are developed from electrolysis reactions at the anode. The flux of H + at the anode has two components, the first is due to the advective flow and the second is due to the electric current.

$$J_H|_{X=0} = c_H^a J_w + \frac{I}{F} \tag{3.75}$$

where c_h^a is the concentration of H^+ at the anode compartment. The electroosmotic advective flux at the anode will carry H + ions generated at the anode into the soil. The first term on the right hand side of Equation 3.75 describes the advective mass flux of hydrogen ion which is equal to the advective fluid flux times the concentration of hydrogen ion at the anode. In the second term, it is assumed that all applied current at the anode will be efficient in generation of H^+ by the following water electrolysis reaction,

$$2H_2O - 4e^- \cdot O_2 + 4H^+ \tag{3.76}$$

Consequently, the boundary condition for H+ at the anode (X=O) is developed by applying Faraday's law for equivalence of mass and charge to the rate of production of H+,

$$\frac{D^*_{H^+}}{L^2}\frac{\partial c_{H^+}}{\partial X} + \frac{\bar{v}_{H^+}}{L} c_{H^+}\Big|_{X=0} = \frac{c^*_j J_w}{L} + \frac{I}{FL} \tag{3.77}$$

where,

$$\bar{v}_{H^+} = -\left(\frac{u^*_{H^+}}{L} + \frac{k_e}{L}\right)\frac{\partial E}{\partial X} - \frac{k_h}{L}\frac{\partial h}{\partial X} \tag{3.78}$$

The boundary condition for H^+ at the cathode ($X=1$), is

$$-\frac{D^*_{H^+}}{L^2}\frac{\partial c_{H^+}}{\partial X} + \frac{\bar{v}_{H^+}}{L} c_{H^+}\Big|_{X=L} = \frac{c_H J_w}{L} \tag{3.79}$$

3.6.2 OH-Transport

Similar to H^+, one dimensional transport of OH- is expressed by,

$$\frac{\partial nc_{OH}}{\partial t} = \left(\frac{D^*_{OH}}{L^2}\right)\frac{\partial^2 c_{OH}}{\partial X^2} + c_{OH}\left[\left(\frac{u^*_{OH}+k_e}{L^2}\right)\frac{\partial E}{\partial X} + \frac{k_h}{L^2}\frac{\partial^2 h}{\partial x^*}\right] + \frac{\partial c_{OH}}{\partial X}\left[\left(\frac{u^*_{OH}+k_e}{L^2}\right)\frac{\partial E}{\partial X} + \frac{k_h}{L^2}\frac{\partial h}{\partial X}\right] - R^{eq}_{OH} \tag{3.80}$$

Boundary conditions for the OH- ion transport are developed from electrolysis reactions at the cathode. The flux of OH- at the cathode ($X=1$) also has two components, due to advective flow and due to the electric current,

$$J_{OH}|_{X=1} = c_{OH} J_w - \frac{I}{F} \tag{3.81}$$

Note in this case that the advective component of mass flux of OH- at the cathode is an outflow (negative), i.e. transporting from the soil to the cathode compartment. The difference between this condition and the condition at the anode is that the fluid flux at the cathode is multiplied by the concentration of OH- in the soil mass while at the anode it is multiplied by the concentration of H^+ of the anode compartment. However, it is assumed that the boundary condition at the cathode will be equal to that in the soil mass. In the second part of Equation 3.81, it is assumed that all applied

current at the cathode will be efficient in generation of OH- by the-following water electrolysis reaction,

$$4H_2O + 4e^- \cdot 2H_2 + 4\,OH^- \tag{3.82}$$

Again applying Faraday's law to the rate of production of OH- at the cathode (X= 1) will result in,

$$-\frac{D^*_{OH}}{L^2}\frac{\partial c_{OH}}{\partial X} + \frac{\bar{v}_{OH}}{L} c_{OH}\Big|_{X=1} = \frac{c_{OH} J_w}{L} - \frac{I}{FL} \tag{3.83}$$

where,

$$\bar{v}_{OH} = -\left(\frac{u_{OH}}{L} + \frac{k_e}{L}\right)\frac{\partial E}{\partial X} - \frac{k_h}{L}\frac{\partial h}{\partial X} \tag{3.84}$$

and the following boundary condition is used for OH- at the anode (X=0),

$$-\frac{D^*_{OH}}{L^2}\frac{\partial c_{OH}}{\partial X} + \frac{\bar{v}_{OH}}{L} c_{OH}\Big|_{X=0} = \frac{c^*_{OH} J_w}{L}.$$

3.6.3 Pore Pressure

One dimensional eletroosmotic soil consolidation is described by

$$\frac{\partial h}{\partial t} = \frac{c_v}{L^2}\frac{\partial^2 h}{\partial X^2} + \frac{k_e}{m_v \gamma_w}\frac{1}{L^2}\frac{\partial^2 E}{\partial X^2} \tag{3.86}$$

Hydraulic head difference between the cathode and the anode is controlled and kept at zero in the experiment conducted in this study. Boundary conditions for this equation are, therefore, constant hydraulic head at both the cathode and the anode,

$$h|_{X=0} = h|_{X=1} = 0 \tag{3.87}$$

3.6.4 Charge Transport Equation

Assuming that the soil medium has zero electrical capacitance, the one dimensional electric

potential distribution in time is given by,

$$0 = F \sum_{j=1}^{N} \left(\frac{z_j D_j^*}{L^2} \right) \frac{\partial^2 c_j}{\partial X^2} + \left(\frac{\sigma^*}{L^2} \right) \frac{\partial^2 E}{\partial X^2} + \left(\frac{1}{L^2} \frac{\partial \sigma^*}{\partial X} \right) \frac{\partial E}{\partial X} \qquad \textbf{(3.88)}$$

once again, the soil effective electric conductivity, σ^*, and its gradient are evaluated **by,**

$$\sigma = F \sum_{j=1}^{N} z_j u_j^* \frac{\partial c_j}{\partial X} \qquad (3.89)$$

$$\frac{\partial d}{\partial X} = F \sum_{j=1}^{N} z_j u_j^* \frac{\partial c_i}{\partial X} \qquad (3.90)$$

Boundary conditions for charge conservation equation are developed from the current value at the boundary. The constant current applied throughout the experiment would result in the following boundary conditions,

$$\left[-F \sum_{j=1}^{N} z_j \frac{D_j^*}{L^2} \frac{\partial c_j}{\partial X} - \frac{\sigma^*}{L^2} \frac{\partial E}{\partial X} \right]_{X=0} = \frac{I}{L} \qquad (3.91)$$

$$E|_{X=1} = 0 \qquad (3.92)$$

3.6.5 Water Auto-ionization Reaction

In aqueous solution water autoionization is an important reaction for H^+ and OH- ions,

$$H_2O \rightarrow H^+ + OH^- \qquad \textbf{(3.93)}$$

Therefore it is essential to incorporate this autoionization to model the soil pH, This reaction will generate equal number of moles **of** H+ and OH-,

$$\Delta c_H = A c, \qquad \textbf{(3.94)}$$

or,

$$R_H^{aq} = R_{OH}^{aq} \qquad (3.95)$$

Also, law of mass action for water ionization requires

$$c_H c_{OH} = K_w = 10^{-14} \qquad \textbf{(3.96)}$$

Six unknowns are defined for modeling soil pH, these are h, E, C_H, C_{OH}, R_H^{aq}, and R_{OH}^{aq}. Equations required for the solution are **4 transport partial differential equations** (Equations 3.74, **3.80, 3.86,** and **3.88)** and two algebraic equations (Equations **3.95** and.3.96).

3.7 Modeling Lead Transport

Lead removal by electrokinetics is modeled in this study in an attempt to assess the principles of the technology and to check the validity of the theoretical model presented. Though various cations and anions might be present in the soil pore fluid at different concentrations, only four ions are included in this model. These arc Pb^{2+} because it is the species of concern, NO^-_3, since lead nitrate salt is used for the experiment, and H+ and OH- because they are necessary in describing the acid/base distribution that has a great influence on the pore fluid chemistry. Four one dimensional partial differential equations are formulated in describing the transport of these ions. Dramatic changes in the concentration of these ions will result in different chemical reactions. Chemical reactions included in this model are the reactions describing precipitation/dissolution of lead hydroxide ($Pb(OH)_2$), thc water auto ionization reaction, and **sorption** reactions.

Other dependent variables included in the model are the changes in distributions of the electrical potential and the hydraulic head. The change in electrical conductivity across **the soil as** a result **of** continuous change of ionic strength of the pore fluid will lead to changes in the electrical potential distribution. The charge transport equation is used to model the changes in the electrical potential. Changes in electrical gradient distribution will develop nonlinear pore water pressures, resulting in suction in this case, across the soil between the electrodes. Development of pore water pressure is modeled using the fluid transport equation, which is the electroosmotic consolidation equation based on Terzaghi's consolidation theory.

Following the theoretical development presented earlier, a system of differential/algebraic equations is developed to model transport and removal of lead from kaolinite by electrokinetics. Boundary conditions for these equations are developed based on the changes in hydro-electro-chemical characteristics of the anode and the cathode. The anode is taken to be at X = 0 and the cathode at X=l.

3.7.1 Pb^{+2} Transport

The following equation is used to describe pb^{2+} transport under hydraulic, electric, and concentration gradients,

$$\frac{\partial nc_{Pb}}{\partial t} = \left(\frac{D^{*}_{Pb}}{L^{2}}\right)\frac{\partial^{2} c_{Pb}}{\partial X^{2}} + c_{Pb}\left[\left(\frac{u^{*}_{Pb} + k_{e}}{L^{2}}\right)\frac{\partial^{2} E}{\partial X^{2}} + \frac{k_{h}}{L^{2}}\frac{\partial^{2} h}{\partial X^{2}}\right] + \frac{\partial c_{Pb}}{\partial X}\left[\left(\frac{u^{*}_{Pb} + k_{e}}{L^{2}}\right)\frac{\partial E}{\partial X} + \frac{k_{h}}{L^{2}}\frac{\partial h}{\partial X}\right] - R^{P}_{Pb} \tag{3.97}$$

Boundary conditions for the given partial differential equation are evaluated assuming that lead is not involved in electrolysis reactions at the cathode and the anode. Therefore, the mass fluxes of lead at the cathode and at the anode are equal its component in the advective mass flux,

$$-\frac{D^{*}_{Pb}}{L}\frac{\partial}{\partial X}c_{Pb} + \bar{v}_{Pb}\, c_{Pb}\Big|_{X=0} = c^{*}_{Pb}\, J_{w} \tag{3.98}$$

$$D^{*}_{Pb}\,\partial\, c_{Pb} + \bar{v}_{Pb}\, c_{Pb}\Big|_{X=} = c^{*}_{Pb}\, J_{w} \tag{3.99}$$

where,

$$\bar{v}_{Pb} = -\left(\frac{u^{*}_{Pb} + k_{e}}{L}\right)\frac{\partial E}{\partial X} - \left(\frac{k_{h}}{L}\right)\frac{\partial h}{\partial X} \tag{3.100}$$

3.7.2 H+ Transport

The differential equation describing H+ transport is given by,

$$Rd_{H}\frac{\partial nc_{H}}{\partial t} = \left(\frac{D^{*}_{H}}{L^{2}}\right)\frac{\partial^{2} c_{H}}{\partial X^{2}} + c_{H}\left[\left(\frac{u^{*}_{H} + k_{e}}{L^{2}}\right)\frac{\partial^{2} E}{\partial X^{2}} + \frac{k_{h}}{L^{2}}\frac{\partial^{2} h}{\partial X^{2}}\right] + \frac{\partial c_{H}}{\partial X}\left[\left(\frac{u^{*}_{H} + k_{e}}{L^{2}}\right)\frac{\partial E}{\partial X} + \frac{k_{h}}{L^{2}}\frac{\partial h}{\partial X}\right] - R^{aq}_{H} \tag{3.101}$$

The electrolysis reactions at the electrode are assumed to be the same as those defined in Section 3.5. Hence, the boundary condition given for H+ and OH- transport are the same as those defined for modeling soil pH in the previous section. For H+ at the anode (X=0),

$$-\frac{D^{*}_{H^+}}{L^2}\frac{\partial c_{H^+}}{\partial x} + \frac{\overline{v}_{H^+}}{L} c_{H^+}\Big|_{X=0} = \frac{c^{s}_{H} J_w}{L} + \frac{I}{FL} \qquad (3.102)$$

where,

$$\overline{v}_{H^+} = -\left(\frac{u_{H^+}}{L} + \frac{k_e}{L}\right)\frac{\partial E}{\partial X} - \frac{k_h}{L}\frac{\partial h}{\partial X} \qquad (3.103)$$

and the boundary condition for H+ at the cathode (X = I),

$$-\frac{D^{*}_{H^+}}{L}\frac{\partial c}{\partial X} + \frac{\overline{v}_{H^+}}{L} c_{H^+}\Big|_{X=L} = \frac{c_H J_w}{L} \qquad (3.104)$$

The transport of H+ through the soil towards the cathode will affect the sorption characteristics of lead on the day surface. H+ is expected to replace the adsorbed lead by ion exchange and at the same time attack the clay surface and result in surface complexation that changes the electrical charge of the soil particle. Consequently, the transport of H+ will be retarded due to sorption reactions (ion exchange and surface complexation). The rate of H+ sorption or retardation has not been thoroughly investigated, however, a retardation factor, Rd_H, can be incorporated in the model to account for these sorption reactions. Evaluation of tbis retardation factor is presented in Section 7.3.1.

3.7.3 OH- Transport

The transport equation for OH- ion is given by,

$$\frac{\partial nc_{OH}}{\partial t} = \left(\frac{D^{*}_{OH}}{L^2}\right)\frac{\partial^2 c_{OH}}{\partial X^2} + c_{OH}\left[\left(\frac{u^{*}_{OH} + k_e}{L^2}\right)\frac{\partial^2 E}{\partial X^2} + \frac{k_h}{L^2}\frac{\partial^2 h}{\partial X^2}\right] + \frac{\partial c_{OH}}{\partial X}\left[\left(\frac{u^{*}_{OH} + k_e}{L^2}\right)\frac{\partial E}{\partial X} + \frac{k_h}{L^2}\frac{ah}{\partial X}\right] - R_{OH} \qquad (3.105)$$

with the boundary conditions, at the cathode (x = 1),

$$-\frac{D^{*}_{OH}}{L^{2}}\frac{\partial c_{OH}}{\partial X}+\frac{\overline{v_{OH}}}{L}\,c_{OH}\Big|_{X=1}=\frac{c^{s}_{OH}\,J_{w}}{L}-\frac{I}{FL} \tag{3.106}$$

and at the anode (X=O),

$$-\frac{D^{*}_{OH}}{L^{2}}\frac{\partial c_{OH}}{\partial X}+\frac{\overline{v_{OH}}}{L}\,c_{OH}\Big|_{X=0}=\frac{c^{s}_{OH}\,J_{w}}{L} \tag{3.107}$$

3.7.4 NO^{-}_{3}, **Transport**

It is necessary to account for NO^{-}_{3}, because it is present at high concentrations since lead nitrate salt is used in spiking the soil. The need to account for NO^{-}_{3} also arises to achieve electrical neutrality in the system. Like other charged species NO^{-}_{3} transport is given by,

$$\frac{\partial ncN}{\partial t}=\left(\frac{D^{*}_{N}}{L^{2}}\right)\frac{\partial^{2}cN}{\partial X^{2}}+c_{N}\left[\left(\frac{u^{*}_{N}+k_{e}}{L^{2}}\right)\frac{\partial^{2}E}{\partial X^{2}}+\frac{k_{h}}{L^{2}}\frac{\partial^{2}h}{\partial X^{2}}\right]$$
$$+\frac{\partial c_{N}}{\partial X}\left[\left(\frac{u^{*}_{N}+k_{e}}{L^{2}}\right)\frac{\partial E}{\partial X}+\frac{k_{h}}{L^{2}}\frac{\partial h}{\partial X}\right]_{I}^{OH} \tag{3.108}$$

with the boundary conditions,

$$-\frac{D^{*}_{N}}{L^{2}}\frac{\partial c_{N}}{\partial X}+\overline{v}_{N}\,c_{N}\Big|_{X=0}=c^{s}_{N}\,J_{w} \tag{3.109}$$

$$\frac{D^{*}_{N}}{L^{2}}\frac{\partial c_{N}}{\partial x}+\overline{v}_{N}\,c_{N}\Big|_{X=1}=c_{N}\,J_{w_{w}} \tag{3.110}$$

$$\overline{v}_{N}=-\left(\frac{u^{*}_{N}+k_{e}}{L}\right)\frac{\partial E}{\partial X}-c_{N}\left(\frac{k_{h}}{L}\right)\frac{\partial h}{\partial X} \tag{3.111}$$

Note that since the global electrical neutrality is necessary (as shown in Section 3.42) concentration of one of the species could be calculated from the equation requiring preservation of

electrical neutrality. For example, since NO^-_3, is the least reactive species among the species present, its concentration can be evaluated by,

$$c_N = -\frac{\sum_{j=1}^{3} z_j c_j}{z_N} = \sum_{j=1}^{3} z_j c_j \qquad (3.112)$$

where i = 1, 2, and 3 refer to Pb^{2+}, H^+, and **OH-.** Significant computation time can be saved when this equation is used.

3.7.5 **Soil Consolidation Equation**

Once again, the soil consolidation equation describing the hydraulic potential distribution is given by,

$$\frac{\partial h}{\partial t} = \frac{c_v}{L^2}\frac{\partial^2 h}{\partial X^2} + \frac{k_s}{m_v \gamma_w}\frac{1}{L^2}\frac{\partial^2 E}{\partial X^2} \qquad (3.113)$$

With the boundary conditions,

$$h|_{X=0} = h|_{X=1} = 0 \qquad (3.114)$$

3.7.6 **Charge Transport Equation**

As described before, the electric potential distribution in time is given by,

$$0 = F\sum_{j=1}^{N}\left(\frac{z_j D_j^*}{L^2}\right)\frac{\partial^2 c_j}{\partial X^2} + \left(\frac{\sigma^*}{L^2}\right)\frac{\partial^2 E}{\partial X^2} + \left(\frac{1}{L^2}\frac{\partial \sigma^*}{\partial X}\right)\frac{\partial E}{\partial X} \qquad (3.115)$$

with the boundary **conditions,**

$$\left[-F\sum_{j=1}^{N} z_j \frac{D_j^*}{L^2}\frac{\partial c_j}{\partial X} - \frac{\sigma^*}{L^2}\frac{\partial E}{\partial X}\right]_{II X=0} = \frac{I}{L} \qquad (3.116)$$

$$E|_{X=1} = 0 \qquad (3.117)$$

3.7.7 Chemical Reactions

Solution of lead transport and removal requires evaluation of the chemical reactions that might occur as a result of changes in the soil chemistry. As presented before, **these** chemical reactions are described by a set of nonlinear algebraic equations under the assumption of local equilibrium. Reactions included in this study are lead hydroxide precipitation/dissolution reaction; water auto-ionization reaction, and lead-sorption.

I. Lead Hydroxide Precipitation/Dissolution

$$Pb(OH)_2 \rightleftharpoons Pb^{2+} + 2OH^- \tag{3.118}$$

Law of mass action for this reaction requires

$$c_{OH}^2 \, c_{Pb} \leq K^p_{Pb(OH)_2} = 2.8 * 10^{-16} \tag{3.119}$$

II. Water Auto-Ionization Reaction

$$H_2O \rightleftharpoons H^+ + OH^- \tag{3.120}$$

Law of mass action for water ionization requires

$$c_H \, c_{OH} = K_w = 10^{-14} \tag{3.121}$$

III. Mass conservation

Dissolution of 1 mole of lead hydroxide will generate 1 mole of Pb^{2+} and 2 moles of OH-. This means that the change in OH- molar concentration due to lead hydroxide dissolution/precipitation reaction is twice the change of Pb^{2+} molar concentration. At the same time the change in molar concentration of OH- due to water autoionization equals the change in molar concentration of H+. Consequently, the total change in OH^- concentration due to both reactions is given by

$$\Delta(c_{OH}) = \Delta(c_H) + 2\Delta(c_{Pb}) \tag{3.122}$$

or,

$$R_{OH} = R_H^{aq} + 2R_{Pb}^p \tag{3.123}$$

IV. Lead Sorption Reaction

Dissolved lead in the soil pore fluid is assumed to have, the form of Pb^{2+} which is highly retarded and adsorbed by different types of clay, compared to other heavy metas, as presented in Table 2.2. Lead sorption characteristics are controlled by a number of variables, most importantly soil pH and lead concentration Yong et al. (1990) describe lead adsorption isotherms at different pH values and concentrations for differnt types of **clay. The results** for lead sorption on kaolinite are used for this study to describe lead sorption at different pH and concentration. The following empirical relation is assumed to describe lead sorption on kaolinite,

$$s_{Pb} = 0.27\, c^t_{Pb}\,(pH - 1)\left(\frac{n}{\rho_d}\right)(207.2 \bullet 1000)\quad 1.0 < pH < 3.7 \tag{3.124}$$

$$s_{Pb} = 0 \quad pH < 1.0 \tag{3.125}$$

$$s_{Pb} = 0.5\,CEC \bullet 207.2 * 10^6 \qquad pH > 4.7 \tag{3.126}$$

where c^t_{Pb} is the total adsorbed and solute concentration in mole/L (= $s_{Pb} + C_{Pb}$), CEC is the cation exchange capacity, which should be substituted in equivalent/gm (for kaolinite used CEC = 1.06 milliequiv/100 gm, = $1.06 * 10^{-5}$ equiv/gm), and 207.2 is the atomic weight of lead. Note that Equation 3.126 and. Equation 3.128 are multiplied by 1000 and 10^6 respectively to evaluate the sorped lead in mg/kg. Figure 3.6 presents a comparison between the empirical relation assumed for lead sorption at different pH values and the experimental results of Yong et al. (1990).

10 unknowns are defined for this study, these are h, E, c_{Pb}, c_H, c_{OH}, c_N, s_{Pb}, R^p_{Pb}, R^{aq}_H, and R_{OH}. Six transport partial differential equations are used, these equations are 3.97 for Pb^{2+} transport, 3.101 for H^+ transport, 3.105 for OH^- transport, 3.108 for NO^-_3, transport, 3.113 for soil consolidation, 3.115 for charge transport. The other four equations required for the solution are the algebraic equations 3.119 for lead hydroxide precipitation/dissolution, 3.121 for water autoionization, 3.122 for charge conservation of the chemical reactions, and one of 3.124-3.126 for lead *sorption* (depending upon the soil pH).

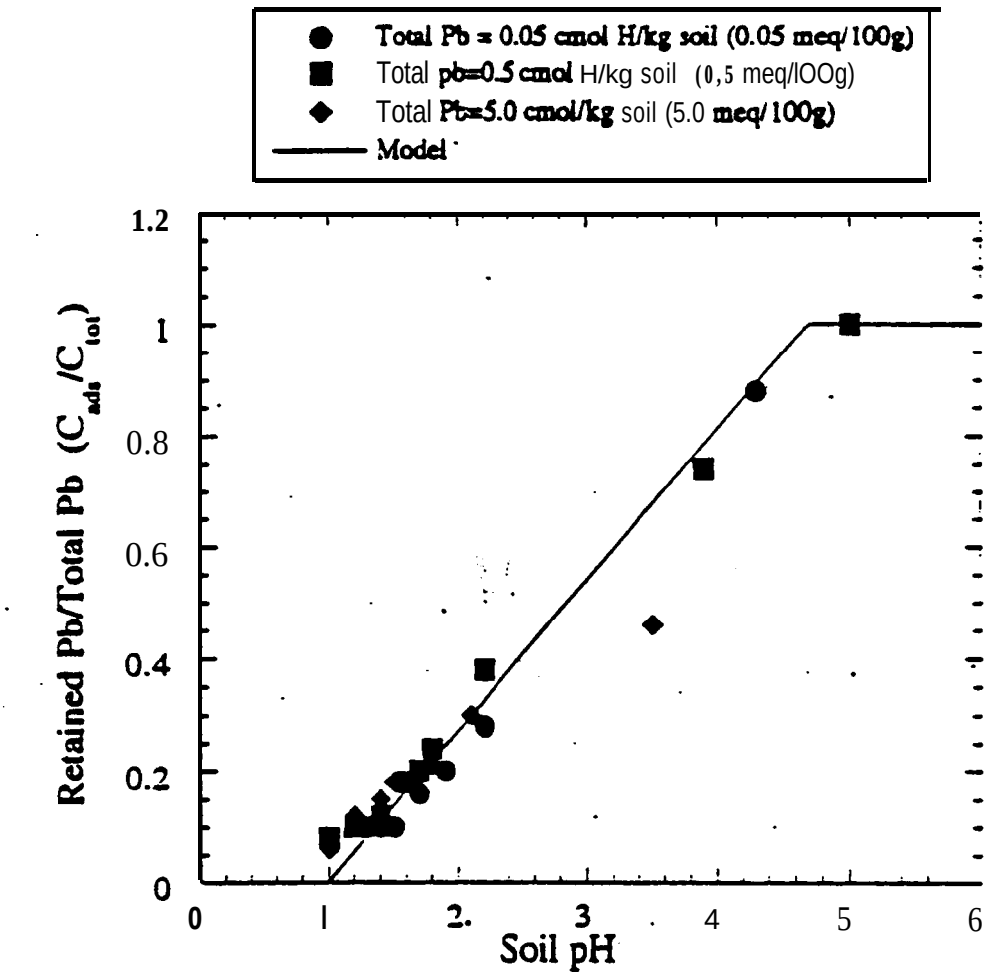

Figure 3.6: Lead Sorption at Different pH Values (Experimental Data from Yong et al., 1990)

Section 4

NUMERICAL SIMULATION

4.1 Introduction

Numerical simulations are of great importance in engineering and science. They are of major interest in providing solutions to the theoretical and mathematical formalism of a particular physical system, specially when analytical forms of solution are not possible,

- they are used to bridge the gap between theoretical developments and experimental results,
- they can be used to evaluate the importance of a specific physical effect on the physical system by turning this effect on or off, changing its strength, or changing its functional form,
- they may be used to test the validity of the theoretical fornalism, and quantitatively test existing theories,
- once a numerical model is tested and verified, it can be used as a design and analysis tool for full practical application, and
- they can be used to quantitatively evaluate new ideas.

Theoretical models and numerical solutions for multidimensional transient coupled species transport in groundwater under hydraulic and chemical gradients have shown significant progress in recent years. In most of these models, a coupled system of partial differential and nonlinear algebraic equations is developed and solved by different numerical approaches. Three of these numerical approaches are identified and used successfully by various authors,

1. providing a solution to the mixed differential and algebraic equations in which the transport equations and chemical equilibrium reactions are solved simultaneously as a system (Miller and Benson 1983; Lichtner 1985),
2. direct substitution **of the** algebraic chemical equilibrium equations into the differential transport equations to form a highly nonlinear system of partial differential equations (Vallocchi et al. 1981; Jennings et al. 1982; Rubin 1983; Lewis et al. 1987), and

3. iterating between the sequentially solved differential and algebraic equations (Kirkner et aL 1984,1985; Yeh and Tripathi 1991).

Detailed reviews of these methods have been presented by Yeh et al. (1989) and Kirkner et al. (1988).

The third approach, sequential iteration between partial differential transport equations and chemical equilibrium algebraic equations, is used in this study because,

- the above described first and second approaches require intensive computer work and CPU time, specially for two or three dimensional applications (Yeh and Tripathi 1991),
- the algebraic equations do not include spatial derivatives, hence they are applicable to a batch system only (point equations) and sequential solution of these equations at every time step is more realistic and a reasonable choice,
- since the transport equations for different species are identical in form, it is convenient to solve them one by one independent of each other and then iterating with the chemical equilibrium equations.

4.2 **Solution** Scheme

The theoretical formalism presented in previous Sections produces a coupled system of partial differential equations, describing transport of fluid, charge, species, and nonlinear algebraic equations describing species chemical reactions. The numerical solution scheme utilized for this system, using the sequential iteration approach, is summarized in Figure 4.1. The procedure is explained in detail in Section 7.

Boundary and initial conditions arc specified at time ($T_i = 0$). The solution starts by solving the differential equations describing species transport to evaluate species concentrations at time ($T = T_i + \Delta t$). Initial values of E and h and their gradients at $T = T_i$ are first used in these equations. The new concentrations of the chemical species are used in the algebraic equations for the chemical reactions to evaluate the rates of production of species due to chemical reactions. The new concentrations are then used to evaluate the electric conductivity distribution and the first and second derivatives of concentrations. These values are used to solve the charge transport equations

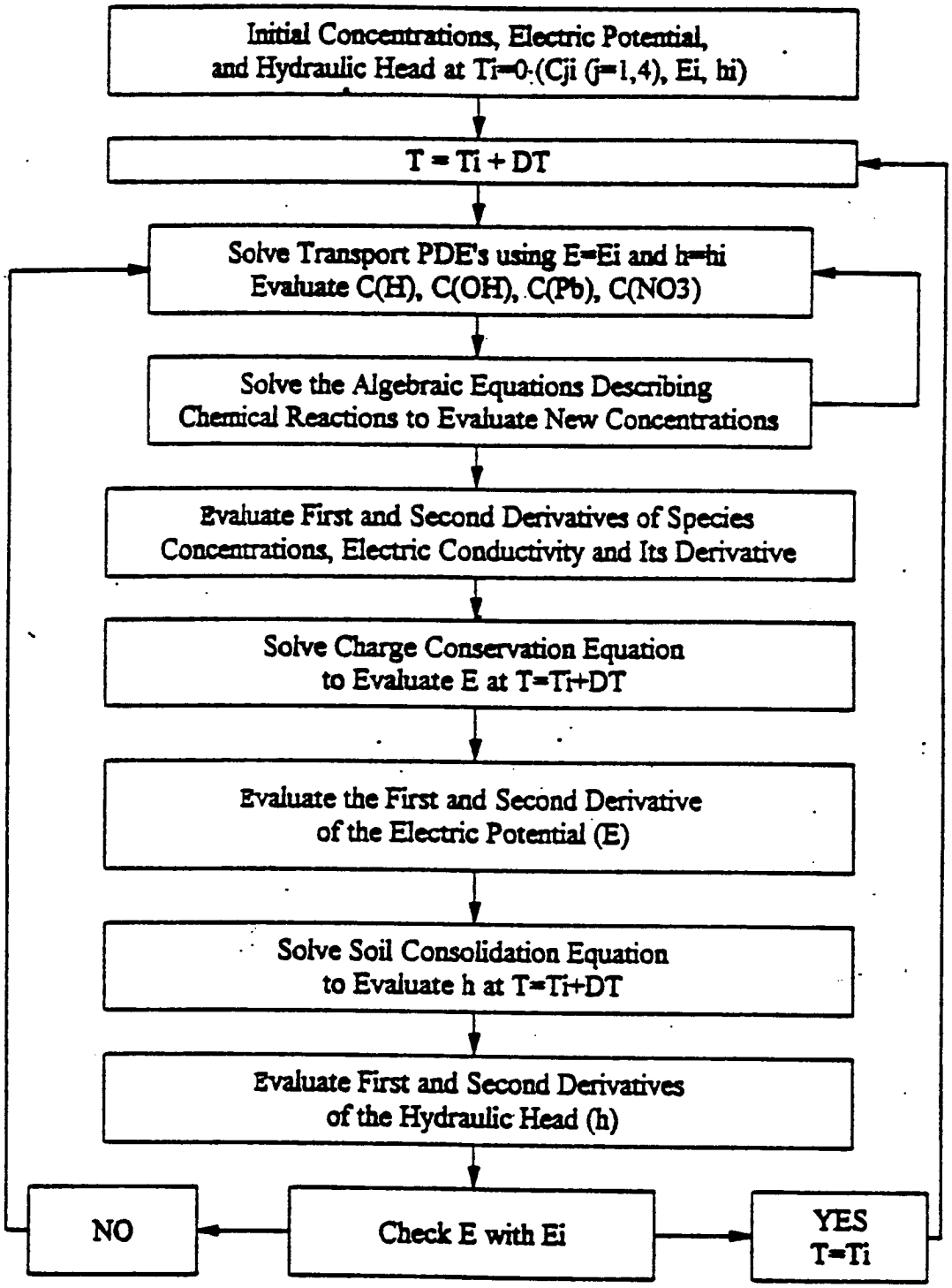

Figure 4.1: Flow Chart Describing the Sequential Iteration Scheme Used

to evaluate the electric potential distribution E at time $T=T_i+\Delta t$. The second derivative of the electric potential is then evaluated across the specimen and used to solve the soil consolidation equation to evaluate the new hybraulic potential distribution at $T=T_i+\Delta t$. The new electric potential distribution is then compared with the distribution used to used to solve species transport equations. If the two distributions do not compare within a specific tolerance, then the new distribution of E is used in the species transport equations and these equation are resolved. If the two distributions agree then the solution proceeds to the next time step.

The computer program developed is discussed in more detail together with its subroutines in Section 7. Appendix A presents a listing of the computer program, while a sample data file pertaining to the pilot-scale study is presented in Appendix.B. The numerical methods used for the solution are described in the following sections.

Extensive literature exists on numerical approximation of different transport partial differential equations with various boundary and initial conditions. Finite-difference methods and finite-element methods are the most widely used numerical approximations for solving transport partial differential equations. Though finite-difference method can provide an adequate and accurate solution for one dimensional transport equations, the finite element method is adopted in this study. The finite element method is more appropriate in treating the f!ux boundary conditions, has the ability to discretely describe complex boundaries, and it is easier to use this procedure in calculating the cross-derivative terms.

The Galerkin weighted-residual method is used as the variational (or weak) method of approximation. In an attempt to prepare a two-dimensional transport model, two dimensional elements are chosen for the finite element discretization in spite of the one dimensional application in this study. The Choleski decomposition method is used for matrix inversion and the bisection method is used for solving the chemical equilibrium algebraic equations.

4.3 Finite Element Solution of PDE's

The general form of the partial differential equation governing two-dimensional advective diffusive species transport with zero and first order production rates is given by,

$$D_x \frac{\partial^2 c}{\partial x^2} + D_y \frac{\partial^2 c}{\partial y^2} - v_x \frac{\partial c}{\partial x} - v_y \frac{\partial c}{\partial y} + \mu c + \gamma = R \frac{\partial c}{\partial t} \qquad (4.1)$$

where D_x, D_y are the diffusion coefficients in x and y directions respectively, v_x and v_y are the flow velocities in x and y respectively, μ is the first order production rate, and y is the zero order production rate. Boundary conditions can be defined as,

$$c = c_0 \qquad (4.2)$$

on the boundary B1, and,

$$(v_x + v_y)c - D_x \frac{\partial c}{\partial x} - D_y \frac{\partial c}{\partial y} = q \qquad (4.3)$$

on the boundary B2, where q is the mass flux of species at the boundary. Figure 4.2 presents a schematic diagram of a two-dimensinal domain for this case with the given boundary conditions.

4.3.1 Variational Formulation

Variational formulation is a weak formulation that describes the differential equation as a recast of an equivalent integral form. A large number of variational formulations have been introduced for deriving approximate solutions. For most linear problems the weak (or variational) formulation is equivalent to the minimization of a quadratic functional I(c), known as the total potential energy, that describes the physical system (Reddy 1985).

The quadratic functional corresponding to Equation 4.1 is described by,

$$I(c) = \int_D (L(c) + \mu c + \gamma)\, dx\, dy \qquad (4.4)$$

where I(c) (or I) is the variational of c, D is the plane region with the boundaries B1 and B2 (Figure 4.2) and the operator L is defined by,

$$L = \left(D_x \frac{\partial^2}{\partial x^2} + D_y \frac{\partial^2}{\partial y^2} - v_x \frac{\partial}{\partial x} - v_y \frac{\partial}{\partial x} - R \frac{\partial}{\text{at}} \right) \qquad (4.5)$$

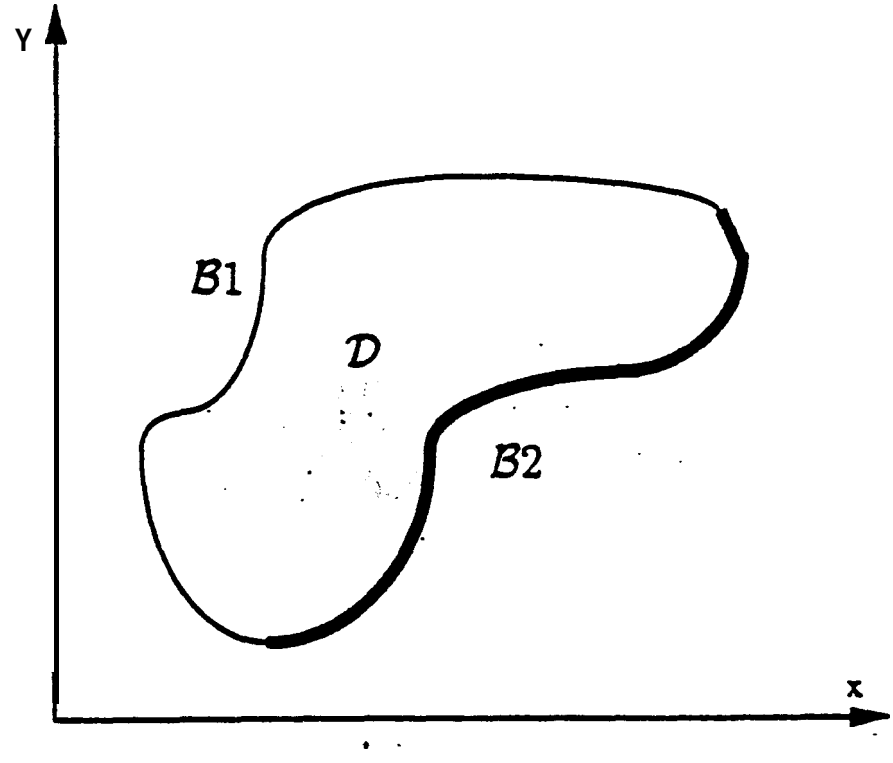

Figure 4.2: General Space Domain for Two-Dimensional Problem with the Boundary Conditions

The first **variation of this integral** equation is

$$\delta_1 I = \delta_c \int_D (L(c) + \mu c + \gamma)\, dx\, dy \tag{4.6}$$

Since the energy must be minimized, the first variation must equal zero;

$$\delta_1 I = 0 \tag{4.7}$$

Equation 6 can be further simplified by utilizing integration by parts. The diffusion terms in x and y directions are expressed as,

$$\int_D \delta_c D_x \frac{\partial^2 c}{\partial x^2}\, dx\, dy = \int_B \left[\delta_c D_x \frac{\partial c}{\partial x}\right]_B ds - \int_D \left[\delta \left(\frac{\partial c}{\partial x}\right) D_x \frac{\partial c}{\partial x}\right] dx\, dy \tag{4.8}$$

$$\int_D \delta_c D_y \frac{\partial^2 c}{\partial y^2}\, dx\, dy = \int_B \left[\delta_c D_y \frac{\partial c}{\partial y}\right]_B ds - \int_D \left[\delta \left(\frac{\partial c}{\partial y}\right) D_y \frac{\partial c}{\partial y}\right] dx\, dy \tag{4.9}$$

where the first term on the right side represents the boundary conditions on the perimeter (B). The boundary conditions are introduced as

$$\begin{aligned} \delta_c D_x \frac{\partial c}{\partial x}\Big\|_B &= \delta_c \left. D_x \frac{\partial c}{\partial x}\right\|_{B1} + \left. \delta_c D_x \frac{\partial c}{\partial x}\right\|_{B2} \\ &= \delta_c D_x \frac{\partial c}{\partial x}\Big\|_{B2} \end{aligned} \tag{4.10}$$

$$\begin{aligned} \left[\delta_c D_y \frac{\partial c}{\partial y}\right]_B &= \left[\delta_c D_y \frac{\partial c}{\partial y}\right]_{B1} + \left[\delta_c D y \frac{\partial c}{\partial y}\right]_{B2} \\ &= \left[\delta_c D_y \frac{\partial c}{\partial y}\right]_{B2} \end{aligned} \tag{4.11}$$

The value on B1 is equal to zero since the variation (δ_c) is zero for the constant concentration boundary condition. From Equation 4.3,

$$D_x \frac{\partial c}{\partial x} + D_y \frac{\partial c}{\partial y} = (v_x + v_y)\, c - q \tag{4.12}$$

$$\int_{B2}\left[D_x \frac{\partial c}{\partial x} + D_y \frac{\partial c}{\partial y} \right] ds = \int_{B2} [(v_x + v_y)c - q]\, ds \qquad (4.13)$$

Substituting Equations 4.8-4.11, and 13 in Equation 4.6,

$$\begin{aligned} \delta_1 I = & -\int_D \left[\delta\left(\frac{\partial c}{\partial x}\right) D_x \frac{\partial c}{\partial x} + \delta\left(\frac{\partial c}{\partial y}\right) D_y \frac{\partial c}{\partial y} \right] dx\, dy \\ & + \int_{B2} \delta_c [(v_x + v_y)c - q]\, ds \\ & + \int_D \delta_c \left[-v_x \frac{\partial c}{\partial x} - v_y \frac{\partial c}{\partial y} + \mu c + \gamma - R \frac{\partial c}{\partial t} \right] dx\, dy \end{aligned} \qquad (4.14)$$

Two-dimensional 8-nodal (quadratic) isoparametric elements are specified for domain discretization. 8-node elements are selected in order to achieve reasonable evaluation of the first and second order derivatives of the dependent variables. Figure 4.3 shows the elements together with the shape functions. Isoparametric element is used because both the dependent variables and the local coordinates can be interpolated from nodal values. Shape functions N_i for this sub-domain are given as (Burnett 1987),

$$\begin{aligned} N_1 &= -\frac{1}{4}(1-\xi)(1-\eta)(1+\xi+\eta) \\ N_2 &= \frac{1}{2}(1-\xi^2)(1-\eta) \\ N_3 &= -\frac{1}{4}(1+\xi)(1-\eta)(1-\xi+\eta) \\ N_4 &= \frac{1}{2}(1+\xi)(1-\eta^2) \end{aligned} \qquad (4.15)$$

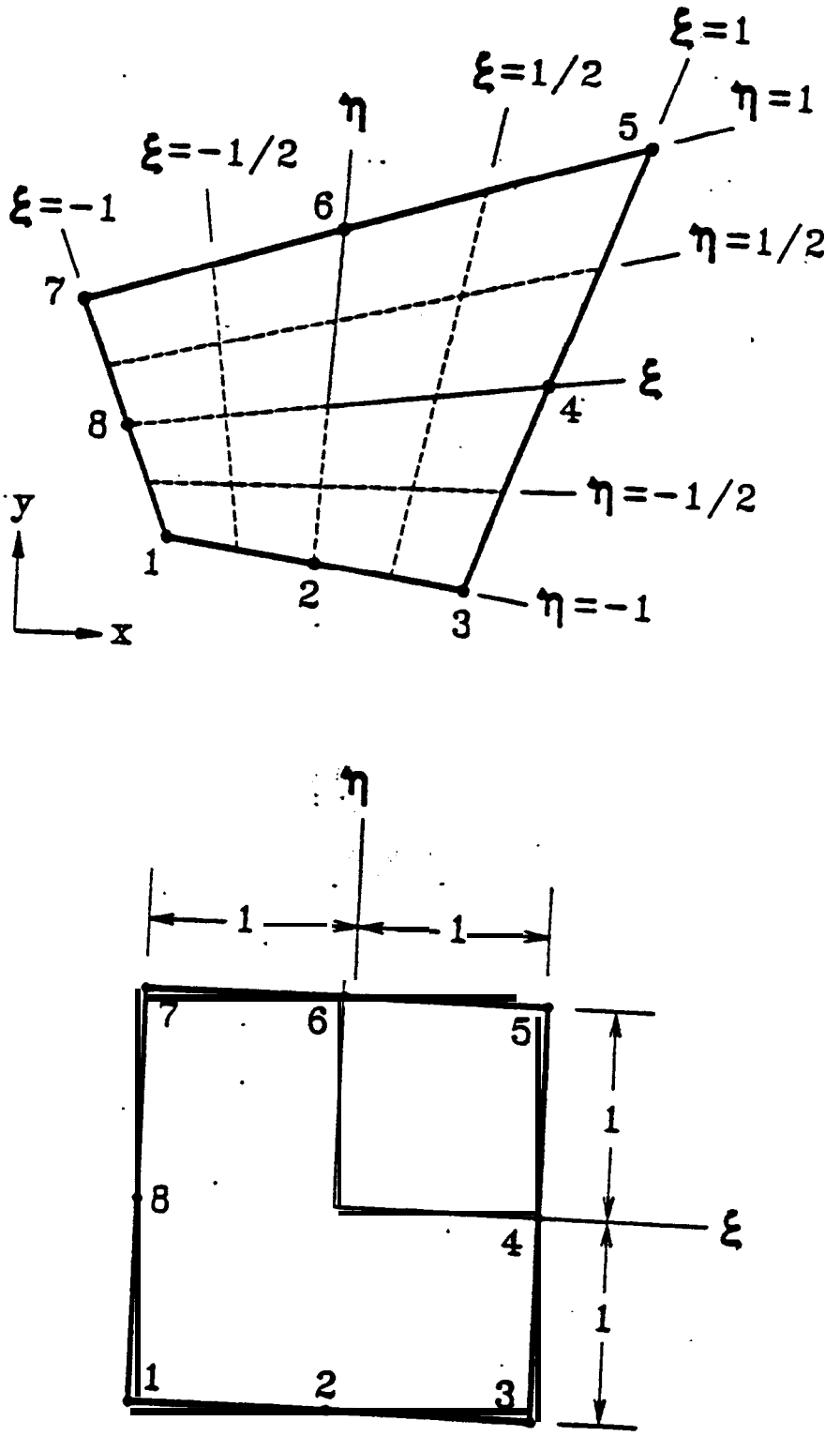

Figure 4.3: Eight Node Quadratic Isoparametric Quadrilateral Element

$$
\begin{aligned}
N_5 &= -\frac{1}{4}(1+\xi)(1+\eta)(1-\xi-\eta) \\
N_6 &= \frac{1}{2}(1-\xi^2)(1+\eta) \\
N_7 &= -\frac{1}{4}(1-\xi)(1+\eta)(1+\xi-\eta) \\
N_8 &= \frac{1}{2}(1-\xi)(1-\eta^2)
\end{aligned}
\tag{4.15}
$$

and,

$$
[N]^T = [N_1\ N_2\ N_3\ N_4\ N_5\ N_6\ N_7] \tag{4.16}
$$

The coordinates and the functions are described by:

$$
\begin{aligned}
x &= [N]^T \{x_i\} = \sum N_i\ x_i \\
y &= [N]^T \{y_i\} = \sum N_i\ y_i \\
c &= [N]^T \{c_i\} = \sum N_i\ c_i
\end{aligned}
\tag{4.17}
$$

where x_i and y_i are the global values of the nodal coordinates and c_i is the nodal concentrations in the specific element Consequently, the function spatial derivatives are

$$
\begin{aligned}
\frac{\partial c}{\partial x} &= \left[\frac{\partial N}{\partial x}\right]^T \{c_i\} \\
\frac{\partial c}{\partial y} &= \left[\frac{\partial N}{\partial y}\right]^T \{c_i\}
\end{aligned}
\tag{4.18}
$$

Since the shape functions are dependent on the local coordinates ξ and η

$$\frac{\partial N_i}{\partial \xi} = \frac{\partial N_i}{\partial x}\frac{\partial x}{\partial \xi} + \frac{\partial N_i}{\partial y}\frac{\partial y}{\partial \xi}$$
$$\frac{\partial N_i}{\partial \eta} = \frac{\partial N_i}{\partial x}\frac{ax}{\partial \eta} + \frac{\partial N_i}{\partial y}\frac{\partial y}{\partial \eta} \qquad \textbf{(4.19)}$$

$$\begin{Bmatrix} \frac{\partial}{\partial \xi} \\ \\ \frac{\partial}{\partial \eta} \end{Bmatrix} = \begin{bmatrix} \frac{\partial x}{\partial \xi} & \frac{\partial y}{\partial \xi} \\ \\ \frac{\partial x}{\partial \eta} & \frac{\partial}{\partial \eta} \end{bmatrix} \begin{Bmatrix} \frac{\partial}{\partial x} \\ \\ \frac{\partial}{\partial y} \end{Bmatrix} = [\mathbf{J}] \begin{Bmatrix} \frac{\partial}{\partial x} \\ \\ \frac{\partial}{\partial y} \end{Bmatrix} \qquad \textbf{(4.20)}$$

where **[J]** is the Jacobian matrix. Hence, the x and y derivatives are evaluated by

$$\begin{Bmatrix} \frac{\partial}{\partial x} \\ \\ \frac{\partial}{\partial y} \end{Bmatrix} = [\mathbf{J}]^{-1} \begin{Bmatrix} \frac{\partial}{\partial \xi} \\ \\ \frac{\partial}{\partial \eta} \end{Bmatrix} \qquad (4.21)$$

$$[\mathbf{J}]^{-1} = \frac{1}{|\mathbf{J}|} \begin{vmatrix} \frac{\partial y}{\partial \eta} & -\frac{\partial y}{\partial \xi} \\ \\ -\frac{\partial x}{\partial \xi} & \frac{\partial x}{\partial \eta} \end{vmatrix} \qquad (4.22)$$

The determinant $|\mathbf{J}|$ **(or the** Jacobian) is given by:

$$|\mathbf{J}| = \frac{\partial x}{\partial \xi}\frac{\partial y}{\partial \eta} - \frac{\partial x}{\partial \eta}\frac{\partial y}{\partial \xi} \qquad (4.23)$$

The determinant of the Jacobian matrix/j/can be regarded as ratio between an infinitesimal area in the parent element to the corresponding infinitesimal area in the real elenent that it is mapped into,

$$dx\,dy = |J|\,d\xi\,d\eta \qquad (4.24)$$

The Jacobian matrix is evaluated using Equation 4.22.

4.3.2. Local Matrices

Equation 4.14 can be formed at the local element k as:

$$\delta_1 I^k = -\int_D \left[\delta\left(\frac{\partial c^k}{\partial x}\right) D_x^k \frac{\partial c^k}{\partial x} + \delta\left(\frac{\partial c^k}{\partial y}\right) D_y^k \frac{\partial c^k}{\partial y}\right] dx\,dy$$

$$+ \int_{B2} \delta c^k [(v_x^k + v_y^k)c^k - q]\,ds$$

$$+ \int_D \delta c^k \left[-v_x^k \frac{\partial c^k}{\partial x} - v_y^k \frac{\partial c^k}{\partial y} + \mu^k c^k + \gamma^k - R^k \frac{\partial c^k}{\partial t}\right] dx\,dy \qquad (4.25)$$

The dependent values for the local element k in **Equation** 4.25 are

$$c^k = [N]^T \{c^k\} \qquad (4.26)$$

$$\delta c^k = [\delta c^k]^T \{N\} \qquad (4.27)$$

$$\delta c^k = [\delta c^k]^T \{N\} \qquad (4.28)$$

$$\delta\left(\frac{\partial c^k}{\partial x}\right) = [\delta c^k]^T \left\{\frac{\partial N}{\partial x}\right\} \qquad (4.29)$$

The local element (k) matrices can be formed by substituting Equations 4.26-4.29 into Equation 4.25,

$$\delta_1 I^k = \{\delta c^k\}^T \left(- \int_D \left(D_x^k \left[\frac{\partial N}{\partial x}\right]\left[\frac{\partial N}{\partial x}\right]^T + D_y^k \left[\frac{\partial N}{\partial y}\right]\left[\frac{\partial N}{\partial y}\right]^T \right) dx\, dy\, \{c\}^k \right)$$
$$+ \{\delta c^k\}^T \left(\int_{C2} (v_x^k + v_y^k)\, [N]\, [N]^T \{c\}^k - [N]\, q]\, ds \right)$$
$$+ \{\delta c^k\}^T \int_D \left(- v_x^k\, [N] \left[\frac{\partial N}{\partial x}\right]^T - v_y^k\, [N] \left[\frac{\partial N}{\partial y}\right]^T \right) dx\, dy\, \{c\}^k \qquad (4.30)$$
$$+ \{\delta c^k\}^T \left(\int_D \left(\mu^k\, [N]\, [N]^T \{c\}^k + \gamma^k\, [N] - R^k [N]\, [N]^T \left\{\frac{\partial c^k}{\partial t}\right\} \right) dx\, dy \right)$$

The time derivative is evaluated using a forward finite difference approach described by,

$$\frac{\partial c}{a\ t} = \frac{\{c\}_{t+\Delta t} + \{c\}_t}{\Delta t} \qquad (4.31)$$

The resulting formulation of the local stiffness matrix can be represented by

$$\delta_1 I^k = \{\delta c\}^{kT} \left[\left([SKF]^k + [\dot{V}L]^k - [AK]^k - [VB]^k + \frac{[E]^k}{\Delta t} \right) \{c\}^k_{t+\Delta t} \right.$$
$$\left. - \frac{[E]^k}{\Delta t} \{c\}^k_t - \{QQ\}^k + \{F\} \right] \qquad (4.32)$$
I

$$[SKF]^k = - \int_D \left(D_x^k \left[\frac{\partial N}{\partial x}\right]\left[\frac{\partial N}{\partial x}\right]^T + D_y^k \left[\frac{\partial N}{\partial y}\right]\left[\frac{\partial N}{\partial y}\right]^T \right) dx\, dy \qquad (4.33)$$

$$[VB]^k = \int_{c2} (v_x^k + v_y^k)\, [N]\, [N]^T ds \qquad (4.34)$$

$$\{F\} = - \int_{c2} [N]\, q\, ds \tag{4.35}$$

$$[VL]^k = \int_D - v_x^k [N] \left[\frac{\partial N}{\partial x}\right]^T - v_y^k [N] \left[\frac{\partial N}{\partial y}\right]^T dx\, dy \tag{4.36}$$

$$\{QQ\}^k = \int_D \gamma^k [N]\, dx dy \tag{4.37}$$

$$[E]^K = \int_D R^k [N]\, [N]^T dx\, dy \tag{4.38}$$

$$[AK]^k = \int_D \mu^k [N]\, [N]^T dx\, dy \tag{4.39}$$

where,

[SKF] represents diffusion terms,
[VL] represents velocity terms,
[E] represents retardation term,
[AK] represents first order production term,
[VL] represents the velocity term at the boundaries,
{QQ} represents zero order production term, and
{F} represents the flux term.

Applying the Transform 4.21, these matrices are equal to,

$$[SKF]^k = - \int_{-1}^{1} \int_{-1}^{1} \left(D_x^k \left[\frac{\partial N}{\partial x}\right] \left[\frac{\partial N}{\partial x}\right]^T + D_y^k \left[\frac{\partial N}{\partial y}\right] \left[\frac{\partial N}{\partial y}\right]^T \right) |J|\, d\xi\, d\eta \tag{4.40}$$

$$VL]^k = \int_{-1}^{1} \int_{-1}^{1} \left(- v_x^k [N] \left[\frac{\partial N}{\partial x}\right]^T - v_y^k [N] \left[\frac{\partial N}{\partial y}\right]^T \right) |J|\, d\xi\, d\eta \tag{4.41}$$

$$\{QQ\}^k = \int_{-1}^{1}\int_{-1}^{1} \gamma^k [N] |J| \, d\xi \, d\eta \tag{4.42}$$

$$[E]^k = \int_{-1}^{1}\int_{-1}^{1} R^k [N] [N]^T |J| \, d\xi \, d\eta \tag{4.43}$$

$$[AK]^k = \int_{-1}^{1}\int_{-1}^{1} \mu^k [N] [N]^T |J| \, d\xi \, d\eta \tag{4.44}$$

4.3.3 **Gauss Legendre Quadrature**

The area integrals in Equations (4.40-4.44) are evaluated numerically using Gauss quadrature. Gaussian product rules (multidimensional Gauss rules) are generated by successive application of one dimensional Gauss rules as follows,

$$\text{Int.} = \int_{-1}^{1}\int_{-1}^{1} c(\xi_i, \eta) \, d\xi \, d\eta \tag{4.45}$$

$$\text{Int.} = \int_{-1}^{1} \left(\sum_i W_i c(\xi, \eta) \right) d\eta = \sum_i \sum_j W_i W_j c(\xi_i, \eta_j) \tag{4.46}$$

where, W^i and W^j are the weight factors for the selected sampling points ζ_i and η_j. Nine sampling points are selected for ζ_i and η_j, $\pm$ 0.7745966692 and $\pm$ 0.0000000000. Weight factors for these points are 0.5555555556 and 0.8888888889, respectively.

4.3.4 Global Matrix

The connectivity of each element is used to generate the global stiffness matrix.

$$\delta_1 I^g = \{\delta c\}^T \left[\left([SKF]^g + [VL]^g - [AK]^g - [VB]^g + \frac{[E]^g}{\Delta t} \right) \{c\}^g_{t+\Delta t} - \frac{[E]^g}{\Delta t} \{c\}^g_t - \{QQ\}^g + \{F\} \right] \tag{4.46}$$

Since the formulated global matrix accounts for all elements of the mesh, then the first variation of the integral equation $\delta_1 I^g$ must equal zero to minimize the energy input to the system. Furthermore, the variations δ_c are arbitrary which renders Equation 4.46 to,

$$\left([SKF]^g + [VL]^g - [AK]^g - [VB]^g + \frac{[E]^g}{\Delta t} \right) \{c\}^g_{t+\Delta t} - \frac{[E]^g}{\Delta t} \{c\}^g_{t+\Delta t} - \{QQ\}^g + \{F\} = 0 \tag{4.47}$$

or,

$$\left([SKF]^g + [VL]^g - [AK]^g - [VB]^g + \frac{[E]^g}{\Delta t} \right) \{c\}^g_{t+\Delta t} = \frac{[E]^g}{\Delta t} \{c\}^g_{t+\Delta t} + \{QQ\}^g - \{F\} \tag{4.48}$$

The above formulation of the finite element solution of the partial differential equation will result in the following matrix form

$$\mathbf{A} \cdot \mathbf{c} = \mathbf{b} \tag{4.49}$$

where **A** is the global matrix developed, **c** is the column vector describing unknown concentrations at time $(t+\Delta t)$, and **b** is the column vector developed for initial and boundary conditions and zero order production rate.

4.3.5 Choleski Decomposition

For any nonsingular square matrix A, the rows can be reordered so that the resulting matrix has an L-U factorization .

$$L - U = A \tag{4.50}$$

where L is the lower triangular and U is the upper triangular. For the case of a 4 x 4 matrix, as an example, Equation 4.50 will be

$$\begin{bmatrix} @_{11} & 0 & 0 & 0 \\ \alpha_{21} & \alpha_{22} & 0 & 0 \\ \alpha_{31} & \alpha_{32} & \alpha_{33} & 0 \\ \alpha_{41} & @_{42} & \alpha_{43} & \alpha_{44} \end{bmatrix} \begin{bmatrix} \beta_{11} & \beta_{12} & \beta_{13} & \beta_{14} \\ 0 & \beta_{22} & \beta_{23} & \beta_{24} \\ 0 & 0 & \beta_{33} & \beta_{34} \\ 0 & 0 & 0 & \beta_{44} \end{bmatrix} = \begin{bmatrix} a_{11} & a_{12} & a13 & a_{14} \\ a_{21} & a_{22} & a_{23} & a_{24} \\ a_{31} & a_{32} & a_{33} & a_{34} \\ a_{41} & a_{42} & a_{43} & a_{44} \end{bmatrix} \tag{4.51}$$

Instead of using an arbitrary Iower and upper triangular factors L and U, Choleski decomposition constructs a lower triangle matrix L whose transpose L^T can itself serve as the upper triangular part (Bathe and **Wilson 1976; Krcyszig** 1988). In other words,

$$L \cdot L^T = A \tag{4.52}$$

The components of L^T are, of course, related to those of L by

$$L^T_{ij} = L_{ji} \tag{4.53}$$

Solving for components of L will result in

$$L_{ii} = \left(a_{ii} - \sum_{k=1}^{i-1} L_{ik}^2 \right)^{\frac{1}{2}} \tag{4.54}$$

$$Lji = \frac{1}{L_{ii}} \left(a_{ii} - \sum_{k=1}^{i-1} L_{ik} L_{jk} \right)^{\frac{1}{2}} \quad j = i+1, i+2, \ldots\ldots n \tag{4.55}$$

4.4 Verification of the Finite Element Solution

It is necessary to verify the computer program to assure that the mathematical formalism and the computer code are correct. Program verification requires comparison of the program results with verified analytical or numerical solutions to known problems.

Various attempts are made to compare the numerical solution with existing analytical solutions of specific problems. Preliminary comparisons are made with ordinary differential equations describing either boundary value problems or initial value problems and the finite element solution showed good comparison with analytical solutions to these cases. Verifications of the numerical model and computer code are accomplished through comparisons with various analytical solutions for initial-boundary value problems, similar to those present in Van Genuchten and Alven (1982). These comparisons are provided in Appendix C for certain practical problems with constant and/or flux type boundary conditions.

Section 5

EXPERIMENTAL MODEL

5.1 Introduction

A laboratory testing program has been developed to investigate the effect of up-scaling bench-scale tests and to demonstrate the feasibility and cost efficiency of electrokinetic soil remediation at dimensions representative of field conditions. Second, it was essential to compare the results of the experimental model with the results of the theoretical formalism developed. Accordingly, a pilot-scale test setup was designed. The following criteria were used in the design,

- one-dimensional conditions and an intermediate case between bench-scale and full-scale in-situ remediation was represented,
- introduction of any boundary effects was minimized.
- constant hydraulic head difference between the anode and the cathode was maintained throughout testing.
- constant electric current or electric potential difference could be applied across the soil mass,
- space and time changes in electric potential, pressure head, and temperature, across the soil mass could be measured, and
- soil samples should be available for chemical analysis during testing.

5.2 Equipment and Instrumentation

There are no standards available for conducting pilot-scale laboratory tests and consequently no standard equipment or instrumentation are available. Standard procedures are used wherever and whenever available.

5.2.1 **Test Container**

Figure 5.1 provides a schematic diagram of the container used for the pilot-scale experimental study. The container was made of plywood so that it did not conduct electricity but resists the lateral compaction pressure. Container dimensions were chosen to be 91.4 cm width x 91.4 cm height x 182.9 cm length (36.0 in x 36.0 in x 72.0 in). These dimensions were selected in an attempt to minimize boundary effects, establish one-dimensional flow conditions, and presented a reasonable electrode spacing between bench-scale experiments and full scale field implementation. The effect of electrode spacing to the efficiency of the process was not well established. A wooden base was used to separate the container from the ground and to detect any leakage.

The inside of the container was sealed with silicon sealant and then wax painted. In order to avoid any fluid leakage from the container, 80-mil High Density Poly Ethylene (HDPE) Gundle liner was fitted inside the plywood container. HDPE/Bentonite composite (Gundseal) also was placed inside the wooden container as a second liner along the walls across the electrodes.

5.2.2 Electrodes

Several types of electrodes can be used in electrokinetic soil remediation. Inert graphite electrodes were used for both the anode and the cathode to prevent introduction of corrosion products that might complicate the electrochemistry due to electrode electrolysis reaction. Electrodes are purchased in rods each 6.35 cm (2.5 in) diameter and 76.2 cm (30 in) length. Each cathode and anode series consisted of a row of five equally spaced electrodes at a center to center spacing of 18.3 cm (Figure 5.1). Electrodes were held by polyacrylite frames that fit inside the anode and cathode compartments (Plate 5.1).

5.2.3 **Power Supply**

Sorensen (DCS 600-1.7) power supply was used that can provide 0-600 V DC and 0-l.7 Amps. The DCS 600-l .7 had two operating modes; constant current and constant voltage. In the constant voltage mode, the output voltage was regulated at the selected value while the output

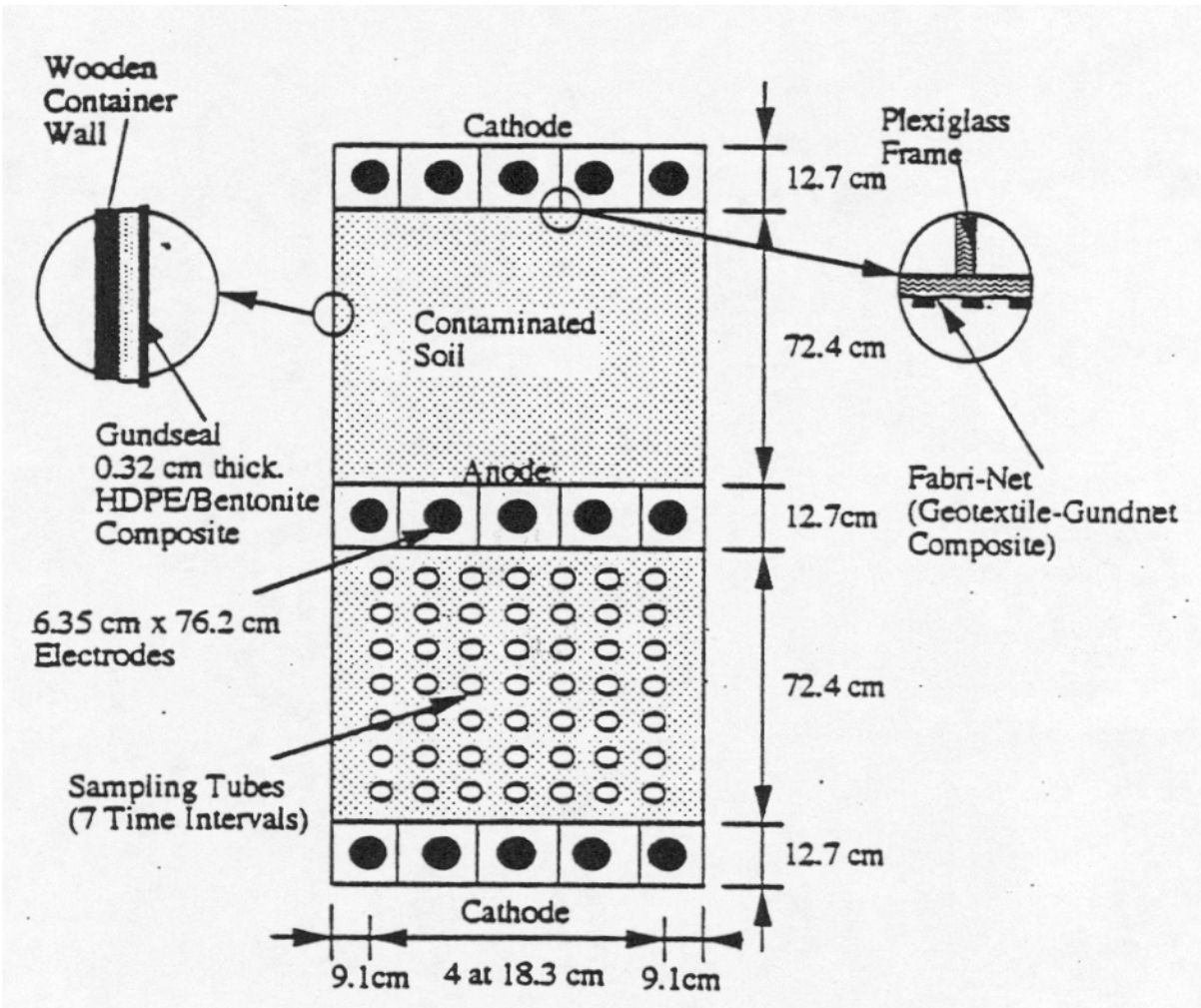

Figure 5.1: A Schematic Diagram of the Wooden Container and Lining Material Used for Testing

Plate 5.1: Graphite Electrodes Used in Pilot-Scale Tests

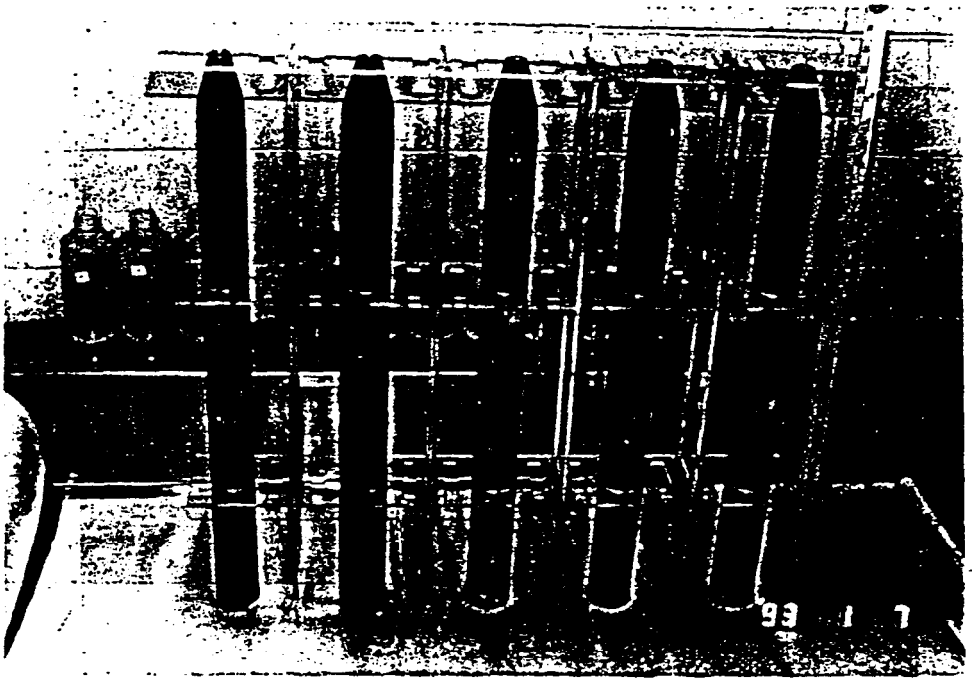

current varied with the load requirements. In the constant current mode, the output current was regulated at the selected value while output voltage varies with the load requirements. The constant current mode was selected to generate the required electric field in order to control the electrolysis reactions at the electrodes such that a constant rate of production of electrolysis products occurred. The current displayed by the power supply was determined to be accurate to 0.1% as specified by the manufacturer and any other current measurement was not found to be necessary.

5.2.4 **Instrumentation**

Various probes and devices were used to monitor physicochemical changes in the soil while processing. Voltage probes were used to monitor the voltage distribution across the soil; thermocouples to monitor temperature changes, tensiometers and transducers to monitor suction, and pH meters to monitor cathode and anode pH values.

Tungsten wires were inserted at different locations and used as voltage probes to measure the electrical potential distribution across the soil mass. It was estimated that a 200 to 300 volt difference will be developed between the electrodes (2-4 V/cm) at 130 μA/cm. A voltage divider was designed and built to attenuate 0-300 V range to a 0-10 V range. **A** schematic diagram of the voltage divider is shown in Figure 5.2. T'he formula used for dropping **the** voltage proportionally is given by

$$\text{Attenuation} = \frac{R1 + R2}{R2} \qquad (5.1)$$

An important factor in deciding the values of resistors used was that the resistors RI and R2 are going to dissipate all the power in the divider. The higher the value of the resistance (R1 + R2) the less power was dissipated by the divider circuit. The values of R1 and R2 used were 10 M ohm and 360 k ohm, respectively.

Suction in the soil across the electrodes was measured using tensiometers connected to transducers linked to a demodulator. Figure 5.3 shows the suction measurement setup. Tensiometers consisted of **a** porous ceramic cup connected through an airtight tube filled with water to a transducer (or manometer). When the porous cup was placed in the soil, the bulk fluid (water) inside came into contact with the soil pore fluid. Generation of suction in **the** soil pore fluid is then transmitted to the fluid inside the cup and consequently to the transducer. The

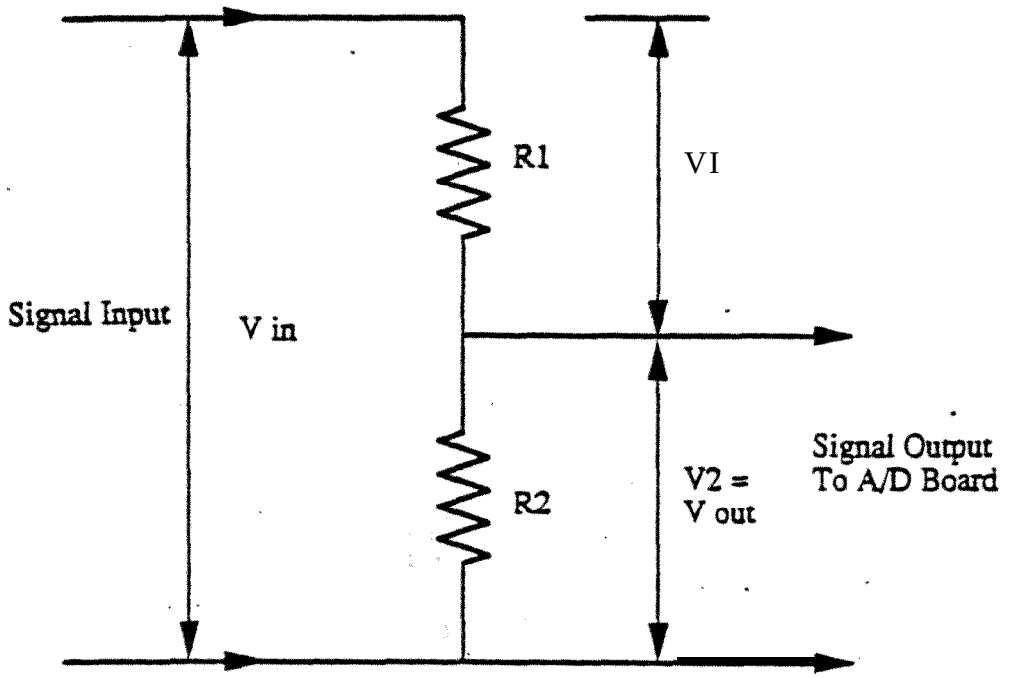

$$\frac{Vin}{V\ out} = \frac{Rl + R2}{R2}$$

Figure 5.2: Voltage Divider

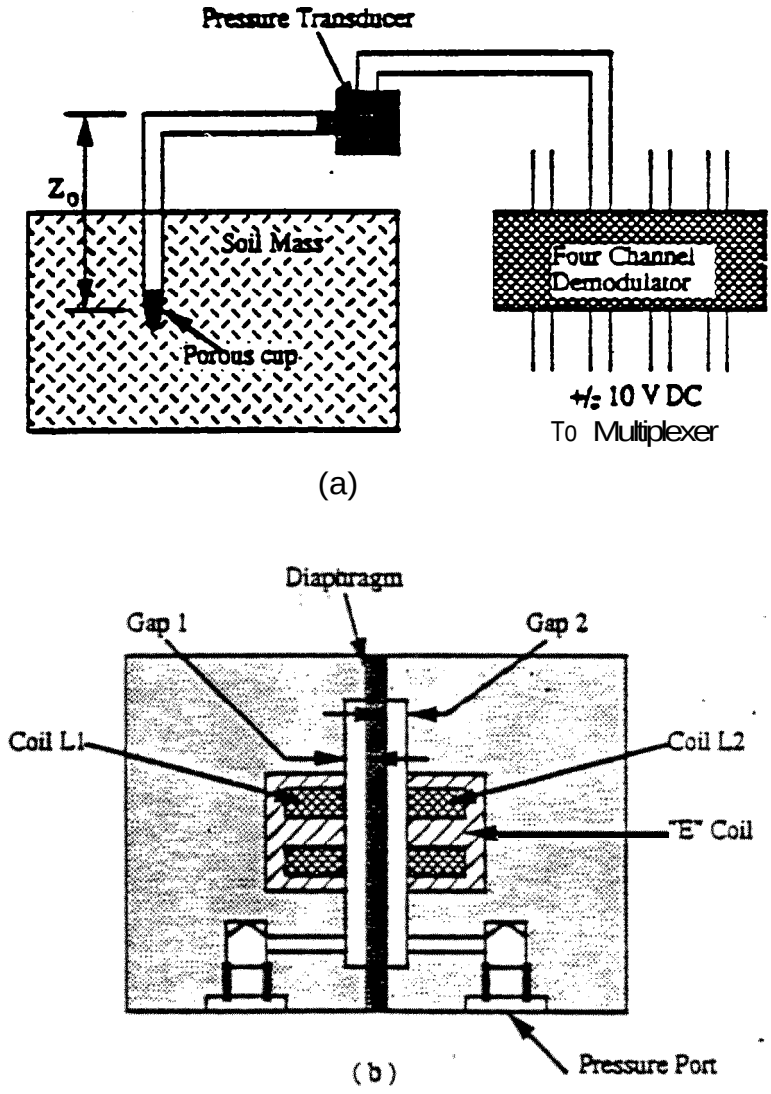

Figure 5.3: A Schematic View of Suction Measurement **Devices**

measured pore water pressure or suction will have a gravitational component that varies with the reference level. As shown in Figure 5.3, the gravitational component of the tensiometer pore fluid, z, was determined from the elevation of the porous cup relative to the reference level. The porous ceramic cups, purchased from Soilmoisture Equipment Corporation, were 2.86 cm (9/8 in) length, 0.64 cm (1/4 in) outer diameter and with 100 kPa air entry value. Plate 5.2 shows the porous cup together with other probes used in large-scale experiments.

Pressure transducers, DP215 purchased from Validyne Engineering Corporation, were used to evaluate the suction generated in the tensiometers. Figure 5.3 presents a schematic diagram of the pressure transducer. The transducer block consists of a diaphragm sensitive to pressure changes placed between two coils. When suction is developed in the tube coming from a tensiometer it will cause the diaphragm to deflect towards the cavity. As a result the magnetic field between the inductance coil emplaced in each block is disturbed and an electric potential is generated across the coil. The magnitude of this potential represents the amount of diaphragm deflection.

Pressure transducers require an AC excitation and return an AC signal. A carrier demodulator, therefore, is needed to provide the AC excitation and convert the AC sensor signal into a high level DC output. CD280 four channel carrier demodulator with ±10 V DC analog output is purchased from Valibyne Engineering Corporation and used for this purpose. It is noted that tensiometers provide the matric suction and they measure suction up to 90-100 kPa.

Measurements of anolyte and catholyte pH vaIues were conducted using a ColeParmer Model 5656-00 pH controller and Model 5593-70 pH eIectrodes. pH electrodes were first immersed in the anolyte and catholyte. Unfortunately, the electric field in the cathode and anode compartments affected the pH readings of the anolyte and catholyte. It was therefore necessary to measure the anolyte and catholyte pH without the interference of this electric field. Water in each compartment was cycled into a separate container using a Cole-Parmet MasterfIex L/S pump. Water level in each container was kept at the same level with the electrode compartments. Water was pumped from these containers to the anode (or cathode) compartment using the pump. If the water level increased at the electrode compartments, it was drained back to the container to keep the same head level (the hydraulic system used is described in details in Section 5.9). However, if water level increased in both of the electrode compartments and the containers due to electroosmotic or hydraulic flow, then it would be drained from the container, collected in a

separate bucket, and the volume of the collected fluid was measured in time. pH meters were then connected to the MUX32 multiplexer to monitor the pH readings by the computer. At the same time, samples of the cathode and anode fluid were taken continuously for pH measurements for cross checking purposes.

Thermocouples were used for temperature measurements during testing. Teflon coated copper-constantan thermocouples, 30.5 cm (12.0 in) length and 0.32 cm (l/8 in) outer diameter, were purchased from OMEGA for this purpose. Thermocouples were formed of two dissimilar metals that were joined together at one end. When this end was heated a thermoelectric (or Seebeck) voltage was generated due to difference in thermoelectric properties of the two metals. Thermocouples were connected to a multiplexer which provides a cold junction compensation and amplifies low level signals.

5.3 Data **Acquisition System**

The hardware utilized in the data acquisition process was a Zenith PC microcomputer with CIO-DAS16 A/D (Analog/Digital) board and CIO-MIX32 multiplexer. The software package used was Labtech-Notebook Version 7.0.

The DAS 16 board, purchased from CyberResearch Inc., supplied 16 single-ended or 8 **difffercntial** input channds (256 differential with multiplexer). The input ranges were 0-l 0 for unipolar inputs, **or ±** 5 for bipolar inputs. The MUX32 panel multiplexes every 16 channels into one input channel on the DAS 16 board, allowing up to 256 differential inputs to one DAS 16 board. The multiplexer also supplies a coldjunction compensation for thermocouple measurement, has selectable 7 Hz input filtering, and can amplify the input readings by a selectable gain. The MUX32 panel was connected to the DAS 16 board through a 37-pin shielded round cable.

Labtech Notebook, an integrated software package for data acquisition, process control, monitoring, and data analysis was used. The software can support up to 500 single channels.

5.4 **Soil Description**

Air floated Georgia kaolinite from Thiele Kaolin Company, Georgia, was used for this study. This mineral was selected because of its low activity (activity is defined as the ratio of the plasticity index to the clay size fraction of the soil) and high electroosmotic water transport efficiency relative to other clay minerals. Table 5.1 presents the physicochemical properties of the soil provided by Thiele Kaolin Company for the soil used in this project. The compositional and engineering properties of Georgia kaolinite, determined by previous research work at Louisiana State University (Putnam 1988; Hamed 1990), are summarized in Table 5.2. These properties were rechecked for this project and they were not found to be significantly different. Chemical analysis of the kaolinite used in this project is presented in Table 5.3.

5.5 Chemical Species

Lead nitrate [$Pb(NO_3)_2$] Salt was used as the source of lead because it has high solubility in water and can provide the necessary ionic forms of lead and nitrate. Lead nitrate solution was prepared by mixing a pre-evaluated weight of lead nitrate salt (depending upon the required concentration) with the required volume of tap water. For example, in PST1, 0.0094 **M** lead nitrate solution is prepared using 31 g of lead nitrate and 10 L of tap water. 20 ml of nitric acid was added to prevent hydroxide precipitation from the hydrolysis of lead ion.

5.6 **Permeation Fluid**

Tap water was used for the cathode and anode compartments. Tap water was supplied at the anode from a source tank and collected at the cathodes, as described in Section 5.9. Chemical analysis was conducted on some tap water samples and Table 5.3 presents the average concentrations of the cations and anions present in the tap water used in this project.

Table 5.1: Physicochemical Properties of Georgia Kaolinite Provided by Thiele Kaolin Company

Hygroscopic Moisture Content (%)	0.5 - 1.5
Specific Surface Area (m^2/g)	20-26
pH (20% Solids)	3.6
Silica (SiO_2) %	43.5 - 44.5
Alumina (Al_2O_3) %	38.0 - 40.5
Iron Oxide (Fe_2O_3) %	0.9 - 1.3
Titanium Dioxide (TiO_2) %	I.4 - 3.5

Table 5.2: Charactaistics of Georgia Kaolinite (Hamed, 1990)

Mineralogical Composition (% by Weight)	
Kaolinite	98
Illite	2
Index Properties (ASTM D 4318)[a]	
Liquid Limit (%)	64
Plastic Limit (%)	34
Specific Gravity (ASTM **D** 845)[b]	2.65
% Finer than 2 μm Size	90
Activity	0.32
Cation Exchange **Capacity** **(milliequivalents/100 gm** *of dry soil)*	1.06
Proctor Compaction Parameters	
Maximum Dry Density ($tons/m^3$)	1.37
Optimum Water **Content** (%)	31.0
Initial pH of Soil[c]	4.7-5.0
Compression Index (C_c)	0.25
Recompression **Index** (C_r)	0.035
Permeability of Specimens Compacted **at** the Wet of Standard Proctor Optimum (x 10^{-8} cm/sec)	6-8

[a] ASTM Method for Liquid Limit, plastic Limit, and **Plasticity** Index of Soils (D 4318)
[b] ASTM Method for Specific **Gravity of Soils (D** 854-58)
[c] **pH Measured** at 50% Water Content
[d] Flexible Wall Permeability **at Full** Saturation

Table 5.3: Chemical Concentrations of Kaolinite and Tap Water

Cation	Kaolinite + DI µg/g	Kaolinite + HNO_3 µg/g	Tap Water mg/l
Pb^{2+}	0.70	2.75	0.05
Fe^{3+}	0.04	109.20	0.00
Ca^{2+}	66.78	183.20	1.48
Mg^{2+}	25.74	125.32	0.06
Si^{4+}	128.80	639.60	10.90
Al^{3+}	3.45	615.00	0.03
Na^{+}	1323.80	1555.00	98.99

Anion	Kaollinite + DI* µg/g	Tap Wata mg/l
Cl^-	502.0	22.8
NO_3^-	126.0	8.2
SO_4^{2+}	114.0	9.0

DI : Deionized Water

5.7 Bench Scale Tests

The procedure used in bench-scale tests was the same as that used by Hamed (1990). Two bench-scale tests were conducted at a concentration of about 1,500 ug/g. For both tests, 0.0165 M lead nitrate solution was prepared using 7.23 g of lead nitrate salt, 1.320 L of tap water and 2.0 ml of nitric acid. 3.0 kg sample of dry kaolinite was mixed with 1.320 L of the solution to bring the soil to 44% water content. The soil sample was cured for 24 hours. The specimen was then divided into two parts and each one was compacted in polyacrylite sleeves of 10.2 cm (4 in) in length and 10 cm (3.94 in) inside diameter. The sleeves were weighed before and after compaction all then directly, inserted in the electroosmotic cell in one-dimensional test.

Electroosmotic test specimens were then assembled as shown in Figure 5.4 (Hamed 1990). Inert graphite discs of 0.13 cm (0.125 in) thickness and 10 cm (3.94 in) diameter were selected as electrodes. Two sheets of 8 μm filter papers were placed at both ends of the specimen. Uniform flow conditions through the electrodes were ensured by drilling fifty holes of 0.3 cm (0.12 in) diameter into the electrodes. The electrodes were held in place by polyacrylite end caps connected with threaded rods. A liquid reservoir of 1100 ml capacity was available at each end. Holes were drilled into the top of each cap above the reservoir to allow venting of gaseous electrolysis products.

5.8 Pilot-Scale Tests

Two pilot-scale tests were conducted on kaolinite spiked with lead at concentrations of about 850 μg/g and 1,500 μg/g. A third pilot-scale test was conducted on a Kaolinite/sand mixture spiked with lead at a concentration of 5,000 μg/g. In these tests, kaolinite samples were mixed with lead nitrate solution in several batches before compaction. In each batch in the first test, 0.0094 M lead nitrate solution was prepared using 31.00 g of lead nitrate salt, 10 L of tap water and 20 ml of 1.6M nitric acid. One bag of kaolinite (22.7 kg (50.0 lb) of dry weight) was placed on the Gundle liner on the laboratory floor. The solution was then added to the dry kaolinite using a sprinkler with continuous mixing using a large shovel. The sample was placed in the concrete mixer and the mixer is turned on for about 10 minutes. Large clods (about 25 cm in diameter) of spiked kaolinite were formed in the mixer. These clods were then cut into smaller pieces (of about

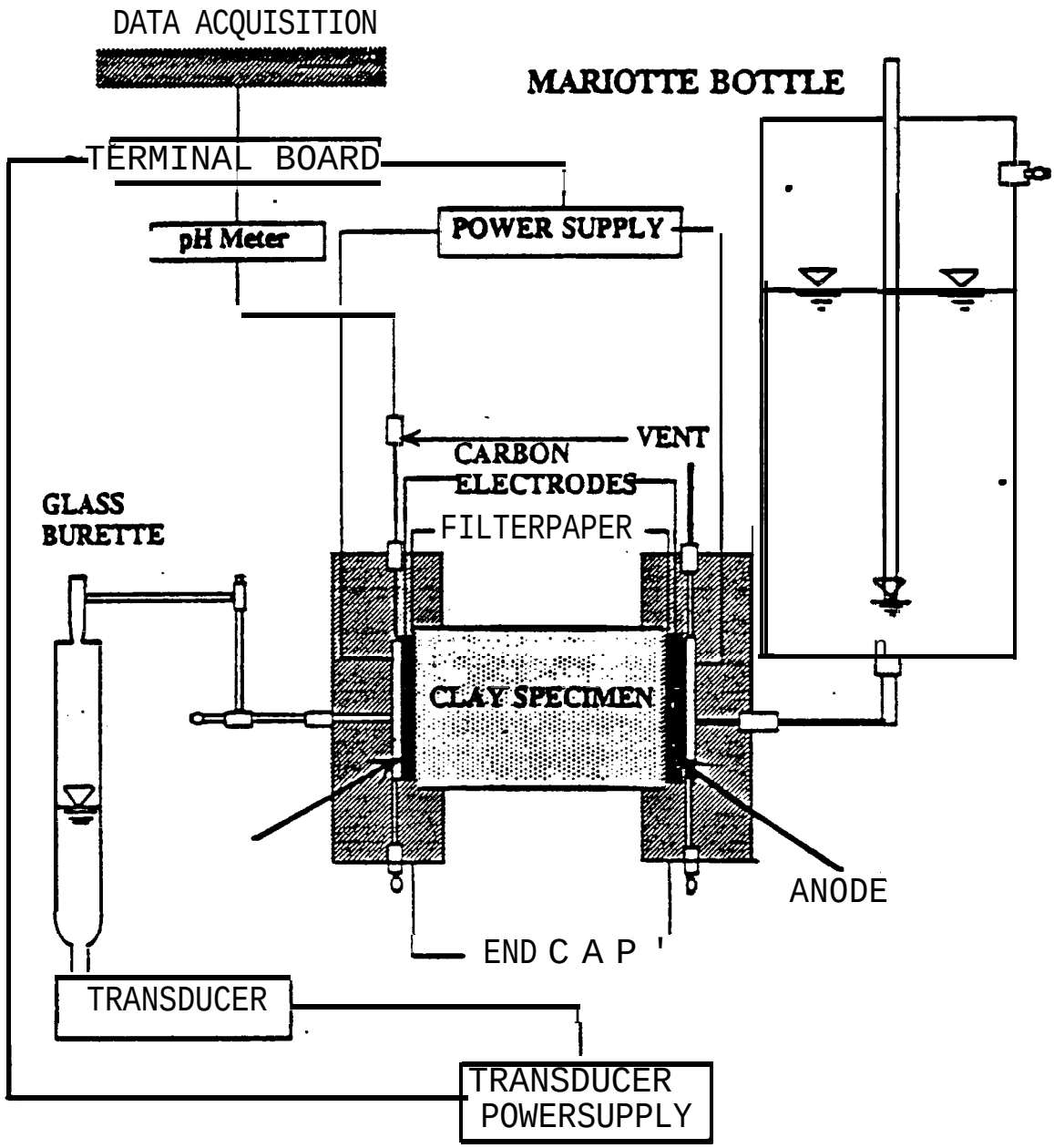

Figure 5.4: Schematic View of the Bench-Scale Test Set-Up (Hamed, 1990)

5 cm in diameter) and placed on the liner inside the box. For every layer, 8 bags were mixed each day and cured for 24 hours. A plastic wrap was used to cover the clay while curing to minimize evaporation.

Compaction was achieved with a hammer manufactured for the purpose. The hammer was a steel rod, 91.44 cm (36.0 in) in length, welded to a steel plate with a contact area of 15.24 cm x 15.24 cm (6.0 in x 6.0 in). The gross weight of the hammer was 4.54 kg (10.0 lb). Each layer was compacted by dropping the hammer a 1000 times on the top of the soil from a height of about 91.44 cm (36.0 in). The compaction energy applied by this procedure was less than the standard proctor compaction energy; however it was enough to bring the soil to 1.2 t/m^3 at the wet of optimum water content dry density at a relatively high degree of saturtion (approximatdy 90%).

Three small wooden boxes were then placed on top of the first layer inside the container. These boxes were placed at middle and at both sides of the container to form the electrode compartments. The outer dimensions of these boxes were 13.5 cm x 89.0 cm x 91.4 cm (5.3 in x 35.0 in x 36.0 in). Gundle composite fabric and geotextile grid were used to separate the wooden boxes from the compacted soil, as shown in Figure 5.1. The three boxes placed in the container were removed using a fork-lift after compaction of all soil layers.

A large fork was used to scarify the surface of the first Iayer before compacting the second layer in an attempt to ensure full integrity between the first and second clay layers. The remaining layers were then compacted using the same procedure.

The same mixing procedure was employed in the second test with only one difference. The lead nitrate solution used in each batch (22.7 kg of dry kaolinite) in the second test was 0.0166 M, prepared using 55.00 g of lead nitrate salt, 10 L of tap water and 20 ml of concentrated nitric acid (16M HNO_3).

For the third pilot-scale test, kaolinite/sand mixture was spiked with lead nitrate solution at a concentration of 5,500 µg/g. 0.1213 M lead nitrate solution was prepared by mixing 400 g of lead nitrate salt with 10 L of tap water. One bag of kaolinite (50.0 lb dry.weight) was mixed with a half bag of fine sand (50.0 lb of dry weight) to form 1:1 kaolinite/sand mixture. The soIution was then mixed with this soil to bring the required lead concentration to a water content of 22%. Compaction was then achieved by using a similar procedure to that above.

5.9 Test Setup

As demonstrated in previous sections, three rows of electrodes were placed in compartments in the soil, as shown in Figure 5.1. A polyacrylite frame is placed in each compartment to hold the electrodes (plate 5.1). Each row was formed of five graphite electrodes. The compartments were then filled with tap water up to a level of 4.0 cm below the clay surface level (the total water volume in each cathode or anode compartment is 70.2 L). The central row of electrodes was selected to be the anode while the two cathode rows are at the ends at a distance of 2.5 ft from the anode row.

Since the electroosmotic flow was expected to occur from the anode towards both cathodes, a water tank was connected to the anode reservoir to supply the rquired amount of flowing fluid. Water was collected from both cathode compartments in separate containers. In order to avoid introduction of advection due to any external hydraulic potential difference, the hydraulic head was kept constant and equal at both cathodes and anode compartments during the experiment with zero head difference (Figure 5.5). This provision permitted evaluation of the effect only of the electrical potential gradients on water flow within the system.

The pilot-scale sample in each test was composed of two identical halfs or cells (plate 5.3). An electric current of 1.7 A was supplied to the sample at the anode. This current was divided to supply the two halves with 0.85 A each. The cross sectional area of the soil treated was 6,398 cm^2 (91.4 cm width x 70.0 cm height) and the applied current density was 0.13 mA/cm.

Voltage probes, tensiometers, and thgermocouples were used to monitor changes in voltage distribution, suction, and temperature across one cell (Figure 5.6), while the second cell was used for sampling, to assess the concentration changes with time. Instruments were calibrated before and after each test. Voltage probes were calibrated using a voltmeter. A power supply was used to feed the data acquisition system with a known voltage (measured with a voltmeter) and the computer reading was adjusted to give the right value. The process was repeated three times with different voltage values and then a check was made on the readings with another two voltage readings. The voltage values used for calibration covered the voltage range expected during testing. Thermocouples were calibrated using ERTCO No. 65514 NBS traceable thermometer. Two different temperature readings were used for calibration, one is for a cold water sample and

Plate 5.2: Various Probes Used in Large-Scale Experiments

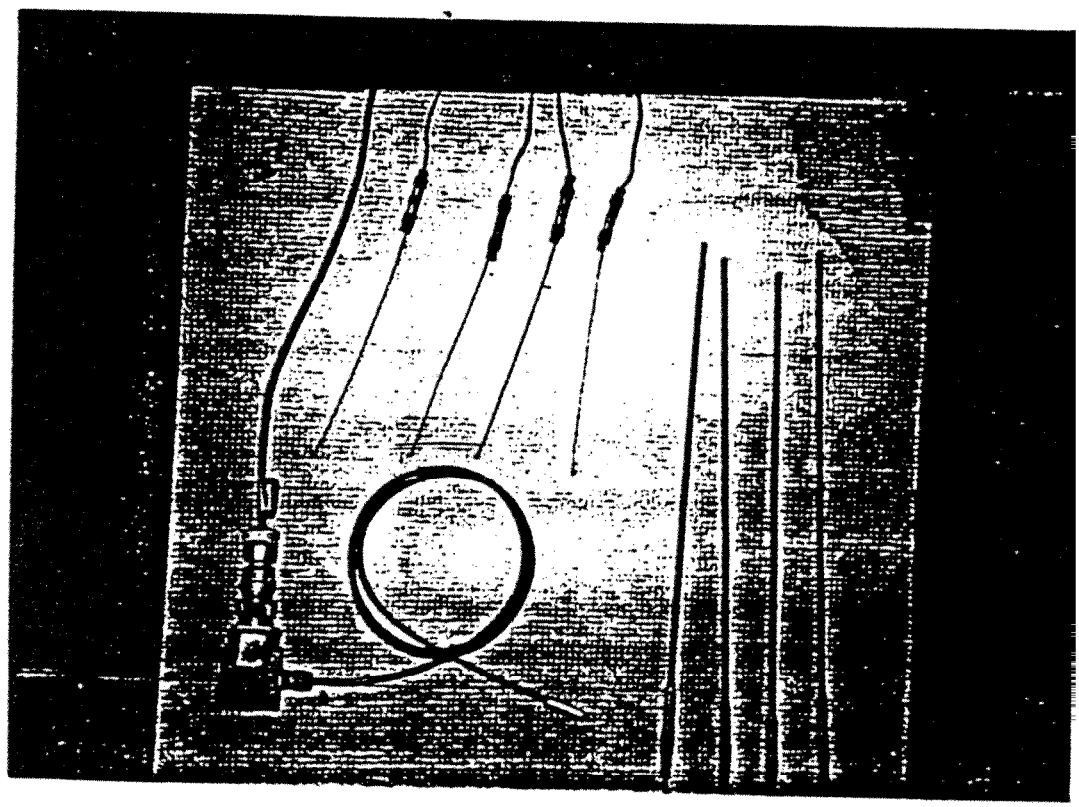

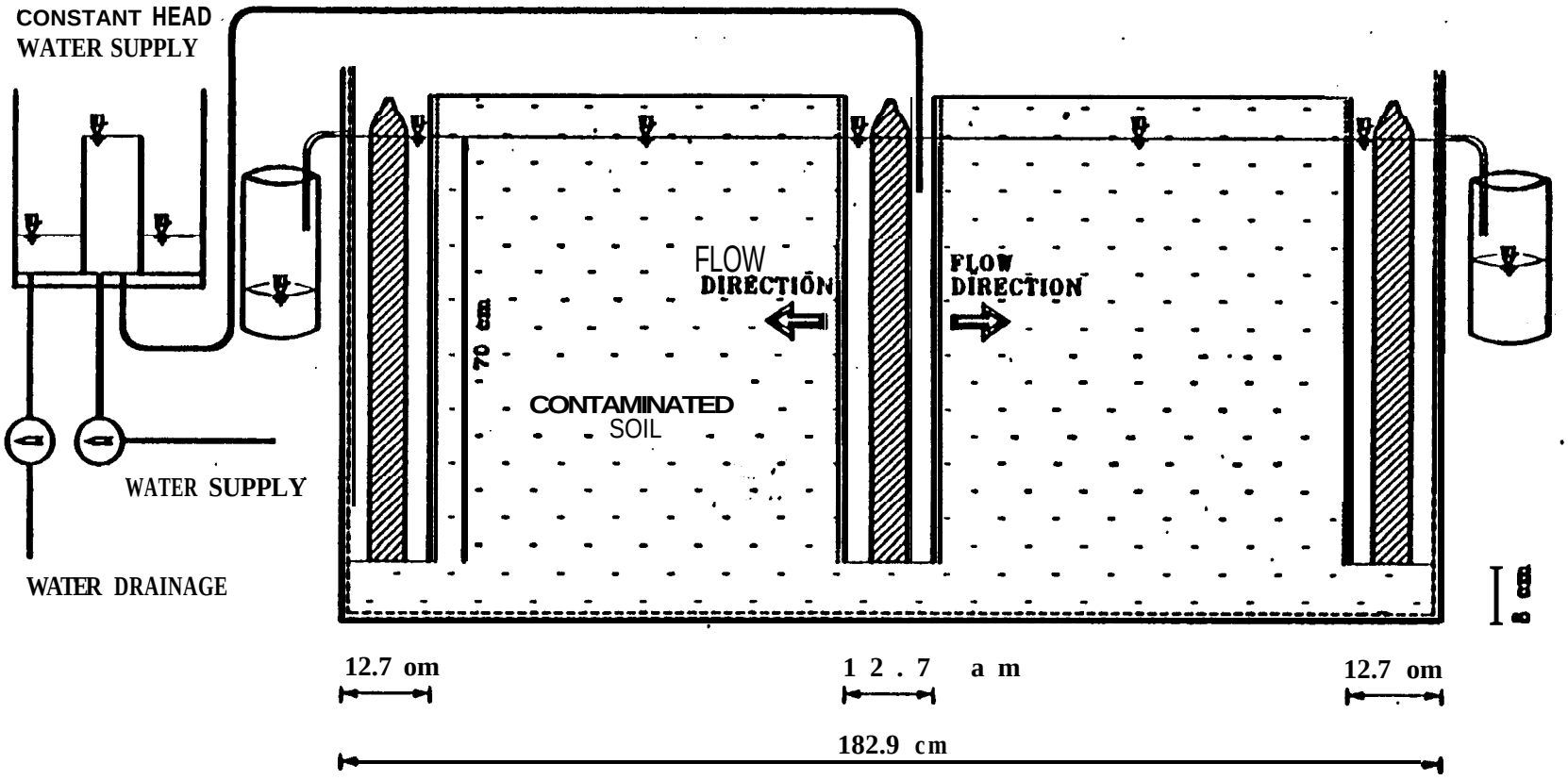

Figure 5.5 Longitudinal Cross-Section of the Pilot-Scale Test Sample Depicting the System Used for the Hydraulic Flow

Plate 5.3 The Wooden Box Used in Pilot-Scale Tests Showing the Two Cells (A and B), the Anode and Two Cathodes.

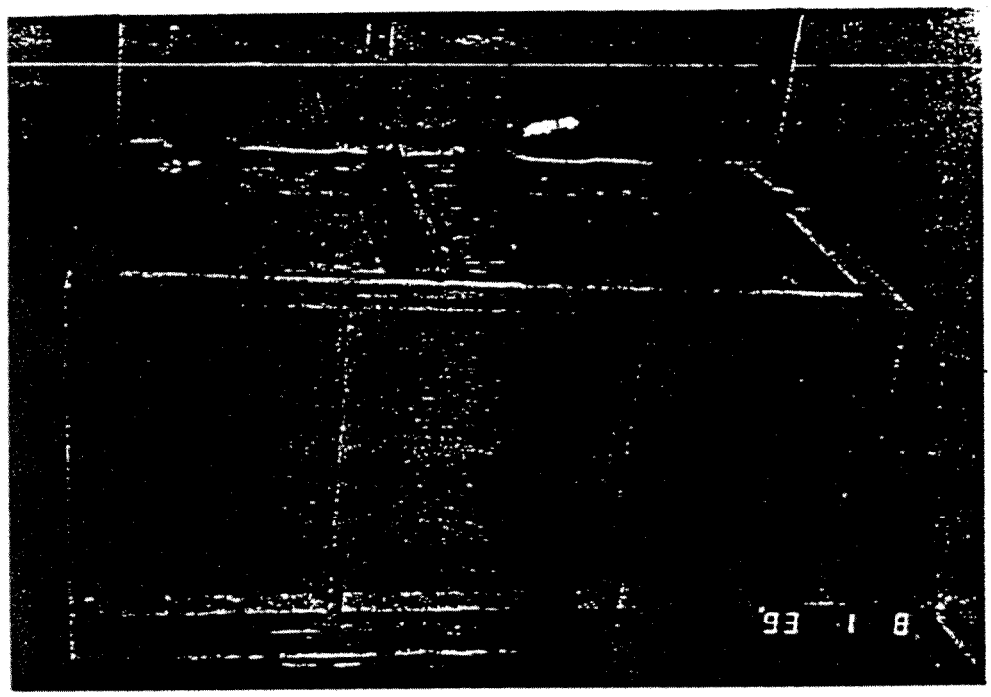

another for a heated water sample. A third reading was taken for a normal water at the ambient room tenperature to check the thermoccouple calibration Tensiometers were calibrated using water columns with different heights to give different pressure heads. The water columns were used to give both positive and negative pressure values for calibration. A check was also made for tensiometer readings at different water levels. After calibration the probes were inserted in the soil as shown in Figure 5.6.

The devices used for measuring voltage distribution, anode and cathode pH, pore water pressure, and temperature were then connected to the MUX32 multiplexer (Figure 5.7). The data generated were then transmitted to the DAS16 A/D board in the 386 Zenith PC, and Labtech Notebook software was used for data acquisition and monitoring

5.10 Chemical Analysis

Chemical analyses of soil and fluid samples were made using inductively coupled plasma (ICP), at the Wetland Biogeochemical Institute of Louisiana State University. Soil samples were oven dried for 24 hours at a 110^0 C. Then, 2 g samples of the oven dried soil were placed in 50 ml centrifuge tubes and mixed with 40 ml portions of 1.6 M nitric acid. The mixtures were treated for 48 hours with continuous shaking to allow dissolution of the salts present and desorption of the adsorbed species. This procedure is a non-standard, simplified version of the standard U.S. EPA procedure for total lead analysis (EPA 1992; SW-846). It was found that the lead concentrations obtained using this method were within 2-4% of those obtained with the EPA method. The mixtures were filtered and the solutions were sent for ICP chemical analysis.

5.11 Soil Sampling

Pilot-scale test specimens were sampled during and after terminating the electrokinetic process. Final analyses of the water content, pH, and chemical concentration were conducted by dividing each bench-scale and pilot-scale soil specimen into samples and subsamples. For bench-scale experiments, the soil specimens were divided into 10 cylindrical sections, each 1.0 cm length and 10.0 cm diameter. pH readings were taken for each section; before oven drying them for chemical analysis and water content evaluation.

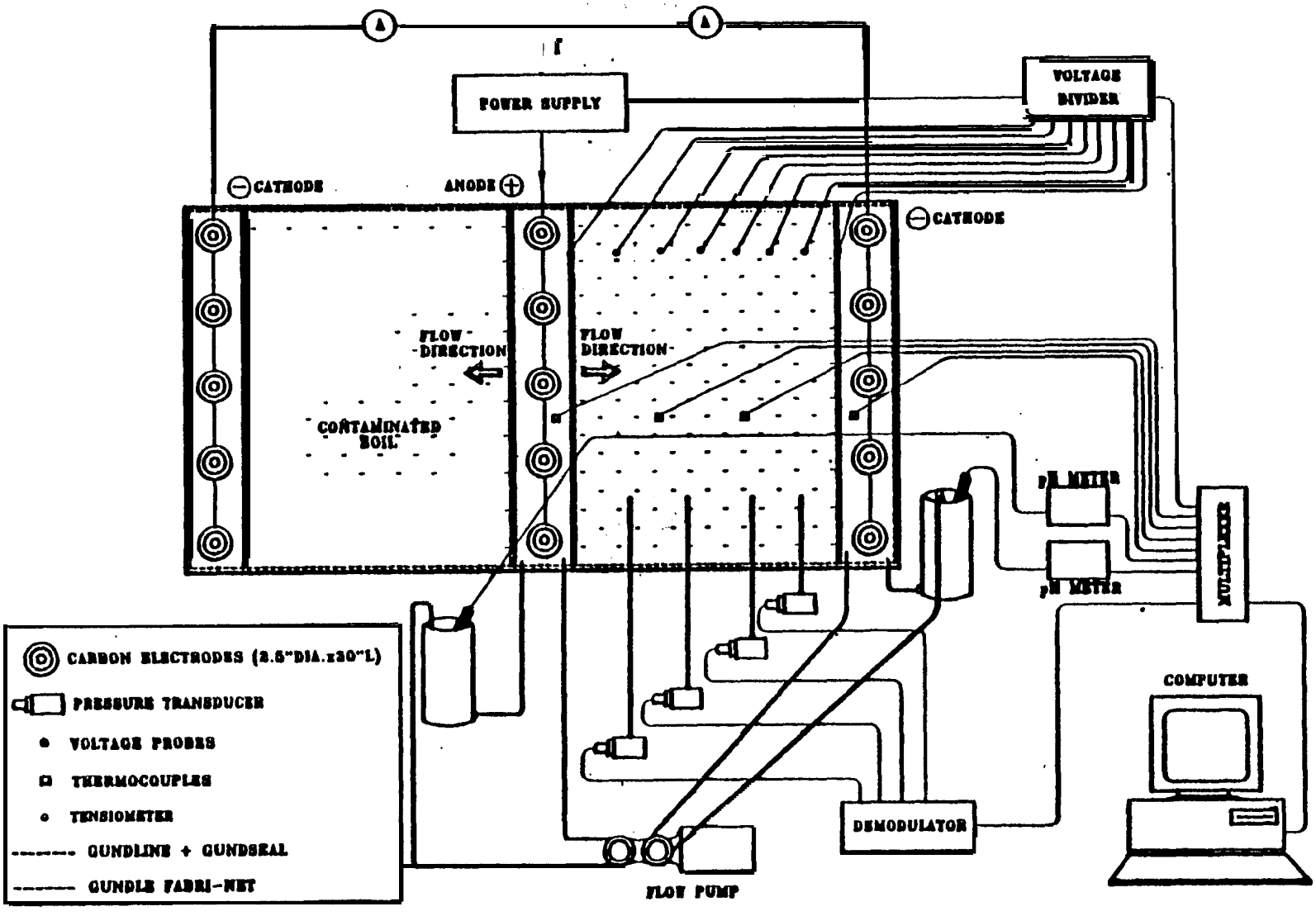

Figure 5.6: A Schematic Diagram of the Pilot-Scale Test Setup

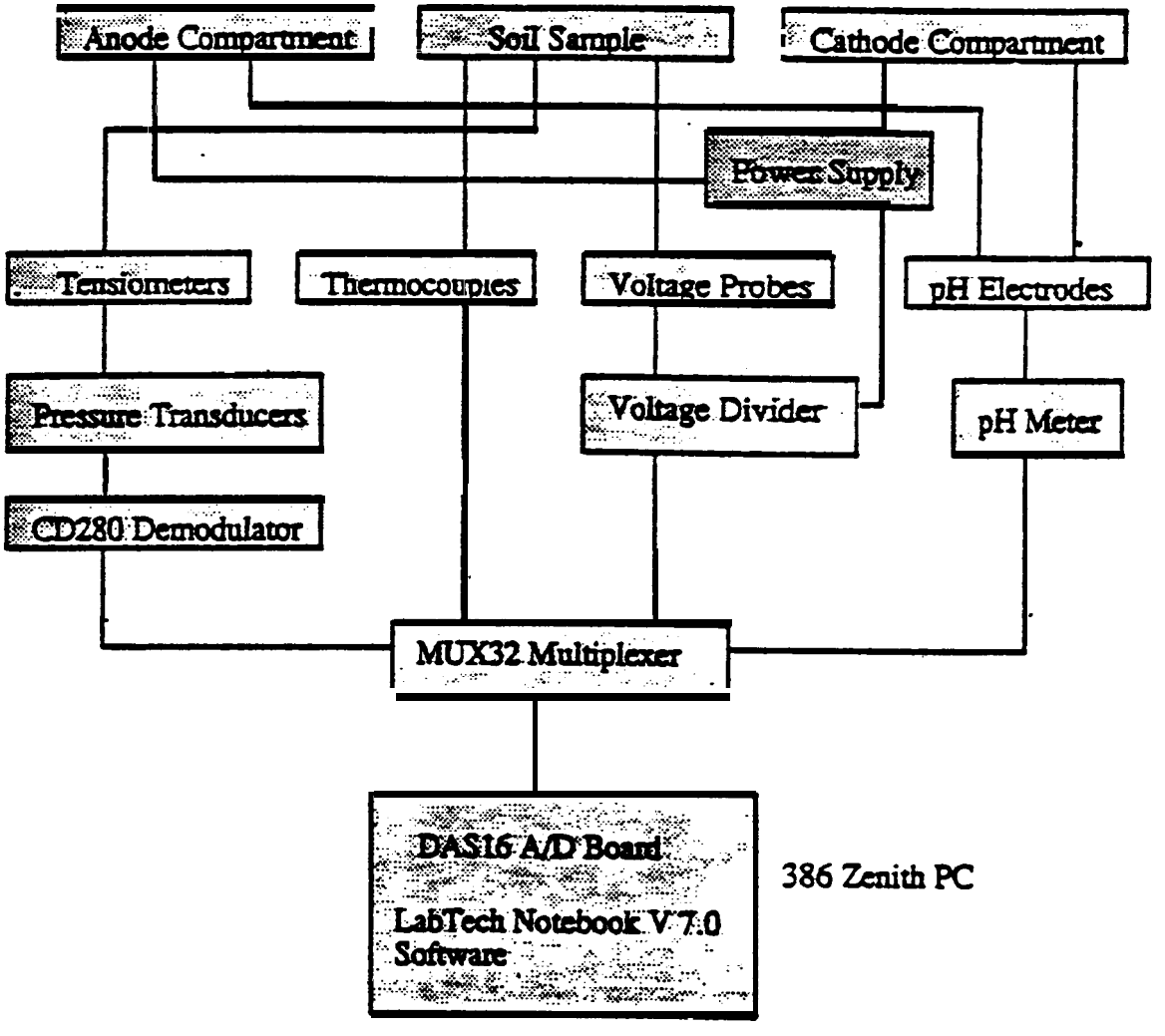

Figure 5.7: A Schematic Diagram of the Data Acquisition System

For the first pilot-scale test, the soil was divided into **3** horizontal layers, top layer (layer l), middle layer (layer **2), and** bottom layer (layer **3).** Each layer was divided into 10 longitudinal sections each of **7.0 cm** length and **6** lateral sections of equal size. As a result, 180 soil samples were taken from the first pilot-scale test; each sample represented a soil volume of (7.0 cm **x** 15.2 cm x 25.4 cm). The same procedure was used for the second pilot-scale test but with a change in size of sections. Each cell of this test was divided into five horizontal layers with the top layer being layer 1 and the bottom layer being layer 5. Each layer was divided into 10 longitudinal sections and 4 lateral sections of equal size. Figure 5.8 displays a schematic diagram of these sections in the second pilot-scale test . Consequently, each cell in the second pilot-scale test was divided into 200 samples of equal volume (7.0 cm x 22.8 cm x 15.2 cm). A total of 400 samples were collected for the second pilot-scale test. Each cell of the third pilot-scale test was divided into three horizontal layers with the top layer being layer I and the bottom layer being layer 3. Each layer was divided into 10 longitudinal sections and 2 lateral sections of equal size. Consequently, each cell in the third pilot-scale test was divided into 60 samples of equal volume (7.0 cm x 45.6 cm x 25.4 cm). A total of 80 samples were collected at the end of processing the third pilot-scale test

Soil sampling for chemical analyses during processing of the pilot-scale-tests were accomplished using sampling probes of 2.54 cm (1.0 in) diameter and 6 1.0 cm (24.0 in) length. These probes were used to take core sample at three different elevations in the soil, each sample representing one third the depth. Each sample was oven dried and mixed thoroughly. Chemical analyses were then made for these specimens as described before. Locations for sampling points are shown in Figure 5.9.

5.12 Standard Methods and Procedures

As mentioned in Section 5.2, there are no standards available for conducting pilot-scale laboratory tests. Standard procedures were used whenever and wherever possible. Measurements conducted in this study include: water content, pH, suction, and cation and anion analysis. The electric current was set constant in all tests. The following methods were used:

water content: The standard method used for water content calculation is ASTM D2216 "Laboratory Determination of Water (Moisture) Content of Soil and Rock". Measurements were conducted immediately after sampling without any holding time.

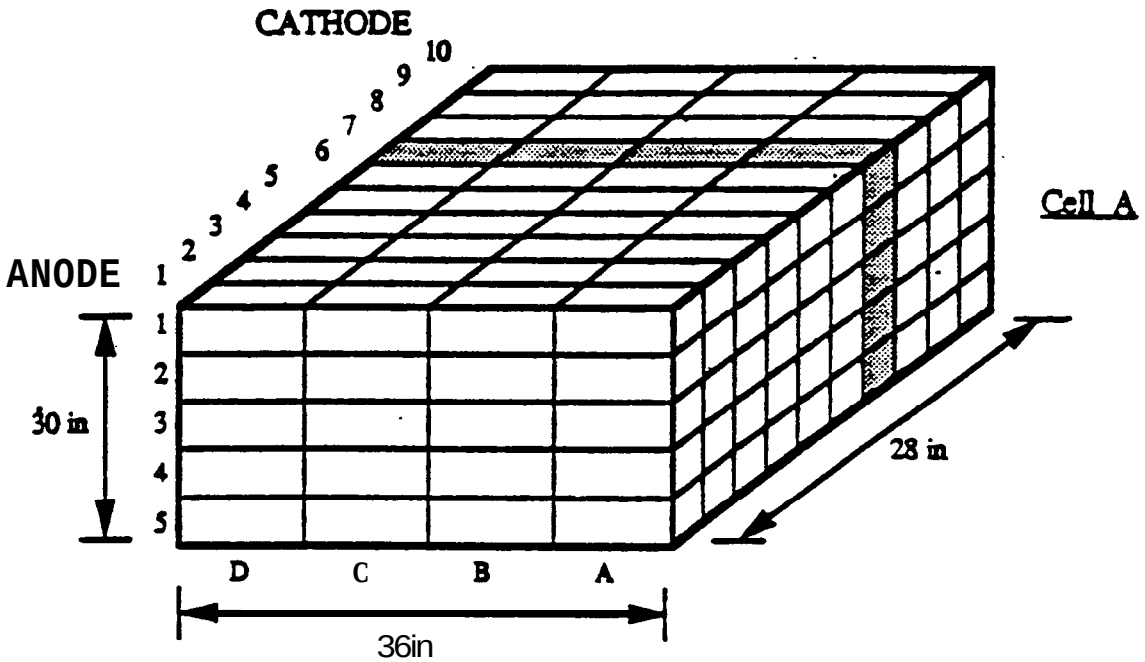

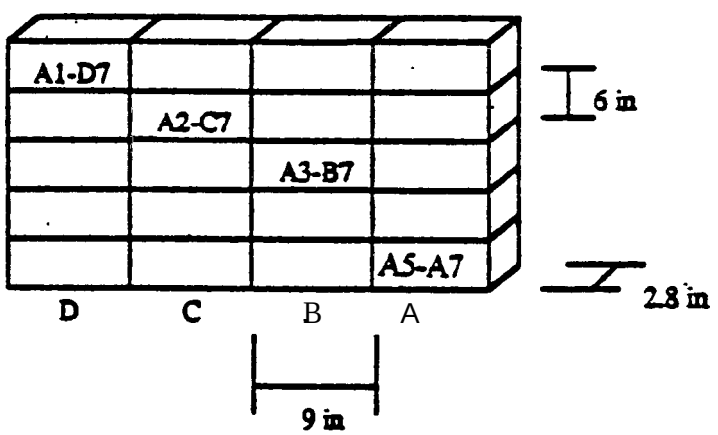

Sample (A3-B7) = Sample in Cell A, Layer 3, Section B7

Figure 5.8: Sampling Locations for Final Analysis in the Second Pilot-Scale Test

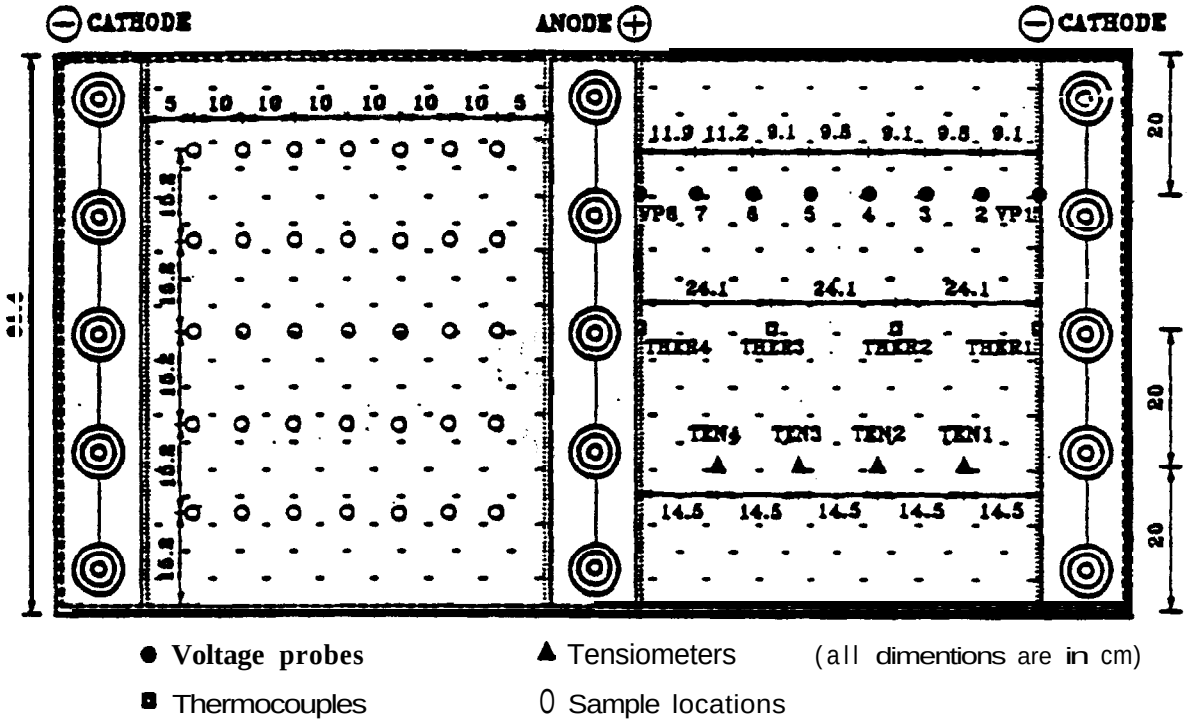

Figure 5.9: Distribution of Monitoring Probes and Locations of Sampling Points

pH: Two methods were used in pH measurement. The first is following the procedure described by Hamed et al. (1991) and the second is ASTM D4972 "Stardard Test Method for pH of Soils". In the first method, all calibration and standardization procedure were conducted similar to ASTM D4972. The difference between the two methods is that in the first procedure the pH electrodes were inserted in the soil at processing conditions. In the second test, the electrodes are inserted in a soil/liquid suspension. Acar et al. (1989) and Hamed (1990) discuss the differences between the two procedures. All pH measurements were conducted immediately without any holding time.

Pore Water presure: Pore water measurements were taken during processing in accordance with ASTMD3404 "Measuring Matric Potential in the Vadose Zone Using Tensiometers".

Metal (lead) analysis: **EPA SW846** Method **6010A** "Inductively Coupled Plasma-Atomic Emission Spectroscopy" was used for metal analysis in the extract Holding times were less than one month for all metal analysis.

Anion analysis: EPA SW846 Method 9056 was used for anion analysis. Holding times for anion analysis were within one week of sampling.

General procedures and methods for sample preparation, mixing, compaction, testing, and sampling are described in Section 5 (Experimental Model; see 5.8 and 5.9). A summary of these procedures is presented:

Sample Preparation and mixing: No standard methods are available for spiking about 1 ton **of soil.** Based on each test requirements (mainly, water content and lead concentration requirements), pre-calculations were made for soil mass, water volume, and lead nitrate mass required for mixing. Accordingly, a specific volume of lead nitrate solution was mixed with a specific weight of the soil. This procedure was the most feasible for the study. Water content and lead concentrations in the soil were evaluated after mixing and compaction.

Soil Compacting: Compaction procedure is described in 5.8 (Pilot-Scale Tests). Compaction was conducted in a way similar to the Proctor Standard Compaction Test (ASTM D698). Compaction effort was applied in a systematic way to minimize variations between the layers. The compaction was achieved in layers of similar thickness. Same compaction energy was applied to each layer. Same personnel were utilized in compaction. Compaction energy was calculated based on dry

density and water content requirements.

Sampling: Soil sampling is conducted in three stages (1) Initial Sampling (2) Sampling during testing, and (3) Final sampling. Sampling was conducted in a systematic manner in all stages. Soil sampling is described in Section 5.11.

Section 6

EXPERIMENTAL RESULTS

6.1 Introduction

The primary objective of the pilot-scale testing was to demonstrate at 80% removal of the lead content in the soil samples. Two bench-scale tests (BST) and three pilot-scale tests (PST) were conducted. Experiment related parameters in these tests are summarized in Table 6.1. Initial conditions, such as dry densities, porosities, degree of saturation, and soil pH were similar in almost all tests. Initial lead concentrations were similar in the bench-scale tests and the second pilot-scale test PST2; both being above the cation exchange capacity of Georgia kaolinite. The current densities were 0.127 mA/cm^2 in bench-scale tests and 0.133 mA/cm^2 in pilot scale-tests. All kaolinite specimens were prepared at a water content of 44%, while the sand/kaolinite specimen (PST3) was prepared at a water content of 24%. These water content levels were chosen to bring the soil above the optimum-water content, which was 31% for kaolinite (Table 5.2) and 20% for 1:1 sand/kaolinite mixture (Nyeretse 1985).

Bench-scale tests (BSTl and BST2) were conducted using kaolinite samples at an initial pH of 4.6 and loaded with lead at a concentration of 1,439 µg/g. The two tests differed in processing periods; the first was disassembled after one week of processing (169 h), while the second, after three and a half weeks of processing (598 h).

The first pilot-scale test (PSTI) was conducted using kaolinite spiked with lead at an initial concentration of 856 µg/g and an initial pH of 4.7. The electrode support used in PST1 was different than that for the other pilot-scale tests (PST2 and PST3). A trench was not used in PST1 for the electrodes. Electrodes were placed in auger holes and they were separated from each other. The decision to use a trench and plexiglas support in PST2 and PST3 was taken to allow homogeneous pore fluid chemistry in the catholyte and anolyte. Unfortunately, the liner in one of the two cells in PST1 was punctured while compacting the clay leading to a leakage of the liquid in one of the cathode compartments. It was decided to shut down that cell and continue processing with the other half of the box by applying half the electric current. Soil samples were not taken for

Table 6.1: Initial Conditions for Bench-Scale and Pilot-Scale Tests

Parameter	BST1	BST2	PST1	PST2	PST3
current (mA)	10.0	10.0	850.0	1,700.0	1,700.0
Dimensions					
Width (cm)	--	--	91.4	91.4	91.4
Depth (cm)	--	--	70.0	70.0	70.0
Length (cm)	10.0	10.0	70.0	70.0	70.0
Diameter (cm)	10.0	10.0	--	--	--
Duration (hr)	169	598	1,300	2,950	2,500
Current, Density ($\mu A/cm^2$)	127.3	127.3	132.8	132.8	132.8
Initial Soil pH	4.6	4.6	4.7	4.5	4.2
Initial Concentration ($\mu g/g$)	1,439	1,439	856	1,533	5,322
Initial Water Content (%)	44.0	44.0	44.1	44.3	24.6
Initial Dry Density (g/cm^3)	1.23	1.23	1.22	1.22	1.80
Initial Saturation (%)	91	91	91	91	90